Research on ECG signal processing for QRS detection and compression in telemedicine system

September 2014

Pu Zhang

Contents

Chapter 1 Introductory chapter

1.1 Research Backgrounds

According to research report by WHO, Cardiovascular diseases (CVDs) killed an estimated 17.3 million people in 2008, representing 30% of all global deaths. And the number of death because of CVDs will increase to reach 23.3 million by 2030 [1]. Eletrocardiogram (ECG) signals acquire cardiac electric activities, which indicate complicated depolarization and repolarization of ventricle and atrium. The waveform pattern and characteristics of ECG signals usually correspond to physiological and pathological changes of heart and human body. Therefore, it becomes a critical index for monitoring patients' situation. Also, ECG signals are the fundamental information to transmit when realizing Telecardiology system as an important sub-system in Telemedicine.

Based on reasons mentioned above, ECG procession and transmission in Telemedicine system have received wide attention in this decade. However, there're some crucial limitations of devices in Telemedicine, such as power consuming, transmission bandwidth, storage capacity, calculation ability and so on. Also Telecardiology system requires real-time transmission and high signal fidelity, which present even more challenges to researches on ECG processing method for Telemedicine system. Nowadays the researchers mainly focus on ECG generation model establishment, noise suppression methods, auto-diagnosis system design, compression and reconstruction strategies built on Telemedicine systems. Meanwhile computational complexity and practical requirement in real-time should also be considered when designing algorithms.

The evaluations for ECG processing methods are mainly implemented in ECG database, which are collected from clinical applications. But the research on abnormal ECG signals, such as ventricular premature contraction (VPC), and corresponding quantitative evaluation of algorithm performances are relatively infrequent. This is because that ECG signal generation models are focus on single type waveform. Therefore, establishing multi-type waveform generation model is critical not only for evaluation of ECG processing methods but also clinical applications, such as ECG classification and auto-diagnosis.

Although ECG pre-processing based on many theories emerge one after another, it is difficult to balance between noise suppression performance and computational complexity while guaranteeing low signal distortion. Take method based on Wavelet for example, when applied to MIT-BIH Arrhythmia Database, the sample rate is 360Hz, at least 10 level decomposition is needed to achieve desirable noise suppression performance. It will bring heave calculation burden on wireless medical devices used in Telemedicine system.

The realization of ECG auto-diagnosis can extremely improve work efficiency of

medical stuff. However, high accuracy is hard to reach. QRS complex detection is the first step to make ECG auto-diagnose come true, as well as R peak interval division that is the precondition for ECG compression and reconstruction. The pseudo-periodicity and waveform mutability are primary causes that 100% positive detection is impossible. To improve the detection accuracy, several kinds of methods based on threshold or math morphology are adopted, but detection method based on single theory cannot adapt to QRS complex with different waveform patterns. Therefore, considering mixed method is the first choice in Telemedicine systems.

Traditional lossless compressing method usually has the disadvantage of low compression ratio and high computational complexity. In Telemedicine system, algorithm design for compression and reconstruction calls for simple compressing at the transmitter, powerful error-correcting ability and high fidelity reconstructing signal at the receiver. New compression theories, such as compressed sensing (CS), can reach above goals and can be adopted in ECG processing models of Telemedicine systems.

1.2 State of the Art Related Work

1.2.1 Research Development in Telemedicine Systems

Telemedicine is defined as the use of telecommunication and information technologies in order to provide clinical health care at a distance. It helps eliminate distance barriers and can improve access to medical services that would often not be consistently available in distant rural communities. It is also used to save lives in critical care and emergency situations [2].

In Telemedicine applications, Tele-diagnosis/monitor is mostly common use, based on which almost all Telemedicine activities can be realized. A typical architecture of Tele-diagnosis/monitor system is illustrated in Figure 1-1.

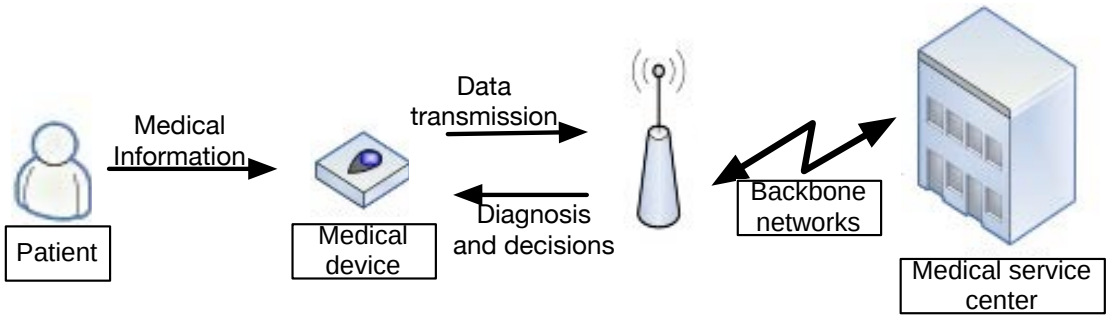

Figure 1-1 A typical architecture of Tele-diagnosis/Tele-monitor system.

Communications between medical devices and medical centers are mainly built up with wireless communication technologies and backbone networks. With rapid development of wireless communication technologies in resent decades, Telemedicine systems have popularized and become an important supplement for routine medical services [3-8]. At the same time, characteristics of medical data

should be considered:

- Variety of data formats and difference of containing information, as shown in Table 1-1. Therefore, it is critical to choose appropriate data formats and strategies for transmission.

Table 1-1 Data formats and data size

Data formats	Data size
Clinical record	3KB
Analysis report	5KB
X-ray imaging	16MB
MR imaging	8MB
CT imaging	20MB
Ultra-sound imaging	5~60MB

- Data transmission security. Medical data usually include personal information; and it is necessary to do encryption during system design.
- Low transmission error and reconstruction distortion. They are the important diagnosis basis for doctors as well as clinical evaluation index for Telemedicine system.
- Real-time transmission in tele-monitor and emergency [9,10]. These will lead to treatment in time for patients in dangerous condition.

Therefore, to realize Telemedicine, several key technologies should be taking into consideration: data encryption; transmission strategies that ensure transmission rate and priority; compression for images and videos with large data sizes; achieving real-time, continuity and coverage through telecommunication technologies [11,12].

1.2.2 ECG Signals' Main Components and Characteristics

ECG signals are cardiac activity waveforms collected by invasive electrodes. A typical normal ECG waveform is illustrated in Figure 1-2, which is consisting of P wave, QRS complex, and T wave:

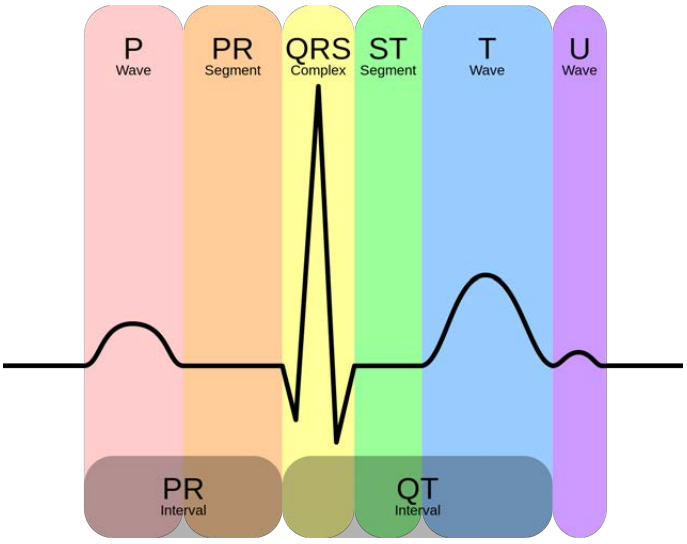

Figure 1-2 A typical normal ECG waveform and its components [13].

- P wave: before QRS complex, consisting of right atrial potential and left atrial potential. Normal P wave is small, smooth and round. Usually the amplitude is under $300\mu V$, and time range is shorter than 0.12s, i.e. frequency range of 10~15Hz. Time range longer than 0.12s, amplitude overtop or sharp, bi-direction, disappearing and other abnormal P wave patterns may be caused by pathologic situation such as arrhythmia, ventricular or atrial hypertrophy and so on.
- QRS complex: reflects the rapid depolarization of the right and left ventricles. Normal time range is 0.07s~0.11s, average amplitude is about 3mV. Time range and PR intervals are helpful when to estimate if there is conduction block. Furthermore, time range becoming longer indicates causes of disease such as right bundle-branch block (RBBB), left bundle-branch block (LBBB), Wolff Parkinson White syndrome (WPW) and so on. Abnormal depth and width of Q wave are considered as a result of myocardial infarction (MI). R wave amplitude is usually related to ages and pathological reasons such as ventricular hypertrophy and anterior MI.
- T wave: represents the recovery of ventricles. The normal pattern is wide and round. Any minute change of T wave, including high-edge, flat and inversion, may be caused by pathological reasons, such as posterior MI, ventricular hypertrophy, pulmonary embolism (PE) and so on.

Clinical ECG signals are collected by 12-lead electrodes, including aVR, aVL, aVF, I~III, V1~V6. The correlations in ECG signals are the basis of processing methods design, and can be divided into three groups:

(1) Correlation between sampling points. ECG signals are generated by continuative myocardium activities, and have very strong correlation between adjacent samples. Figure 1-3 illustrates Lead-II of Sample No. 100 in MIT-BIH Arrhythmia Database and the unbiased estimation of its autocorrelation function:

$$R_{xx,unbias}(m) = \frac{1}{N-|m|} R_{xx}(m) \tag{1-1}$$

where $N = 3000$ is sample number. From Figure 1-3, it is obvious that the correlation between sampling points is stable and strong with cyclical peaks, which proves the pseudo-periodicity of ECG signals.

(2) Correlation between RR intervals. This kind of correlation is manifested in the waveform pattern of P wave, QRS complex and T wave, as well as on/off set positions and characteristics of time intervals. It is also can be found in Figure 1-3.

(3) Correlation between different leads. For instance, RR intervals and R peak positions of different leads are almost the same. However, multi-lead ECG observes cardiac activities from different angles, and there're extreme variation in amplitudes and waveform patterns. And due to pathological, physiological and medicine effects, correlation reduces between leads. Figure 1-4 illustrated two leads of Sample No. 107 in MIT-BIH Arrhythmia Database and the unbiased estimation of its cross correlation function.

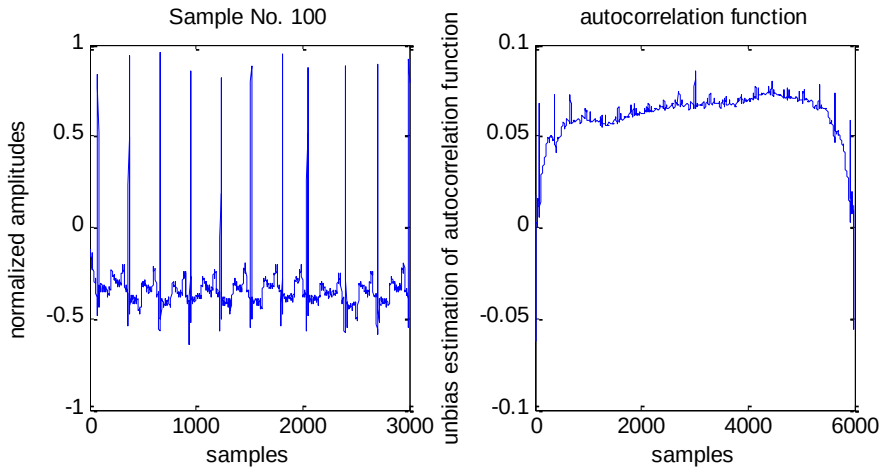

Figure 1-3 ECG of Sample No. 100 in MIH-BIH database and its unbiased estimate of autocorrelation function

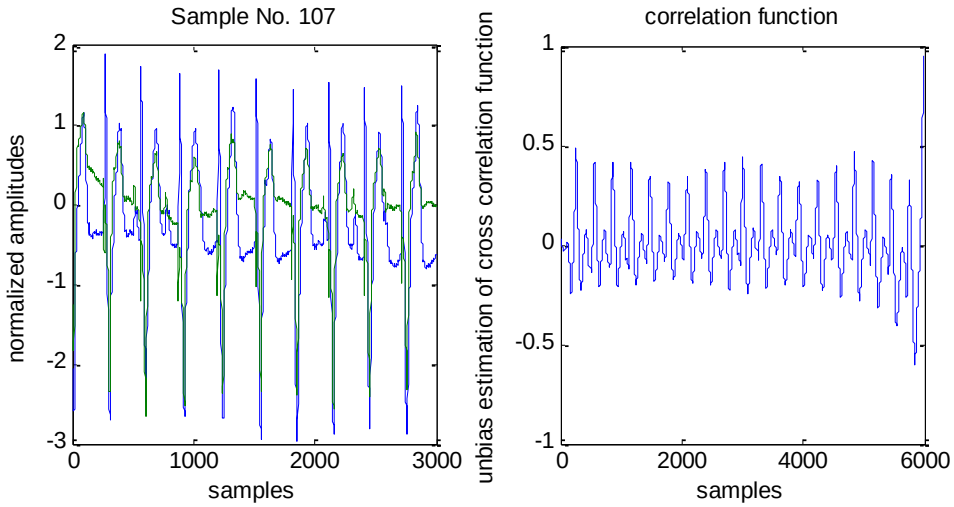

Figure 1-4 ECG signals of Sample No. 107 in MIH-BIH database and its unbiased estimate of cross correlation function.

1.2.3 Interference in ECG signals

In ECG signal processing, three kinds of interference are taken into consideration: power line interference, baseline wandering and high frequency noise.

(1) Power line interference: its frequency is power frequency and its harmonics. In MIT-BIH Arrhythmia Database, power frequency is 60Hz. Therefore, a 60Hz trap has to be designed to filter it. Its harmonics fall into high frequency noise.

(2) Baseline wandering: it is caused mainly by respiration and electrodes contact problems. The frequency is usually under 1Hz, and the amplitude is smaller than 15% of peak-to-peak value.

(3) High frequency noise: it is mainly consisting of EMG interference. The frequency range is wide and up to 10kHz. It can be assumed as zero mean

Gaussian noise with short burst of 50ms.

1.2.4 ECG processing methods

ECG processing in Telemedicine system includes: pre-processing, QRS complex detection, compressing and reconstructing. A typical ECG signal processing system is shown in Figure 1-5.

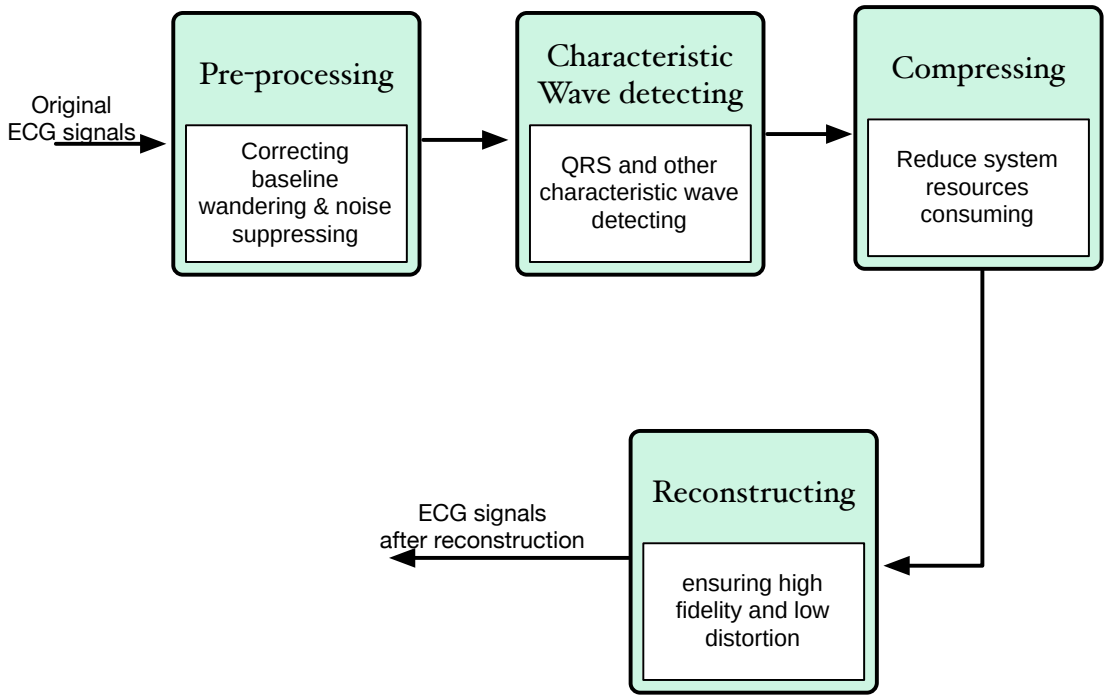

Figure 1-5 A typical ECG processing model in telemedicine system.

(1) ECG pre-processing: its main target is to filter power line interference, baseline wandering and high frequency noise. Early days, noise suppression methods are based on band-pass filters [14,15]. However, band-pass linear filter has constant cut-off frequency, which will cause severe distortion of ST segment and QRS complex. Also, it cannot adaptively follow time-variant characteristic of ECG signals. Adaptive filtering technologies are used to achieve noise suppression, and the core algorithms are based on least mean square (LMS) or iteractive least square (RLS) [16-19]. Difficulties in getting appropriate reference signals limit the application of this kind of methods. With the rapid development of Wavelet Analysis technology, it is widely used in ECG pre-processing field for its good performance in time-frequency characteristic [20,21]. But it is difficult to separate signal and baseline wandering or high frequency noise. This will cause poor performance in noise suppression or waveform distortion. Methods based on Mathematical Morphology (MM) are also adopted as an efficient nonlinear filter [22,23]. The basic idea is that correcting baseline wandering by linear segment element (SE) and high frequency noise suppression by triangular SE. However, the block effects caused by these SEs cannot meet the requirement of high fidelity.

(2) QRS Complex detection: it ensures dividing cardiac cycles correctly, which is

usually the first step before ECG compression, and has deep impact on utilization of correlations between cardiac cycles or different leads. There are many algorithms designed for QRS detection purpose. Before Wavelet techniques are adopted, the derivative and its related information of ECG are mainly used for QRS detection, as it can access the deep slops of the R waves [24,25]. Such kind of methods has the characteristics of less calculation and easy implementation, but with lower positive rate and noise immunity. QRS detection algorithms based on Wavelet Techniques have been popular since last decade. The main idea is that QRS Complex's analyzing components are different between levels, and by choosing the level with local maximum, it is easier to distinguish modulus maximum that are related to QRS Complexes [26,27]. However, for QRS Complex with steep slope, methods based on Wavelet techniques are likely to mix it with EMG or other noise, and result in leak detection. Mathematical morphology (MM) methods have been introduced into ECG signal processing field in 1980s [28]. Mostly, algorithms based on MM methods are adopted in the pre-procession for its robustness and self-adaptability in extracting morphological information [29]. And then QRS detection based on MM method was mainly implemented by triangle structure elements (SE) [30]. In 2002, Goutsias et al proposed nonlinear multi-resolution signal decomposition scheme based on MM [31], which can achieve good performance for ECG signals, especially in ECG pre-processing [32]. QRS complex detection can also be realized by multi-resolution decomposition scheme based on MM (MDMM) [33]. However, QRS complex detection methods based on MM distinguish steep R peaks more easily than gentle ones.

(3) ECG signal compression and reconstruction: in Telemedicine system, the compression algorithm should be simple to limit power consuming, and the reconstruction should be low distortion. It can be classified into three groups: first is direct compressing method, such as the turning point method, Fan algorithm, and amplitude zero phase encoding method and so on. This kind of method cannot achieve desired compressing ratio (CR) and limited distortion performance (PRD) [34]. Second is linear transforming domain methods, i.e., using Fourier, Walsh, Kahunen Loeve, discrete cosine, or wavelet transform to calculate ECG signals to another domain, then compression is done. The disadvantage is that the computing complexity is high at the transmitter and the balance between CR and PRD is hard to reach [35-39]. Third is parameter extraction method, after analyzing ECG signals, characteristic values and waveform patterns are extracted as compressing results, the reconstruction is to recover ECG signals by these characteristics. This kind of method is hard to implement in Telemedicine system for its computing complexity is very high [40,41].

1.3 Main Contributions and Framework of the Thesis

This thesis focuses on ECG processing methods in Telemedicine system, and the research methodology and contributions of the thesis are illustrated in Figure 1-6.

Chapter 1 introduces research backgrounds and the state of the art related work; chapter 2 does some research on ECG multi-resolution decomposition methods based on Wavelet and Hilbert and their use in ECG processing process; chapter 3 presents an efficient ECG pre-processing method based on lifting scheme constructing mathematical morphology multi-resolution decomposition (MMMD); chapter 4 proposes a mixed QRS complex detection method based on MMMD and Wavelet decomposition; chapter 5 puts forward an ECG compressing and reconstruction method based on compressive sensing (CS); and chapter 6 comes to the conclusion.

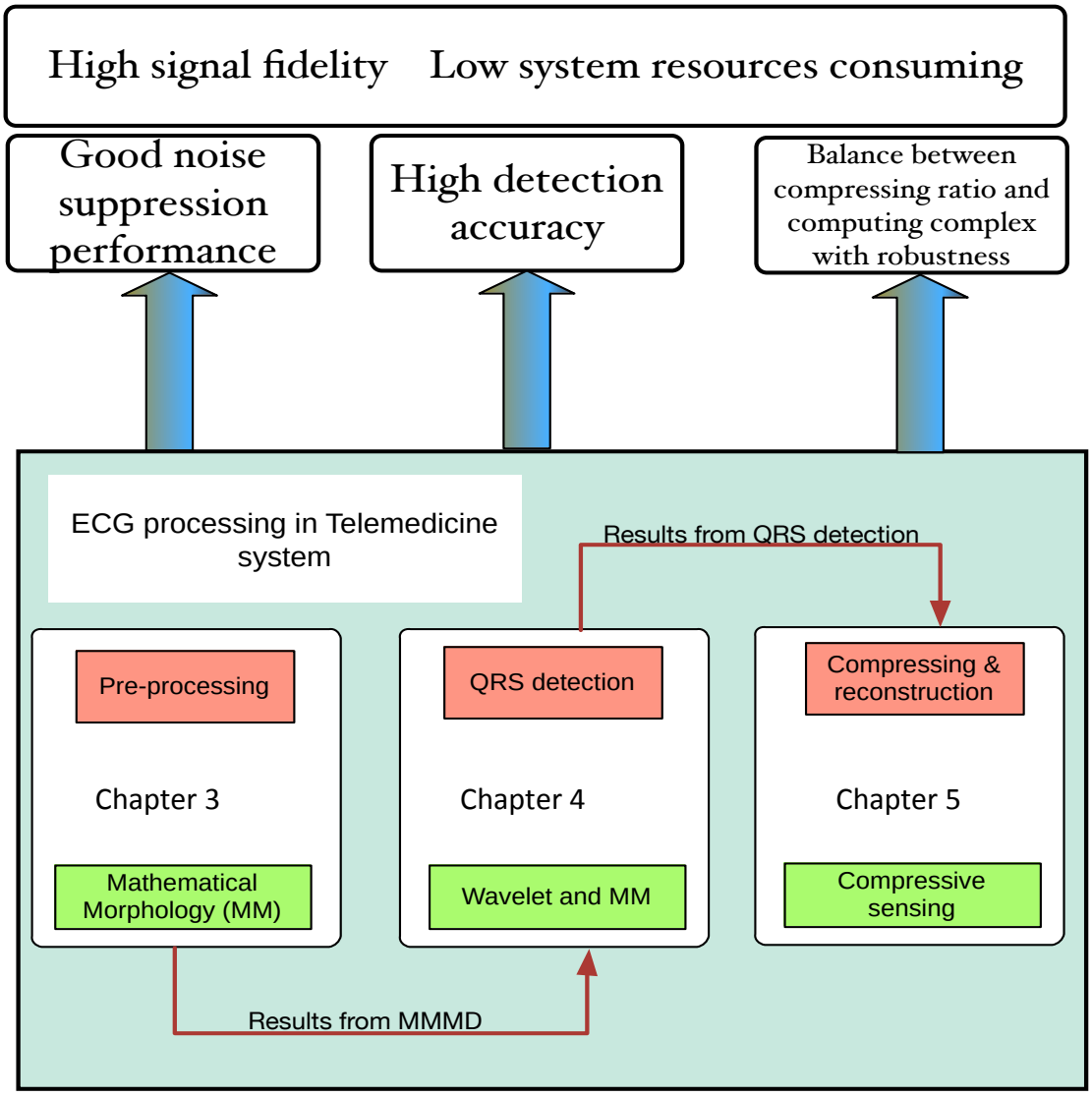

Fig.1-6 Research methodology and contributions of the thesis

Chapter 2 Wavelet Transform and Hilbert Transform for ECG signals

ECG signals record electrical activities of the heart, and are collected from long-term observation with high resolution. It is one of the most important vital signs helping medical staff to diagnose heart diseases and monitor patients. The typical ECG signals include P, QRS, T waveforms with interference such as EMG, baseline drift caused by respiration.

Modeling and analyzing ECG signal generation can be useful for acquaintance with characteristics of ECG waveform patterns; can provide standard testing database for evaluation of ECG processing methods; and it is also a time domain compression method itself.

Since 1990s, Wavelet Transform has become an efficient time domain analyzing and coding tool. Continuous Wavelet Transform (CWT) is an powerful analyzing tool for non-stationary signals, and is very suitable for analyzing high-resolution ECG signals; Discrete Wavelet Transform (DWT) and Wavelet Packet Transform (WPT) provide strong foundation for separations of signal components, which is the theory basis for ECG signal compression.

Hilbert transform is also useful in QRS complex detection. Furthermore, Hilbert-Huang transform can decompose the ECG signal by EMD method, which is more efficient in R peak detection. And Hilbert spectrum analysis has recently been adopted as a technique for measuring arrhythmia.

2.1 Wavelet Transform for ECG signals

2.1.1 Continuous Wavelet Transform

Wavelet Transform can be adopted in many aspects of ECG procession, such as denoising, QRS detection, RR interval division, compression and reconstruction.

Continuous Wavelet Transform (CWT) is a time-domain analyzing method. Comparing to typical STFT, it can receive the time-domain location with arbitrary sensitivity of high frequency component. Also, it is not limited to only use sinusoid analyzing functions, instead, arbitrary function meeting the following three mathematical criterions. The CWT for a continuous signal $x(t)$ can be defined as follows:

$$T(a,b) = \frac{1}{\sqrt{a}} \int_{-\infty}^{+\infty} x(t) \psi^*(\frac{t-b}{a}) dt \qquad (2\text{-}1)$$

where, $\psi^*(t)$ is the complex conjugate of analyzing wavelet function $\psi(t)$, a is scale factor, b is shift factor. $\psi(t)$ should meet the following three mathematical criterions:

(1) Energy limitation criterion

$$E = \int_{-\infty}^{+\infty} |\psi(t)|^2 dt < \infty \tag{2-2}$$

(2) If $\hat{\psi}(f)$ is Fourier transform (FT) of $\psi(t)$, i.e.,

$$\hat{\psi}(f) = \int_{-\infty}^{+\infty} \psi(t) e^{-i2\pi ft} dt \tag{2-3}$$

2-4 should be ensured,

$$C_g = \int_0^{+\infty} \frac{|\hat{\psi}(f)|^2}{f} df < \infty \tag{2-4}$$

this means that wavelet doesn't have zero order spectrum, i.e., $\hat{\psi}(0) = 0$, in other words, $\psi(t)$ should have volatility and zero mean.

(3) For complex wavelet, FT should be real numbers without negative frequency components. Information energy distribution at scale *a* and position *b* can be presented by two dimension wavelet energy density function:

$$E(a,b) = |T(a,b)|^2 \tag{2-5}$$

In practice, $\frac{|T(a,b)|^2}{C_g f_c}$ is also called as Wavelet Transform Spectrum, and f_c is the characteristic frequency of Wavelet function. The overall information energy can be denoted by the following equation:

$$E = \int_{-\infty}^{+\infty} x(t)^2 dt = \frac{1}{C_g} \int_{-\infty}^{+\infty} \int_0^{+\infty} |T(a,b)|^2 \frac{da}{a^2} db \tag{2-6}$$

Therefore, the energy distribution at scale *a* is determined as:

$$E(a) = \frac{1}{C_g} \int_{-\infty}^{+\infty} |T(a,b)|^2 \, db \tag{2-7}$$

Peak in $E(a)$ determines dominant scale in signal, we can change energy relied $E(a)$ to frequency relied $E_\omega(f)$. To achieve this target, *a* in scale should be transformed as characteristic frequency of wavelet:

$$f = \frac{f_c}{a} \tag{2-8}$$

where, mother wavelet ($a = 1, b = 0$) has characteristic frequency of f_c, and f is the frequency at arbitrary scale *a*.

Correspondingly, the original signal $x(t)$ can be reconstructed by Inverse Wavelet Transform, as is shown in 2-9:

$$x(t) = \frac{1}{C_g} \int_{-\infty}^{+\infty} \int_0^{+\infty} T(a,b) \psi_{a,b}(t) \frac{da}{a^2} db \tag{2-9}$$

Define two kinds of Maximum values that are often adopted in practice:

(1) Wavelet ridge:

$$\frac{d(|T(a,b)|^2/a)}{da} = 0 \tag{2-10}$$

It is used to determine instantaneous frequency and amplitude [42,43]. In addition, the amplitude of the ridge is used for calculating the amplitude of instantaneous frequency component.

(2) Wavelet Modulus Maximum:

$$\frac{d|T(a,b)|^2}{db} = 0 \tag{2-11}$$

It is used to locate and characterize singularity points such as inflection points [44,45].

Many kinds of QRS detection algorithms are based on Wavelet Modulus Maximum. Take Mexican Hat wavelet for example, wavelet function is defined as:

$$\psi(t) = (1 - t^2)e^{-\frac{t^2}{2}} \tag{2-12}$$

As is shown in Figure 2-1, Mexican Hat wavelet is second derivative of Gaussian function, and the Modulus Maximum curve of the CWT coefficients at singularity points is continuous. Relation between Scale factor a and characteristic frequency of mother wavelet can be described as:

$$f = \frac{f_c}{a \times f_s} \tag{2-13}$$

where f_c for Mexican Hat wavelet is $f_c = 0.251$, ECG signals in MIT-BIH database has sample rate $f_s = 360Hz$. The target frequency, i.e. the frequency of QRS complex in ECG signals $f = 15 \sim 18Hz$, then $a = 5,6$. Therefore, in QRS detection, a Mexico Hat wavelet at scale 5 or 6 can be adopted.

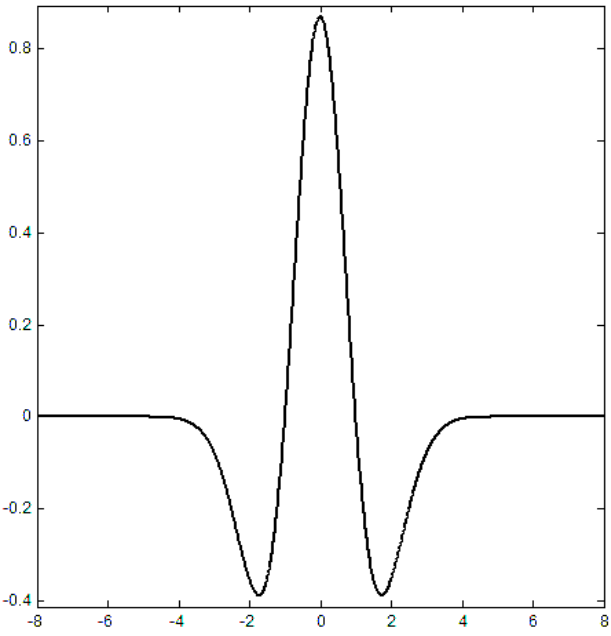

Figure 2-1 Mexican hat wavelet

We choose Sample No. 100 in MIT-BIH Arrhythmia Database, and do CWT by Mexican Hat wavelet at scale 6, as is shown in Figure 2-2. It is obvious that QRS complex can be identified from CWT results by using Modulus Maximum method.

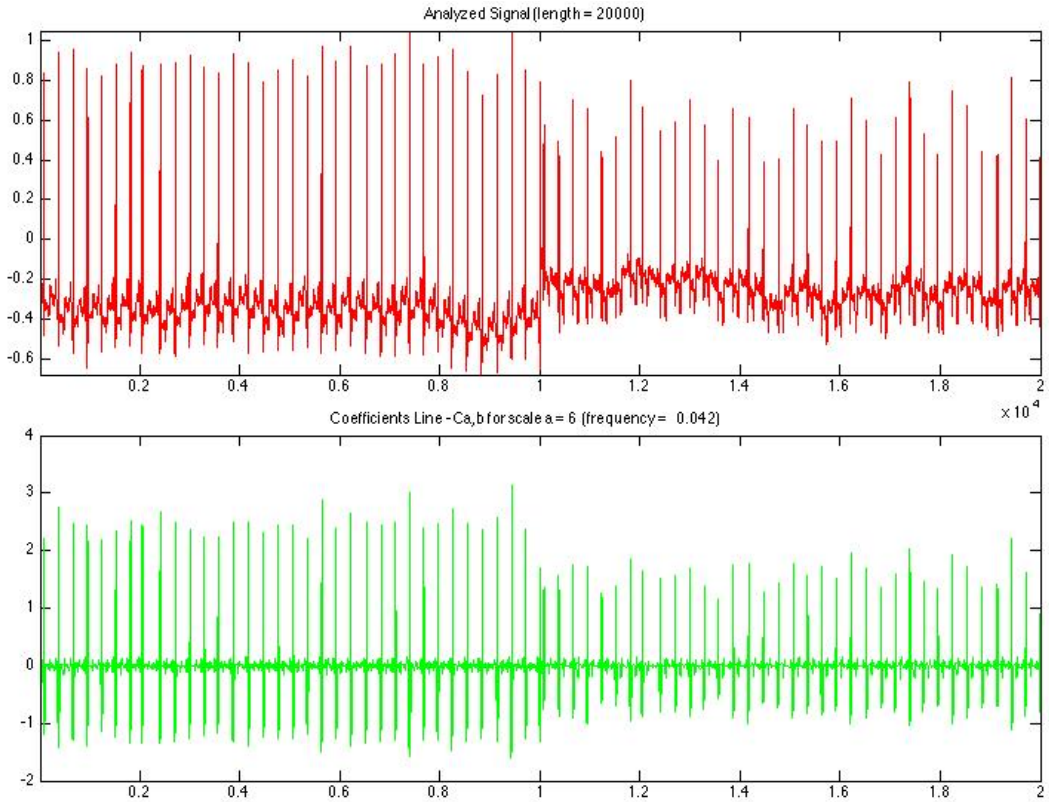

Figure 2-2 Sample No. 100 ECG signal in MIT-BIH database and its CWT by Mexican Hat wavelet at scale 6.

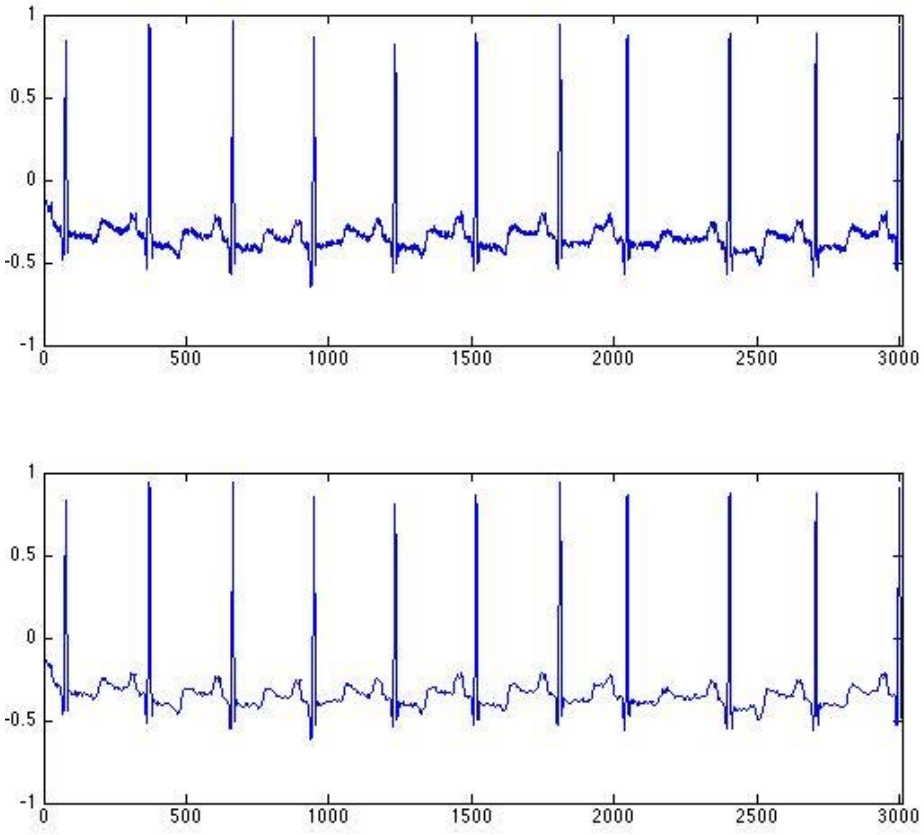

Figure 2-3 Denoising of Sample No. 100 ECG signal in MIT-BIH database by db9

Besides, ECG denoising can also be done by CWT. For instance, Sample No. 100 ECG signal in MIT-BIH database has been decomposed to by db9, and the high frequency noise is mostly contained in detail component level 1 and 2, Therefore, after thresholding, noise has been suppressed, as is shown in Figure 2-3, and for clarity, only first 3000 samples are presented. However, waveform distortion cannot be avoided, because useful information is included in each approximation and detail component at arbitrary level. How to control the distortion to an acceptable extent is the target for ECG denoising by wavelet transform.

2.1.2 Discrete Wavelet Transform

In Discrete Wavelet Transform (DWT), a and b are integer power of 2, and orthogonal wavelet basis are adopted to achieve zero redundancy. Actually, Transform integration is still continuous for DWT, except for defining in the grid at scale a and position b. In practice, to implement with fast calculation, a and b are usually discrete as follows:

$$a = {a_0}^m, b = n \times b_0 \times {a_0}^m \ (a_0 > 1, b_0 > 0, m, n \in Z) \tag{2-14}$$

And Wavelet Transform can be changed as 2-15:

$$\psi_{m,n}(t) = \frac{1}{\sqrt{{a_0}^m}} \psi(\frac{t - n \times b_0 {a_0}^m}{{a_0}^m}) \tag{2-15}$$

Usually, $a_0 = 2, b_0 = 1$ are chosen to construct dyadic grid, as is shown in 2-16:

$$\psi_{m,n}(t) = 2^{-\frac{m}{2}} \psi(2^{-m}t - n) \tag{2-16}$$

The discrete dyadic grid wavelet meets orthogonal normalization, which means:

$$\int_{-\infty}^{+\infty} \psi_{m,n}(t) \psi_{m',n'}(t) dt = \begin{cases} 1 \ if \ m = m' \ and \ n = n' \\ 0 \qquad otherwise \end{cases} \tag{2-17}$$

i.e., wavelet coefficients $T_{m,n}$ contain no redundancy and can complete reconstruct the original signal.

$$T_{m,n} = \int_{-\infty}^{+\infty} x(t) \, \psi_{m,n}(t) dt \tag{2-18}$$

Normalized orthogonal dyadic wavelet is determined by scaling function and scaling equation. And scaling function is associated with smoothness of signal, and has the same form with wavelet function:

$$\phi_{m,n}(t) = 2^{-\frac{m}{2}} \phi(2^{-m}t - n) \tag{2-19}$$

$$\int_{-\infty}^{+\infty} \phi_{0,0}(t) \, dt = 1 \tag{2-20}$$

$\phi_{0,0}(t) = \phi(t)$ can be called as father wavelet or father scaling function. Approximation coefficients are convolution of scaling function and the signal:

$$S_{m,n} = \int_{-\infty}^{+\infty} x(t) \phi_{m,n}(t) dt \tag{2-21}$$

Continuous approximation to signal can be obtained by sum up sequence consisting of products of scaling function and approximation coefficients:

$$x_m(t) = \sum_{n=-\infty}^{+\infty} S_{m,n}\, \phi_{m,n}(t) \quad (2\text{-}22)$$

when $m \to -\infty$, $x_m(t)$ converges to $x(t)$. And $x(t)$ can be denoted by approximation coefficients and detail coefficients:

$$x(t) = \sum_{n=-\infty}^{+\infty} S_{m_0,n}\, \phi_{m_0,n}(t) + \sum_{m=-\infty}^{m_0} \sum_{n=-\infty}^{+\infty} T_{m,n} \psi_{m,n}(t) \quad (2\text{-}23)$$

It is obvious that the original continuous signal can be denoted as sum of approximation signal at scale m_0 and all detail components from scale m_0 to negative infinite. Detail component at scale *m* is defined as:

$$d_m(t) = \sum_{n=-\infty}^{+\infty} T_{m,n} \psi_{m,n}(t) \quad (2\text{-}24)$$

Therefore, 2-22 can be changed as follows:

$$x(t) = x_{m_0}(t) + \sum_{n=-\infty}^{+\infty} d_m(t) \quad (2\text{-}25)$$

And

$$x_{m-1}(t) = x_m(t) + d_m(t) \quad (2\text{-}26)$$

Which means that if we sum up Detail component and Approximation component at arbitrary scale, we will have Approximation component at one scale higher. A multi-resolution decomposition is formed.

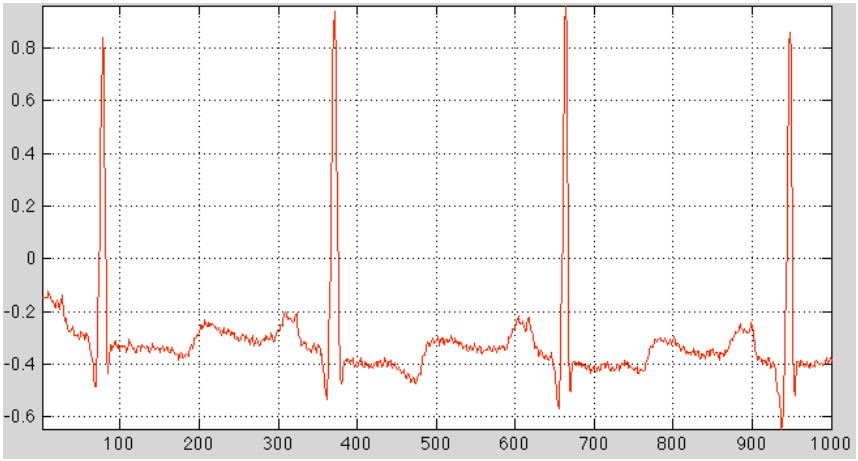

(a) The original ECG samples of the first 1000 samples of Sample No. 100 in MIT-BIH Arrhythmia Database

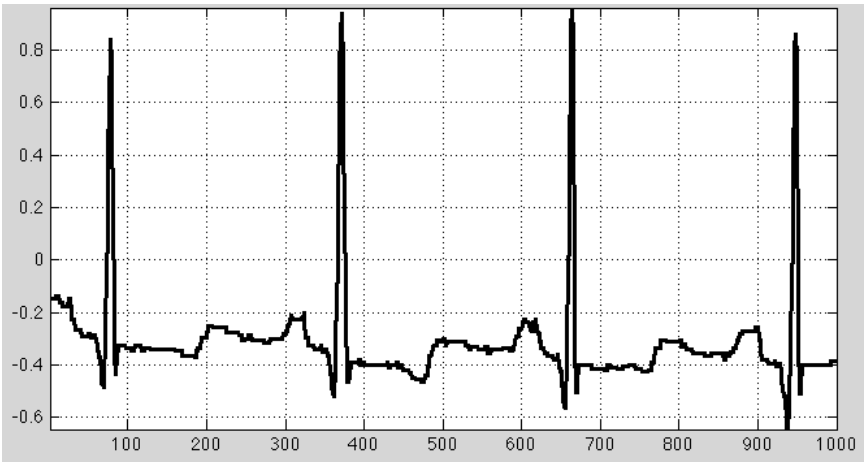

(b) Compressed ECG signal at CS=4.70

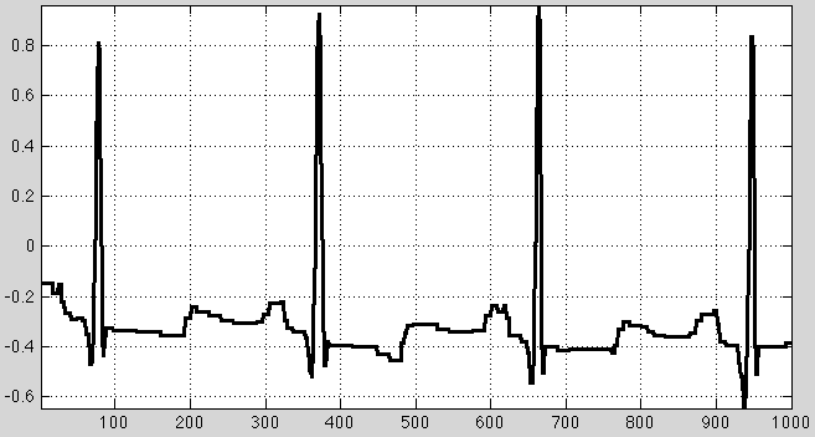

(c) Compressed ECG signal at CS=7.16

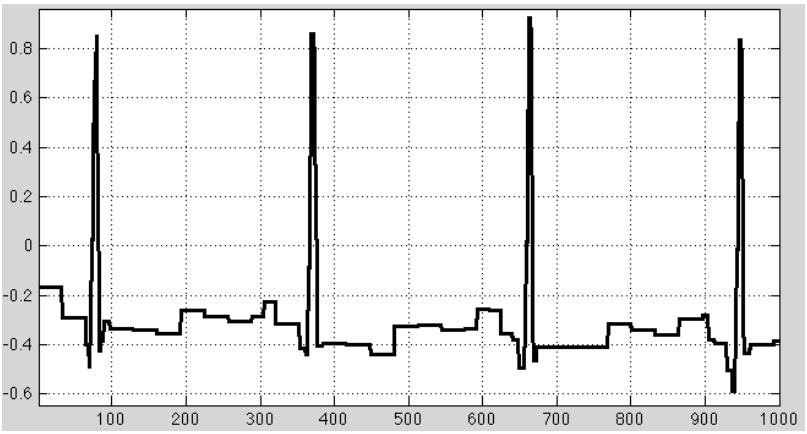

(d) Compressed ECG signal at CS=12.69

Figure 2-4 Sample No. 100 in MIT-BIH Arrhythmia Database (the first 1000 samples) and compression results at CS=4.70, 7.16, and 12.69

In practice, DWT are often used as a powerful tool for the encoding of data required for compression systems.

ECG signals are collected over long-term and at high resolution (250Hz~1000Hz), and create huge amount of data when transmission and storage. Take Sample No. 100 in MIT-BIH Arrhythmia Database for example, db1 wavelet is used for compression. The compression results are illustrated in Figure 2-3. For clarity, the first 1000 samples are shown at compression ratio (CS) of 4.70, 7.16 and 12.69

It is obvious that when CS is bigger, the waveform distortion becomes bigger too. And when CS=12.69, the distortion is unacceptable visually. In practice, to improve compression performance, DWT is often combined with embedded algorithms such as Embedded Zerotree Wavelet (EZW), Set Partitioning In Hierarchical Trees (SPIHT), and so on. We will discuss them in detail in Chapter 5.

2.1.3 Wavelet Function Selection for ECG Signal Processing

Wavelet Transform is related to many aspects in ECG processing, such as denoising, QRS complex detection, RR interval division, local abnormal waveform detection, compression and reconstruction, and so on. However, not all the wavelet functions

are appropriate for ECG processing. The characteristics such as orthogonality, Lipschitz regularity, vanishing moments, compact support, symmetry and so on, should be considered with different needs. For instant, in QRS complex detection, there are high requirements for compact support and vanishing moments; while in ECG signal compression, vanishing moments and Lipschitz regularity are the key consideration.

2.2 Hilbert Transform for ECG signals

2.2.1 Hilbert Transform and Hilbert Space

According to linear calculation and length concept in $\mathbf{R}^n$, as well as important characteristics such as angle and orthogonality between vectors, Inner Product Space and Hilbert Space are introduced.

Assume K is number field (real or complex), and U is linear space over K For arbitrary $x, y \in U$, there's unique corresponding number $(x, y) \in K$ meeting the following conditions:

(1) $(\alpha x, y) = \alpha(x, y) \qquad \alpha \in K$

(2) $(x + z, y) = (x, y) + (z, y) \qquad z \in U$

(3) $(x, y) = \overline{(y, x)}$

(4) $(x, y) \geq 0 \; and \; (x, x) = 0 \Leftrightarrow x = 0$

Then, (x, y) is the inner product of $x \; and \; y$, and U is the **Inner Product Space**. There are four useful properties in the Inner Product Space:

(1) In the Inner Product Space, "norm" can be induced by the inner product:

$$\|x\| = \sqrt{(x, x)} \tag{2-27}$$

And it meets the four axioms above.

(2) In the Inner Product Space, the norm satisfies Parallelogram formula:

$$\|x + y\|^2 + \|x - y\|^2 = 2(\|x\|^2 + \|y\|^2) \tag{2-28}$$

(3) If the norms in normed linear space meet Parallelogram formula, the inner product can be denoted by norm (in real number space):

$$(x, y) = \frac{1}{4}(\|x + y\|^2 - \|x - y\|^2) \tag{2-29}$$

(4) In the Inner Product Space, the inner product (x, y) is continuous with x and y, i.e. when $x \longrightarrow x_n, \; y \longrightarrow y_n, \; (x, y) \longrightarrow (x_n, y_n)$.

If norm $\|x\| = \sqrt{(x, x)}$ in the Inner Product Space U is complete, U is called a **Hilbert space**.

For a real-time function $x(t)$, the Hilbert transform is presented as [46]:

$$X(t) = H[x(t)] = \frac{1}{\pi}\int_{-\infty}^{+\infty} \frac{x(\tau)}{t-\tau} d\tau = (\frac{1}{\pi t}) * x(t) \tag{2-30}$$

Rewrite 2-30 by applying Fourier Transform:

$$F\{X(t)\} = \frac{1}{\pi} F\left\{\frac{1}{t}\right\} F\{x(t)\} \quad (2\text{-}31)$$

as $F\left\{\frac{1}{t}\right\} = -j \operatorname{sgn} f$, we have

$$F\{X(t)\} = -j \operatorname{sgn} f \; F\{x(t)\} \quad (2\text{-}32)$$

Therefore, we can conclude that the signal $x(t)$ and its Hilbert transform $X(t)$ are orthogonal, and $X(t)$ is the harmonic conjugate of the original signal $x(t)$.

The correlation between $X(t)$ and $x(t)$ is strong, and they together formulate a powerful analytic signal, which can be denoted by amplitude and phase, where the derivative of phase can be identified as the instantaneous frequency.

$$y(t) = x(t) + jX(t) \quad (2\text{-}32)$$

The envelope $B(t)$ of $y(t)$ is

$$B(t) = \sqrt{X(t)^2 + x(t)^2} \quad (2\text{-}33)$$

and its instantaneous phase angle in the complex plane can be defined by

$$\phi(t) = \arctan\left(\frac{X(t)}{x(t)}\right) \quad (2\text{-}34)$$

As is shown in Figure It is obvious that $B(t)$ has the same slope and magnitude of the original signal $x(t)$ where $X(t) = 0$, i.e., at or near its local maximum. It is very useful characteristic for designing R peak detection method in ECG processing.

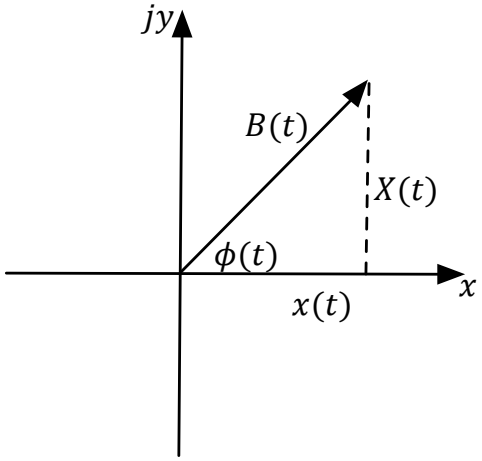

Figure 2-5 Complex representation of the envelope [47]

The main idea of R peak detection based on Hilbert Transform can be described as: first, do first-order difference calculation on the ECG signal; second, calculate Hilbert Transform to the derivation; third, decide the zero-crossing points between two positive and negative peaks, i.e., the R peaks; finally, confirm the R peak by using the envelop.

We also take Sample No. 100 in MIT-BIH Arrhythmia Database for example, as is shown in Figure 2-6, (b) presents the first differential of the ECG waveform, in which the zero crossing points between positive peaks and negative peaks are corresponding to R peaks, and it is obvious the Hilbert transform and the envelop of the first order deviation of ECG signals can both used for R peak detection, especially

the envelop.

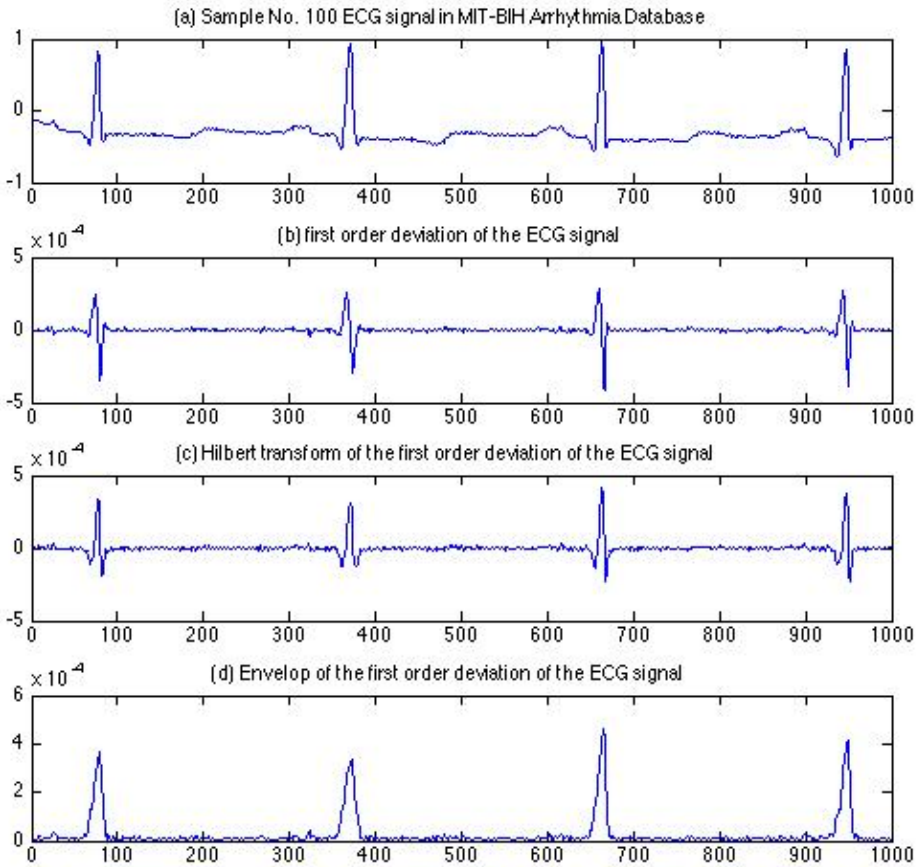

Figure 2-6 the Hilbert transform and the envelop of the first order deviation of Sample No. 100 ECG signal in MIT-BIH Arrhythmia Database

2.3 Hilbert-Huang transform for ECG signals

2.3.1 Huang transform

Hilbert-Huang Transform (HHT) method [48,49], which includes Huang transform and Hilbert spectrum, is an efficient method for analysis of non-stationary signal. In HHT, different intrinsic mode function (IMF) can be separated by using empirical mode decomposition (EMD). Different from Fourier spectrum, Hilbert spectrum is a three-dimension figure of time, frequency and amplitude, which points out the signal change in both time and frequency domain. Therefore, it is very appropriate for analyze ECG signals.

The key to Huang transform is EMD, which considers that any complex time sequence consists of several different, simple, non-sinusoidal functional empirical mode functions. Therefore, the complex time sequence can be decomposed from high frequency to low frequency as intrinsic mode functions, which is also called as basic time sequence. The intrinsic mode function should meet the following two

conditions:

(1) For all the time sequence, the difference between the number of the extreme values and zero crossing points equals to one or zero.

(2) At any point, the mean value of the maximum envelop and the minimum envelop is zero.

In practice, assuming time domain signal $x(t)$,

(1) using cubic spline function to connect the maximum and the minimum, acquire maximum envelop and minimum envelop respectively.

(2) Then connect the mean value of maximum envelop and minimum envelop and get a mean value line m_1. Then we have $h_1(t) = x(t) - m_1(t)$. If $h_1(t)$ meets the EM function condition, $h_1(t)$ is the first level intrinsic EM function. Otherwise, $h_1(t)$ is assumed as new time domain signal, and repeat the aforementioned process, we have $h_{11}(t) = h_1(t) - m_{11}(t)$.

(3) Repeat the method (1) and (2) k times, until $h_{1k}(t)$ meeting the EM function condition, we have $c_1(t) = h_{1k}(t)$ denoting the first level intrinsic mode function, containing the high-frequency component of the signal $x(t)$.

(4) Define the residue $r_1(t) = X(t) - c_1(t)$, repeat (1) to (3), we have $c_j(t)$ and $r_j(t) = r_{j-1}(t) - c_j(t)$, $j = 2,3, \dots, n$.

(5) When one of the following two conditions is satisfied, the EMD is over: $c_n(t)$ or $r_n(t)$ is smaller than pre-determined error; $r_n(t)$ is a monotone function, and no more intrinsic mode function can be extracted. And the original signal $X(t)$ can be denoted as:

$$x(t) = \sum_{j=1}^{n} c_j(t) + r_n(t) \tag{2-35}$$

Figure 2-7 illustrated the EMD of Sample No. 100 of MIT-BIH Arrhythmia Database. We can see that the frequency of the EMD component decreases level by level, and for this sample, the EMD is up to 8 level IMF, and the last subplot is the residue.

Comparing with Fourier transform, whose transform result is series of waveforms with the same amplitude and frequency, Huang transform result is series of intrinsic mode functions with different frequency components and amplitudes. Therefore, Huang transform has more general meaning than Fourier transform. And the EMD result of the ECG signal can be used as identification of people.

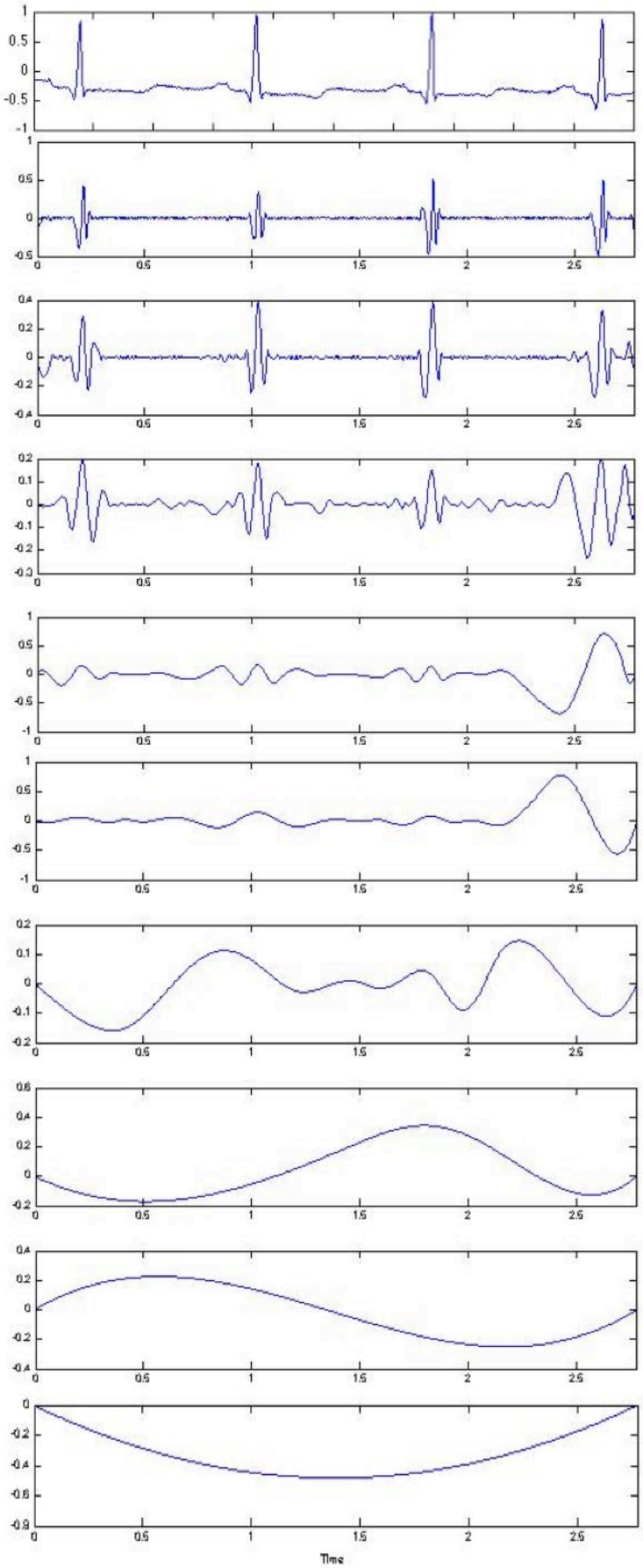

Figure 2-7 EMD of Sample No. 100 of MIT-BIH Arrhythmia Database

2.3.2 Hilbert spectrum analysis

According to 2-32 to 2-34, which are rewrite as follows:

$$y(t) = x(t) + jX(t) \tag{2-36}$$

$$B(t) = \sqrt{X(t)^2 + x(t)^2} \tag{2-37}$$

$$\phi(t) = \arctan\left(\frac{X(t)}{x(t)}\right) \tag{2-38}$$

And $y(t)$ can be denoted as:

$$y(t) = B(t)\exp[t\phi(t)] \tag{2-39}$$

Then define the instantaneous frequency as $\omega(t) = \mathrm{d}\,\phi(t)/\mathrm{d}t$. The Hilbert transform of the IMF of $x(t)$ is:

$$H(t) = \sum_{j=1}^{n} B_j(t) exp[\mathrm{i}\int \omega_j(t)\mathrm{d}t] \tag{2-40}$$

Hilbert spectrum is defined as the real part of 2-40, and is denoted as $H(\omega, t)$ for it's a function of both time and frequency.

In medical field, there are many applications of Hilbert-Huang Transform and its spectrum. Harvard Medical School has adopted them to measure arrhythmia. And they also can be used to test blood pressure change. Figure 2-8 illustrated the Hilbert-Huang spectrum of Sample No. 100 of MIT-BIH Arrhythmia Database.

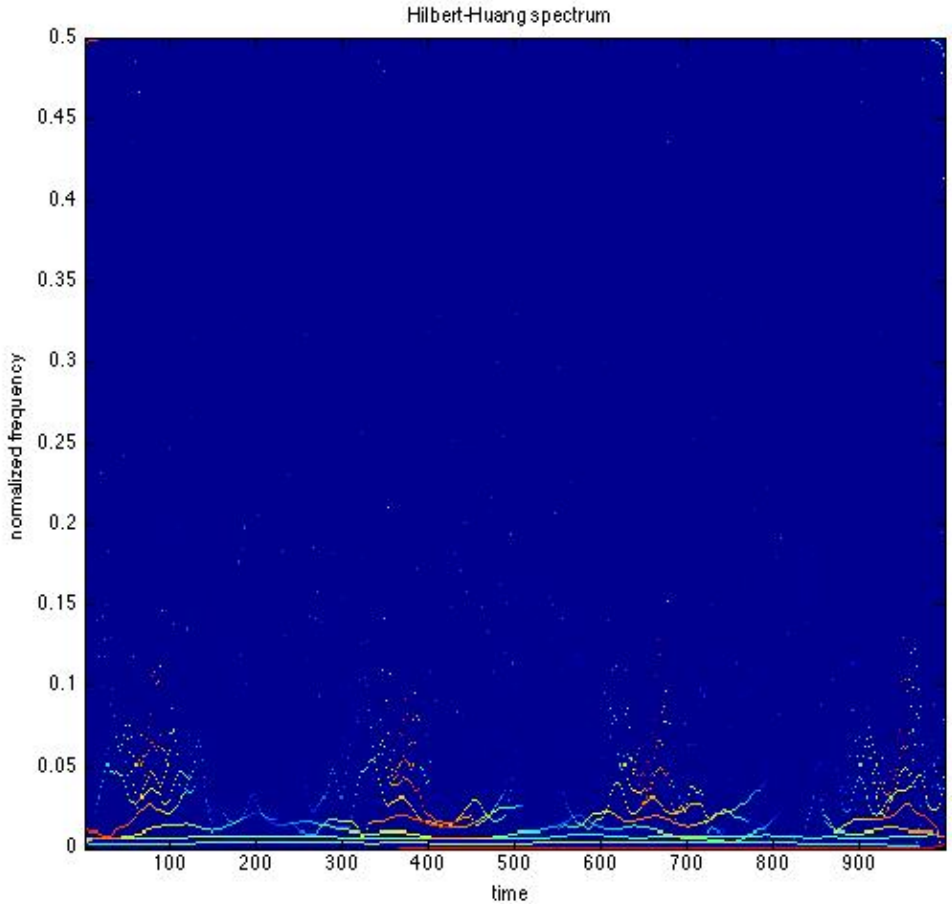

Figure 2-8 the Hilbert-Huang spectrum of Sample No. 100 of MIT-BIH Arrhythmia Database

Chapter 3 ECG Preprocessing Methods based on Lifting Scheme Constructing MMMD

Mathematical Morphology method has robustness and self-adaption in extraction of shape information, and can be implemented by simple and quick set operations. Therefore, it is adapted widely in signal and image processing. By modification of ECG signal local geometric characteristic, mathematical morphology can realize noise suppression and baseline correction and is proper for ECG pre-processing. However, the selection of structure elements has significant impact on filtering high frequency noise and will cause signal distortion because of the high frequency fluctuation.

In this chapter, a novel pre-processing method based on lifting scheme constructing multi-resolution morphological decomposition is proposed. The algorithm adopts cubic spline interpolation for design of predicting and updating operators to effectively reduce the block effect. By simulation to standard test ECG signals and comparison with other pre-processing algorithms based on wavelet transform and multi-resolution morphological decomposition, it is concluded that this algorithm can achieve good performance in mean absolute differences, max difference and root mean square error. The waveform distortion is visually acceptable and the computing complexity is not high.

3.1 Basic Operation in Mathematical Morphology

Generally, mathematical morphology method (MM) is designed for binary images or gray images, which can be considered as increasing gray information based on binary images. From set theory point of view, MM filtering for can be explained as: assuming the binary image as the set of foreground pixels (values equal to 1), and belong to Z^2, let the set of structure element (SE) be a probe moving in the image and searching the set of central position SEs which meet some criterion, and acquire specific information of shape of the image. Therefore, the set operation can be used directly in the set of binary image. Besides basic operation (intersection, union and so on), mapping and shifting are also defined for set. The mapping and shifting set A can be denoted as:

$$\hat{A} = \{w | w = -a, a \in A\} \tag{3-1}$$

$$(A)_z = \{c | c = a + z, a \in A\} \tag{3-2}$$

Dilation and erosion are basic operators for image processing. There are usually three kinds of combination of dilation and erosion: Open, Close and Hit transform.

3.1.1 Dilation and Erosion

In binary image processing, dilation denotes “lengthen” and “thicken” operation.

A and B is sets in Z^2, A dilated by B is defined as the original set of the overlap part between A and B after mapping and shifting, as 3-3:

$$\begin{aligned} A \oplus B &= \{z \mid (\hat{B})_z \cap A \neq \varnothing\} \\ &= \{z \mid (\hat{B})_z \cap A \subseteq A\} \end{aligned} \tag{3-3}$$

Dilation is similar with convolution in arithmetic operation. They are both let one element (set) mapping relative to the origin and shifting by the other element (set).

In binary image processing, erosion denotes "shorten" and "thin" operation. A and B is sets in Z^2, A eroded by B is defined as, the origin position set where after shifting, set B is not intersectional with background A:

$$\begin{aligned} A \Theta B &= \{z \mid (B)_z \cap A^c = \varnothing\} \\ &= \{z \mid (B)_z \subseteq A\} \end{aligned} \tag{3-4}$$

An simple application of erosion is deleting the detail component that is not related in binary images.

Dilation and Erosion is the dual of the complement and inverse of the set, i.e.,

$$(A \Theta B)^c = A^c \oplus \hat{B} \tag{3-5}$$

There are several useful properties for algorithm designing in image processing and analyzing. For example, associative law and the distributive law can be used for improve implementation speed of the algorithm, i.e., they can make complicated structure element decomposed as union of several simple SE and by using simple SE, image is manipulated. The important properties of Dilation and Erosion is described as follows:

(1) Commutative law:

$$A \oplus B = B \oplus A \tag{3-6}$$

(2) Associative law:

$$A \oplus (B \oplus C) = (A \oplus B) \oplus C \tag{3-7}$$

(3) Conservation law:

$$\begin{aligned} A \subseteq B &\Rightarrow A \oplus C \subseteq B \oplus C \\ A \subseteq B &\Rightarrow A \Theta C \subseteq B \Theta C \end{aligned} \tag{3-8}$$

(4) distributive law:

$$\begin{aligned} (A \cup B) \oplus C &= (A \oplus C) \cup (B \oplus C) \\ A \oplus (B \cup C) &= (A \oplus B) \cup (A \oplus C) \\ A \Theta (B \cup C) &= (A \Theta B) \cap (A \Theta C) \\ (B \cap C) \Theta A &= (B \Theta A) \cap (C \Theta A) \end{aligned} \tag{3-9}$$

Dilation and erosion are basic operators for image processing. In practice, we are often adopt combinations of dilation and erosion.

3.1.2 Open, Close and Hit Operation

(1) Open Operation: Assuming A is the original image, B is SE, as is shown in 3-10, A being open operated by B is defined as the result of A is eroded by B is dilated by B. Geometrically, A being open operated by B means the union of shifting B's complete mapping in A.

$$\begin{aligned} A \circ B &= (A \Theta B) \oplus B \\ &= \cup\{(B)_z \mid (B)_z \subseteq A\} \end{aligned} \tag{3-10}$$

Open operation can completely delete object area not include SE. For one-dimension signal, sharp peaks can be filtered.

(2) Close Operation: Assuming A is the original image, B is SE, as is shown in 3-11, A being close operated by B is defined as the result of A is dilated by B is eroded by B. Geometrically, A being close operated by B means the union of B's shifting that is not overlapped A.

$$\begin{aligned} A \bullet B &= (A \oplus B) \Theta B \\ &= \cup\{(B)_z \mid (B)_z \subseteq A^c\} \end{aligned} \tag{3-11}$$

Close operation can fill the holes that are smaller than B. For one-dimension signal, sharp troughs can be filtered.

(3) Hit operation: Assuming A is the original image, B is SE pair $B = (B_1, B_2)$, as is shown in 3-12, A being Hit operated by B is defined as the combination that complete mapping of B_1 and not mapping of B_2.

$$A \otimes B = (A \Theta B_1) \cap (A^c \Theta B_2) \tag{3-12}$$

This operation can recognize the specific shape of the image, such as isolated points and endpoints of the segments.

3.1.3 ECG processing by MM filtering

MM operations aforementioned are defined for binary images. ECG signals can be manipulated as binary images or one-dimension signals. In this paper, ECG signals are assumed as one-dimension signals, and MM operations are defined as follows:

Define ECG signal as $f(n), n = 0,1, \dots, N-1$, symmetrical SE as $B(m), m = 0,1,2, \dots, M-1$. In practice, we usually choose SE as segments or Isosceles Triangle. And erosion and dilation of ECG signal can be denoted as following, and open and close operations are the same as in binary images.

$$(f \Theta B)(n) = \min\{f(n+m) - B(m)\} \quad m \epsilon 0,1, \dots, M-1 \tag{3-13}$$

$$(f \oplus B)(n) = \max\{f(n-m) + B(m)\} \quad m \epsilon 0,1, \dots, M-1 \tag{3-14}$$

Opening operator is $f \circ B = (f \Theta B) \oplus B$ while closing operator is $f \cdot B = (f \oplus B) \Theta B$.

Using MM filter to ECG signals for baseline correction and noise suppression, we often adopt combination of several different SE and symmetrical manipulation. For example, line SEs are usually used for baseline correction and triangle SE are often chosen for high frequency noise suppression. The shape design of SE (often denoted by matrix) are relied on the shape specifics of reversed ECG characteristic waveforms; while the length of SE are determined by the lasting time of the characteristic waveform and sampling rate. For example, for ECG signals in MIT-BIH database with the sample rate of 360Hz, according to research to the lasting time of ECG characteristic waveforms, select line SE with the length of 78 for baseline correction. Take Sample 222 with obvious baseline drift as example, the erosion, dilation, open and close operations are illustrated in Figure 3-1, and it is obvious that the erosion operation decides the basic morphology of the baseline, and dilation operation is interested in peak extraction. Therefore, open operation is responded to low pass filter for ECG signals, and the close operation is high pass filter correspondingly.

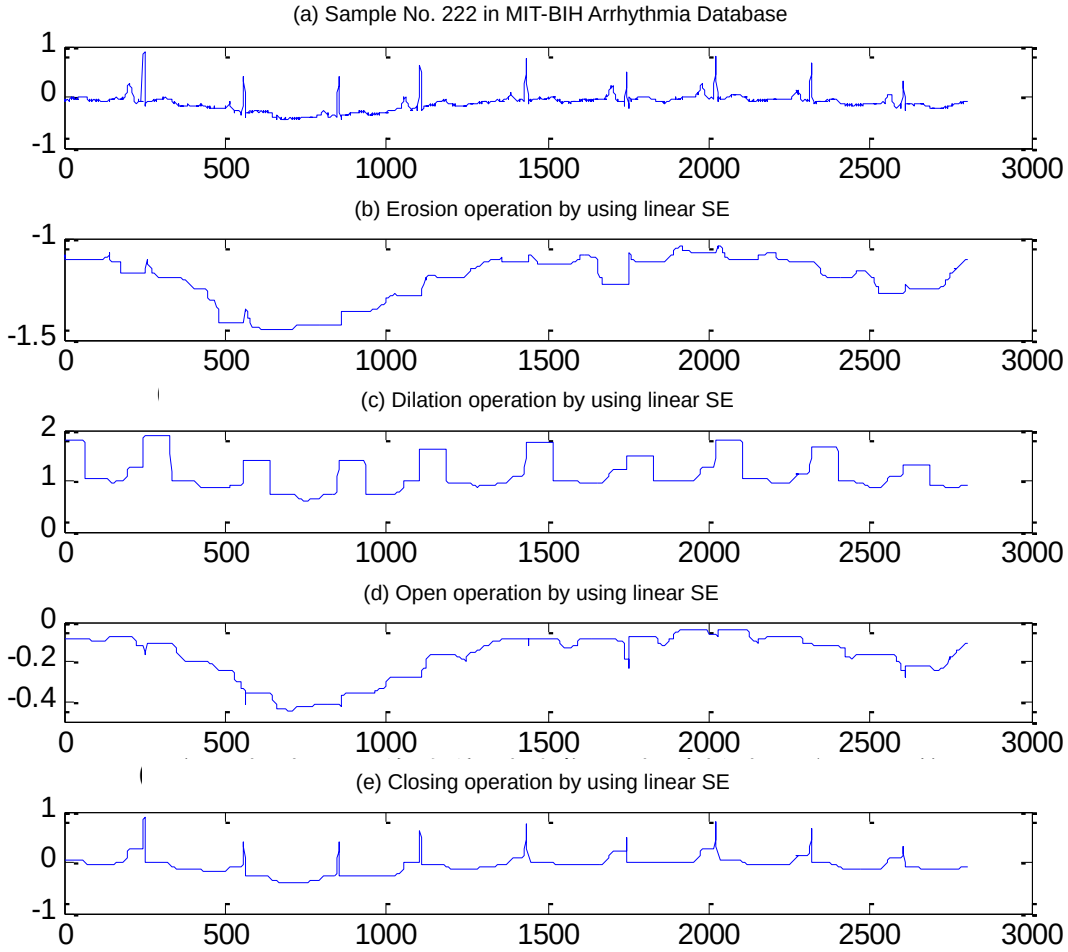

Figure 3-1 Erosion, Dilation, open and close operations using a line SE for Sample 222 in MIT-BIH database.

One kind of basic baseline correction and noise suppression method is described as follows [29] and is called as MF method. Baseline correction is conducted by the following morphological filter described as:

$$f_b = f_o \circ B_o \cdot B_c \qquad B_o = 0.2F_s \qquad B_c = 1.5B_o = 0.3F_s = 360Hz \tag{3-15}$$

noise suppression is done by 3-16:

$$f = \frac{1}{2}[(f - f_b) \circ B \bullet B + (f - f_b) \bullet B \circ B] \tag{3-16}$$

where f_0 is the original ECG signal, f_b is the detected baseline, f is the ECG signal after baseline correction. B_0 is used to remove the signal peaks while B_c is used to remove the signal troughs. Therefore, the length of B_c is longer than that of B_0, and they are both line SE. the length depend on the duration of characteristic waveforms in ECG signals T_ω and sampling rate F_s. Commonly, $T_\omega < 0.2s$, therefore, let $B_o = 0.2F_s$ and $B_c = 1.5B_o = 0.3F_s$. And $B = (0\ 1\ 5\ 1\ 0)$ is triangle SE for noise suppression.

In reference [30], noise suppression method is improved and is called as MMF method: SE pair $B_{pair} = (B_1, B_2)$ is adopted, B_1, B_2 have the same length but $B_1 \neq B_2$. $B_1 = (0\ 1\ 5\ 1\ 0)$ and B_2 is line SE. The filter can be described as:

$$\begin{aligned} f &= \frac{1}{2}(f_{bc} \bullet B_{pair} + f_{bc} \circ B_{pair}) \\ &= \frac{1}{2}(f_{bc} \oplus B_1 \Theta B_2 + f_{bc} \Theta B_1 \oplus B_2) \end{aligned} \tag{3-17}$$

where f_{bc} is ECG signals after baseline correction by 3-15.

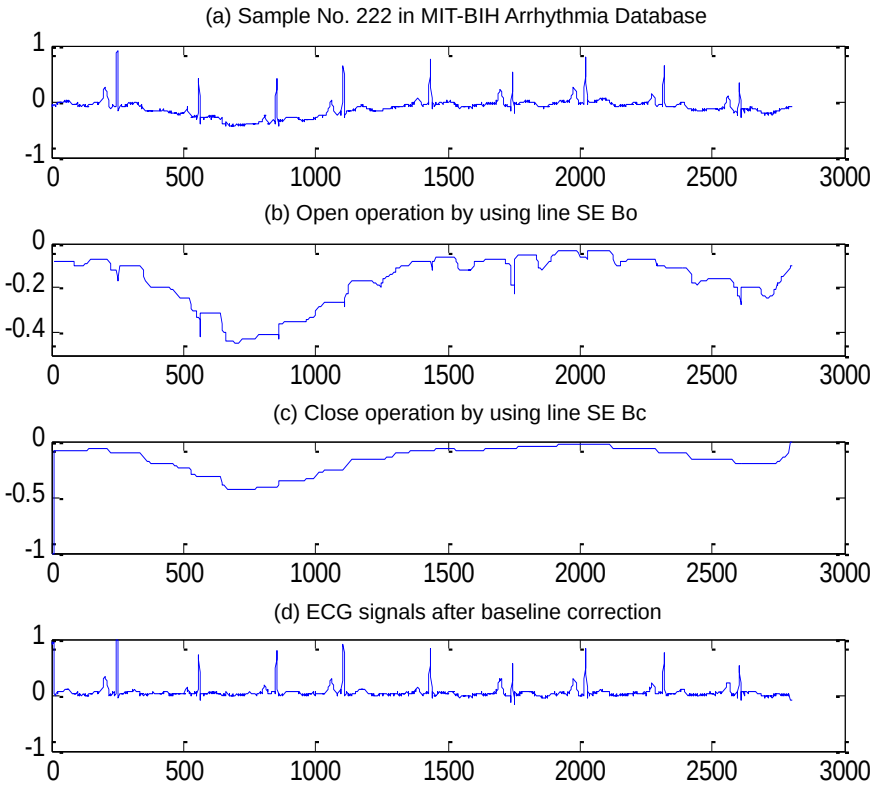

Figure 3-2 Using morphological operators with, $B_o = 72$, and $B_c = 108$ to correct the baseline wander of sample 222.

We tested these two typical baseline correction methods on Sample No. 222, and as is shown in Figure 3-2, after baseline correction, ECG signals are almost on the same horizontal line. However, from Figure 3-2(c), the baseline component by line SE

has obvious block effect, and this will cause waveform distortion in the ECG signals.

And after baseline correction, the noise suppression method of MF and MMF are also tested for Sample number 222. The simulation results are illustrated in Figure 3-3. These two methods both can filter the noise in good performance, and there's not significant difference between them, we need to design simulation for quantitative analysis.

3.2 simulation design for quantitative analysis

Three performance evaluation criterions had been chosen as well as considering computing complexity. Let $s(i)$ be the input signal, $\hat{s}(i)$ be the signal after filtering. N was the number of samples, and R was peak-to-peak value of the input signal. The three criterions were given by

(1) Mean absolute difference (MAD)

$$MAD = \frac{1}{RN}\|s(i) - \hat{s}(i)\|_1 = \frac{1}{R}\frac{1}{N}\sum_{i=1}^{N}|s(i) - \hat{s}(i)| \tag{3-18}$$

(2) Maximum difference (MaxD)

$$MaxD = \frac{1}{R}\|s(i) - \hat{s}(i)\|_\infty = \frac{1}{R}\underbrace{max}_{i=1,\dots,N}|s(i) - \hat{s}(i)| \tag{3-19}$$

(3) Root mean square error (RMSE)

$$RMSE = \frac{1}{R\sqrt{N}}\|s(i) - \hat{s}(i)\|_2 = \frac{1}{R}\sqrt{\frac{\sum_{i=1}^{N}|s(i)-\hat{s}(i)|^2}{N}} \tag{3-20}$$

The values of these parameters were smaller, the pre-processing performances of algorithms were better.

Creating a standard testing ECG signal for simulation is necessary to provide a common platform to evaluate the performance of pre-processing methods. A "clean" ECG signal generated by a bedside monitor was mixed with simulated baseline wandering and high-frequency noise, given by

$$S(n) = I(n) + N(n) + B(n) \tag{3-21}$$

Where $S(n)$ was the combining signal; $I(n)$ was the clean ECG signal generated by a bedside monitor with sampling rate equals to 250Hz; $N(n)$ was high frequency noise consisting of two parts, probability distribution function is defined as

$$N(n) = (1-\varepsilon)G_1\left(\frac{n}{\sigma_1}\right) + \varepsilon G_1\left(\frac{n}{\sigma_2}\right) \tag{3-22}$$

Where G_1 and G_2 denoted probability distribution function of Gaussian random variables and represent background noise and high-frequency noise respectively. Typical setting was $\varepsilon = 0.2, \sigma_1 = 0.01, \sigma_2 = 0.1$. $B(n)$ was baseline wandering given by

$$B(n) = B + mn + Acos\left(2\pi\frac{n}{N} + \varphi\right) \tag{3-23}$$

let $m = 0.0001, B = -0.2, A = 0.2, N = 5000, \varphi = 0$. The standard testing ECG signal generated by above was shown in Figure3-3.

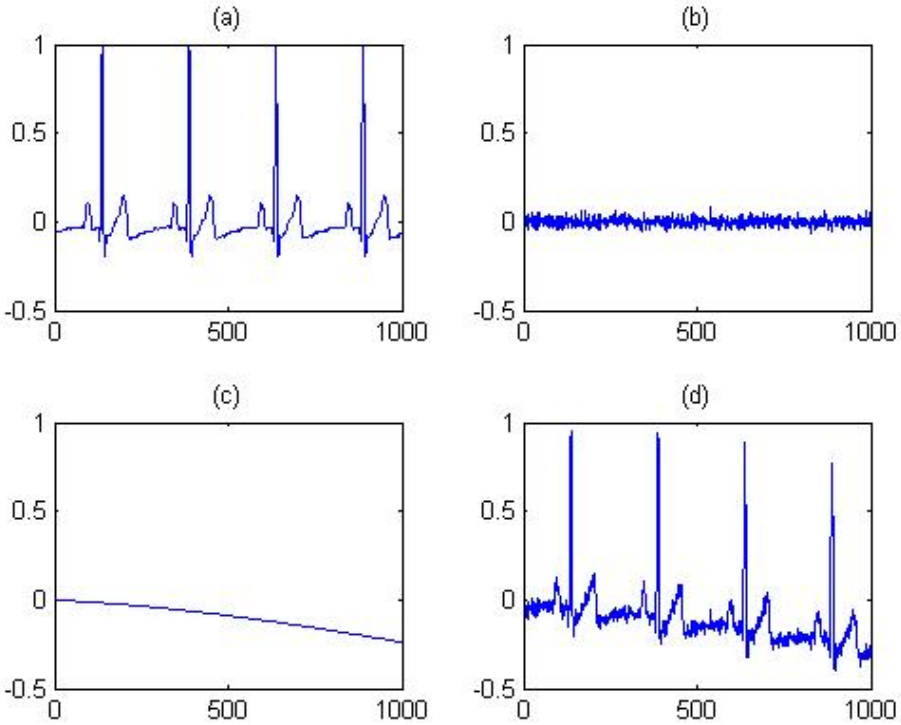

Figure 3-3 A standard testing ECG signal generated by mixing a clean signal with noise and baseline wandering. (a) A clean ECG signal generated by a bedside monitor. (b) Simulated noise. (c) Simulated baseline wandering. (d) The standard testing ECG signal.

3.3 Multi-resolution Decomposition Method

Definition 3-1 Complete lattice [33,50]:

If each subset K in set L has a minimum supremum $\vee K$ and a maximum infimum $\wedge K$, set L a complete lattice.

Definition 3-2 Adjunction:

Assuming L and M are two complete lattice, define operator $\mathcal{E}: L \to M$ and $\delta: M \to L$, if (ε, δ) meet 3-24, it constructs the adjunction between L and M.

$$\delta(y) \le x \Leftrightarrow y \le \varepsilon(x), \qquad x \in \mathrm{L}, y \in \mathrm{M} \tag{3-24}$$

and for arbitrary $\{x_i | i \epsilon I\} \subseteq L$ and $\{y_i | i \epsilon I\} \subseteq M$, we have

$$\varepsilon\left(\underset{i\in I}{\wedge} x_i\right) = \underset{i\in I}{\wedge} \varepsilon(x_i) \text{ and } \delta\left(\underset{i\in I}{\vee} y_i\right) = \underset{i\in I}{\vee} \delta(y_i) \tag{3-25}$$

therefore, ε, δ are monotonous operators, and ε and δ are called as **erosion** and **dilation** respectively. Define $\psi: L \to L$ and id is the unit operator. If $\psi^2 = \psi\psi = \psi$, ψ is idempotent and called as morphological filter. If $\psi \le id$, it is open operation; while $\psi \ge id$, it is close operation. For (ε, δ), which is the adjunction between L and M, $\varepsilon\delta$ constructs close operation on M and $\delta\varepsilon$ constructs open operation on L.

For further explanation, given complete lattice T and nonempty set E, define set

$T(E)$ include all functions $x: E \to T$, for arbitrary $x, y \in T(E)$, and meet 3-26,

$$If\ x(p) \le y(p), and\ x \le y, for\ \forall p \in E \tag{3-26}$$

and $T(E)$ is a complete lattice.

For d-dimension discrete space Z^d, there are erosion operator ε_A and dilation operator δ_A on set $T(Z^d)$, defined as 3-27 and 3-28:

$$\varepsilon_A(x)(n) = (x \Theta A)(n) = \bigwedge_{k \in A} x(n+k) \tag{3-27}$$

$$\delta_A(x)(n) = (x \oplus A)(n) = \bigvee_{k \in A} x(n-k) \tag{3-28}$$

where $A \subseteq Z^d$ is the **structure element**. As a result, 3-27 and 3-28 have the same meaning with 3-13 and 3-14.

Then we will discuss multi-resolution decomposition method. Let $j \in J \subseteq Z$ be the scale in multi-resolution decomposition. Define signal component on scale j as V_j. In this frame, define analysis operator $\psi_j^{\uparrow}: V_j \to V_{j+1}$ and composition operator $\psi_j^{\downarrow}: V_{j+1} \to V_j$. By using 3-28 and 3-29, we can realize analysis and composition transform at different level i, j $(i < j)$.

$$\psi_{i,j}^{\uparrow} = \psi_{j-1}^{\uparrow} \psi_{j-2}^{\uparrow} \cdots \psi_i^{\uparrow} \tag{3-29}$$

$$\psi_{j,i}^{\downarrow} = \psi_i^{\downarrow} \psi_{i+1}^{\downarrow} \cdots \psi_{j-1}^{\downarrow} \tag{3-30}$$

Then define analysis and composition transform from scale j to scale i, as 3-31:

$$\hat{\psi}_{j,i} = \psi_{j,i}^{\downarrow} \psi_{i,j}^{\uparrow} \tag{3-31}$$

Because the analysis operator is actually used for compressing the signal, the process is nonreversible. By composition, it is unable to lossless reconstruct the original signal. Therefore, $\hat{\psi}_{j,i}$ is the approximate signal at scale j.

Definition 3-3 Pyramid Condition:

For analysis operator $\psi_j^{\uparrow}$ and composition operator $\psi_j^{\downarrow}$, satisfying $\psi_j^{\uparrow} \psi_j^{\downarrow} = id$ on scale V_{j+1}, and are called as **Pyramid Condition**, and there are the following deduction:

- $\psi_j^{\uparrow}$ is surjective;
- $\psi_j^{\downarrow}$ is injective;
- $\psi_j^{\uparrow} \psi_j^{\downarrow} \psi_j^{\uparrow} = \psi_j^{\uparrow}$ and $\psi_j^{\downarrow} \psi_j^{\uparrow} \psi_j^{\downarrow} = \psi_j^{\downarrow}$ established;
- $\psi_j^{\downarrow} \psi_j^{\uparrow} \psi_j^{\downarrow} \psi_j^{\uparrow} = \psi_j^{\downarrow} \psi_j^{\uparrow}$.
- If $\psi_j^{\downarrow}$ is injective, the composition transform will not cause information loss,

i.e., assuming $\psi_j^{\uparrow}$ is surjective, let $y \in V_{j+1}$, $x \in V_j$, and $x = \psi_j^{\downarrow}(y)$, then $\psi_j^{\uparrow}(x) = \psi_j^{\uparrow}\psi_j^{\downarrow}(y) = y$.

Theorem 3-1:

Assuming that $\psi_j^{\uparrow}$ and $\psi_j^{\downarrow}$ meeting pyramid condition, 3-32 and 3-33 establish, and $\hat{\psi}_{i,j}$ is idempotent:

$$\psi_{j,i}^{\uparrow}\psi_{j,i}^{\downarrow} = id \text{ on } V_j \ , \ i < j \tag{3-32}$$

$$\hat{\psi}_{j,i}\hat{\psi}_{k,i} = \hat{\psi}_{j,i} = \hat{\psi}_{k,i}\hat{\psi}_{j,i} \ , \ i < k \le j \tag{3-33}$$

Theorem 3-2:

In 3-33, the first equality sign presents that for $x \in V_j$, the approximation $\hat{\psi}_{k,i}(x)$ at scale k can provide enough information for the approximation $\hat{\psi}_{j,i}(x)$ at scale j $(j > k)$; and the second equality sign means that calculation by $\hat{\psi}_{k,i}$ cannot change the result of $\hat{\psi}_{j,i}(x)$. It means that when scale in multi-resolution decomposition increases, the information included decreases.

Then we consider the situation that the signal domain is a complete lattice and analysis and composition operators between adjacent scales form an adjunction. Assuming that $V_j, j = 0,1,2,\ldots$ are complete lattices; $(\psi_j^{\uparrow}, \psi_j^{\downarrow})$ is adjunction between V_j and V_{j+1}. Under this condition, $\psi_j^{\uparrow}$ is an erosion operator and , $\psi_j^{\downarrow}$ is an dilation operator. It is easy to know that if and only if $\psi_j^{\downarrow}$ is injective ($\psi_j^{\uparrow}$ is surjective), the pyramid condition is satisfied. At the same time, we know that, $\psi_j^{\downarrow}\psi_j^{\uparrow}$ is an open operator and , $\psi_j^{\downarrow}\psi_j^{\uparrow} \le id$.

Furthermore, for $V_j = T(Z^d), j = 0,1,2,\ldots$, according to definition 3-2, we have:

$$x_{j+1} \le \psi_j^{\uparrow}(x_j) \Leftrightarrow \psi_j^{\downarrow}(x_{j+1}) \le x_j \qquad x_j \in V_j, x_{j+1} \in V_{j+1} \tag{3-34}$$

For arbitrary shifting on Z^d, $(\tau x)(n) = x(n-k)$, where $n, k \in Z^d$, has the property of shift invariance, as is shown in 3-35:

$$\psi_j^{\uparrow}\tau^2 = \tau\psi_j^{\downarrow}$$
$$\psi_j^{\downarrow}\tau = \tau^2\psi_j^{\uparrow} \tag{3-35}$$

Theorem 3-3:

Assuming that $(\psi_j^{\uparrow}, \psi_j^{\downarrow})$ is an adjunction on $T(Z^d)$, and meeting 3-35, and every pair of adjunctions should satisfy the following equations:

$$\psi_j^{\uparrow}(x)(n) = \bigwedge_{k\in Z^d} a_{k-2n}(x(k))$$
$$\psi_j^{\downarrow}(x)(k) = \bigvee_{n\in Z^d} b_{k-2n}(x(n)) \tag{3-36}$$

where (a_k, b_k) for each $k \in Z^d$ define a pair of adjunctions on T.

Definition 3-4: Support

Define support A of $(\psi_j^{\uparrow}, \psi_j^{\downarrow})$ meeting 3-36 contains all $(a'_{k,0}, b'_{k,0})$, where $a'_{k,0}$ is not always equal to the maximum element in T and $b'_{k,0}$ is not always equal to the minimum element in T.

For $n \in Z^d$, define $Z^d[n] = \{k \in Z^d | k - n \in Z_2^d\}$, where Z_2^d contains all the vectors with even coordinate in Z^d. For $A \subseteq Z^d$ and $n \in Z^d$, let $A[n] = A|Z^d[n]$, and A can be divided into no more than 2^d non-empty and independent discontinuous subsets.

Theorem 3-4:

Considering $(\psi_j^{\uparrow}, \psi_j^{\downarrow})$ meeting theorem 3-3, let $A \subseteq Z^d$ be its support. Assuming that existing an $a \in A$ satisfying $A[a] = \{a\}$, and $b'_{0,a}$ is injective, then $(\psi_j^{\uparrow}, \psi_j^{\downarrow})$ satisfies pyramid condition.

3.2 Lifting Scheme Constructing Multi-resolution Decomposition

Lifting scheme was provided by Sweldens [51-53] and has the following metrics: it can construct wavelet decomposition method on arbitrary domain; it has higher vanishing moments; it can be fast implemented by quick integer calculation. The lifting scheme can be divided into three steps: decompose, predict and update. For simplicity's sake, we only discuss at scale 1.

(1) Decompose: assuming scale analysis/composition operators are $\psi^{\uparrow}: V_0 \to V_1$ and $\psi^{\downarrow}: V_1 \to V_0$; wavelet analysis/composition operators are $\omega^{\uparrow}: V_0 \to W_1$ and $\omega^{\downarrow}: W_1 \to V_0$; the original signal is x_0, the signal component at scale 1 is $x_1 = \psi^{\uparrow}(x_0)$ and the wavelet component is $y_1 = \omega^{\uparrow}(x_0)$.

(2) Predict: define predict operator $\pi: V_1 \to W_1$, because of the redundancy in wavelet transform, at scale 1, predict wavelet component $\pi(x_1)$ by signal component, by using 3-37, we will have finer detail component than wavelet

component y_1'.

$$y_1' = y_1 - \pi(x_1) \tag{3-37}$$

(3) Update: define update operator $\lambda: W_1 \to V_1$, to maintain some scalar characteristic (such as unchangeable vanishing moments or mean value, and so on), signal component x_1 can be updated by new detail component y_1':

$$x_1' = x_1 - \lambda(y_1') \tag{3-38}$$

and the original signal can be reconstructed step by step by x_1' and y_1', as is shown in 3-39 and 3-40:

$$\hat{x}_1 = x_1' + \lambda(y_1') \tag{3-39}$$

$$\hat{x}_0 = \psi^{\downarrow}(\hat{x}_1) + \omega^{\downarrow}(y_1' + \pi(\hat{x}_1)) \tag{3-40}$$

On the other hand, predict and update operators can be used independently. For instants, we can adopt 3-37 to predict detail component, and 3-41 as the reconstructing expression:

$$\hat{x}_0 = \psi^{\downarrow}(x_1) + \omega^{\downarrow}(y_1' + \pi(x_1)) \tag{3-41}$$

When using update operator independently, 3-42 is adopted for signal component prediction, and 3-43 as the reconstructing expression:

$$x_1' = x_1 + \lambda(y_1) \tag{3-42}$$

$$\hat{x}_0 = \psi^{\downarrow}(x_1' + \lambda(y_1)) + \omega^{\downarrow}(y_1) \tag{3-43}$$

3.3 LMMMD ECG Pre-processing method

LMMMD ECG pre-processing algorithm can be divided into two parts: baseline correction and noise suppression. Baseline correction is conducted by the following morphological filter:

$$f_b = f_o \circ B_o \cdot B_c \tag{3-43}$$

f_o is the original ECG signal, f_b is the detected baseline wandering, $B_o$and$B_c$are two linear SEs which

According to multi-resolution mathematical morphological decomposition method (MMMD), ECG signals after baseline correction can be decomposed at level j as following

$$x_{j+1} = \psi_j^{\uparrow}(x_j) = MF_j(x_j) \tag{3-44}$$

$$y_{j+1} = \omega_j^{\uparrow}(y_j) = x_j - MF_j(x_j) \tag{3-45}$$

where $MF_j(f)$ is defined as multi-resolution morphological filter at level j.

$$MF_j(f) = \frac{1}{2}(f \circ B_j \cdot B_j + f \cdot B_j \circ B_j) \tag{3-46}$$

where B_j is a linear SE with length equals to $j+1$ while x_j is the approximate

signal and y_j is the detail signal at level *j*. x_j is the approximate signal, i.e., the ECG signal after de-noising.

More improvement in noise suppression performance may be achieved by lifting scheme constructing MMMD method (LMMMD algorithm). Consider lifting scheme constructing new detail and signal component at level *j* as

$$y_j' = y_j - \pi(x_j) \tag{3-47}$$

$$x_j' = x_j - \lambda(y_j') \tag{3-48}$$

where $\pi: V_j \to W_j$ is the predicting operator and $\lambda: W_j \to V_j$ is the updating operator. Reconstructions at level j and $j-1$ are defined as

$$\hat{x}_j = x_j' + \lambda(y_j') \tag{3-49}$$

$$\hat{x}_{j-1} = \psi_j^{\downarrow}(\hat{x}_j) + \omega_j^{\downarrow}\left(y_j' + \pi(\hat{x}_j)\right) \tag{3-50}$$

Block effect is the main cause of waveform distortion in morphological filter based ECG pre-processing method. To address this issue, a novel updating and predicting operator based on cubic spline interpolation is proposed as

$$\pi(x_j)(n) = x_j(n) - x_j(n+1) \tag{3-51}$$

$$\lambda(y_j)(n) = \mathrm{spline}\big(x_j(n-1), x_j(n+1)\big) \tag{3-52}$$

Where the predicting operator is the difference between adjacent samples; and updating operator is the interpretation according to the forward and backward sample. Because of the smoothing characteristic of cubic spline interpolation, LMMMD algorithm can reduce the block effect and improve the waveform distortion.

3.4 Simulation Applied to standard testing ECG

LMMMD algorithm was applied to a standard testing ECG signal which mixes "clean" ECG signal generated by a bedside monitor and simulated baseline wandering and high-frequency noise. Then the performance of the algorithm as well as comparison with other pre-processing methods was presented in this section.

3.4.1 Baseline correction

An algorithm based on wavelet transform was considered as a comparison. Firstly, the ECG signal was decomposed by db6 wavelet to the 8th level, and a_8 signal component was set to 0 to remove the baseline component. The simulation results of baseline correction by wavelet transform and morphological operations were shown in Figure 3-4, 3-5 and Table 3-1. Although wavelet transform method had

superiority in MAD and RMSE, waveform distortions in samples near 1000 were distinguished, which should be strictly kept in small range for ECG signals. Baseline correction method based on morphological operations could not achieve good performance in RMSE for block effect brought by linear SE and waveform distortions were visually acceptable.

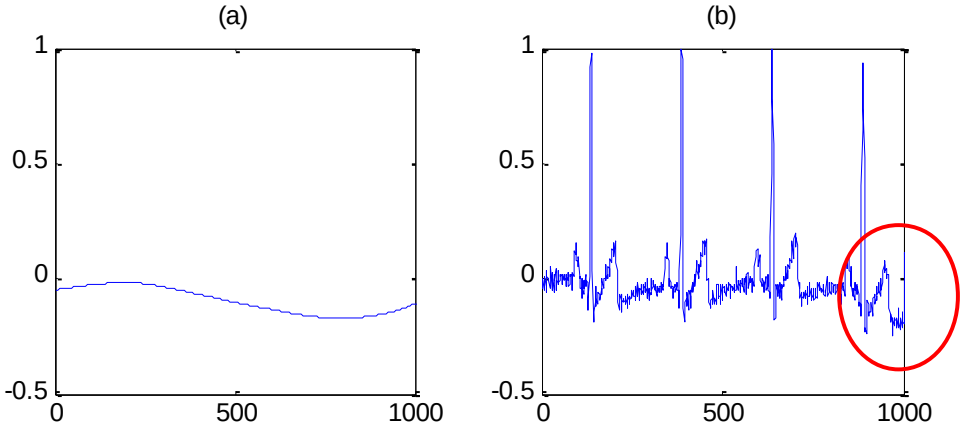

Figure 3-4 Baseline correction by db6 wavelet transform. (a) Baseline component. (b) ECG signal after baseline correction.

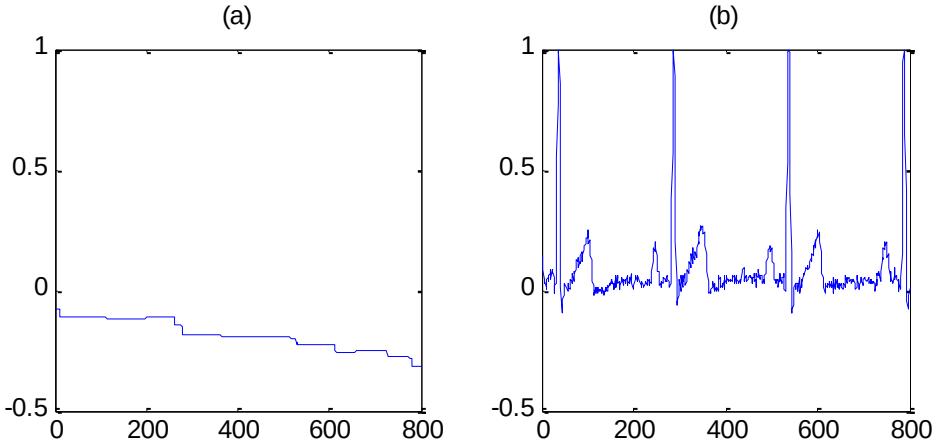

Figure 3-5 Baseline correction by morphological operations. (a) Baseline component. (b) ECG signal after baseline correction.

Table 3-1 Performance evaluation of baseline correction by db6 wavelet transform and morphological operation.

	db6 wavelet transform	morphological operations
MAD	0.0197	0.0518
MaxD	1.04×10^{-4}	1.04×10^{-4}
RMSE	0.0299	0.0543

3.4.2 Noise suppression

One comparative algorithm was method based on db6 wavelet transform. Based on ECG signals after baseline correction and the db6 wavelet transforming results of the original signal, noise suppression was dealt with detail signals on level 1, 2 and 3. De-noised wavelet coefficients were given by

$$\widehat{w}_{j,k} = \begin{cases} \mathrm{sgn}(w_{j,k})(|w_{j,k}| - \lambda) & |w_{j,k}| \geq \lambda \\ 0 & otherwise \end{cases} \tag{3-53}$$

where $\lambda = \sigma\sqrt{2\ln N}$, σ was mean square error of the noise and N was the length of signals. Simulation results were as shown in Figure 3-6. There were waveform distortions in QRS complex.

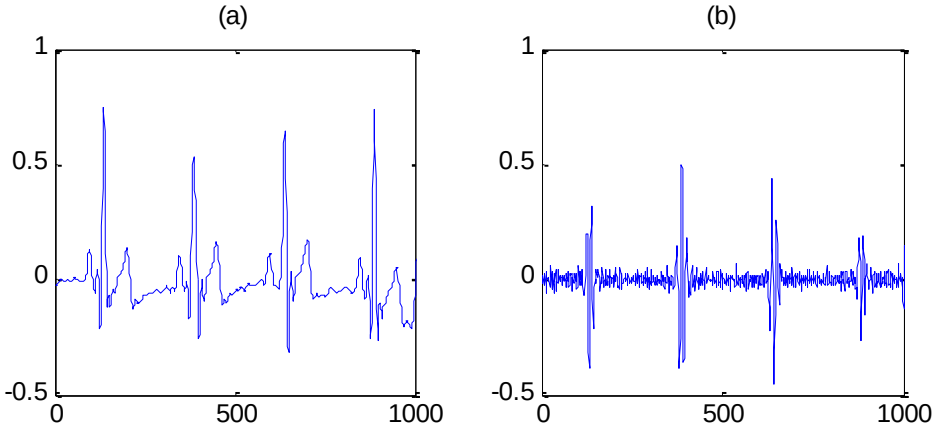

Figure 3-6 Noise suppression by db6 wavelet transform method. (a) ECG signals after pre-procession. (b) Noise suppressed from the signal.

Another comparative algorithm was method based on MMD. Firstly, the signal was decomposed to level 3, as was shown in Figure 3-7. Detail signals on level 1 and 2 mainly consisted of noise while detail signal on level 3 mainly included information of ECG signal. Therefore, the ECG signal was decomposed to level 2 to achieve best noise suppression performance.

Simulation by LMMMD algorithm was shown in Fig3-8. Approximate signal on level 2 was chosen as the result of noise suppression for the same reason in simulation by MMMD method. The performance evaluations of the three noise suppression methods were shown in Table 3-2. Block effect was improved than that of simulation by MMD method, which could be noticed in Figure 3-8 and verified by the improvement of MAD, MaxD and RMSE values described in Table 3-2. Exception of MAD and computing time, LMMMD algorithm achieved better performance than the other two methods. For MAD value, LMMMD algorithm and MMMD algorithm were based on baseline correction by morphological operation, which had worse performance than baseline correction by db6 wavelet transform. By using lifting scheme, the computing time was increased, but still much less than methods by db6 wavelet transform.

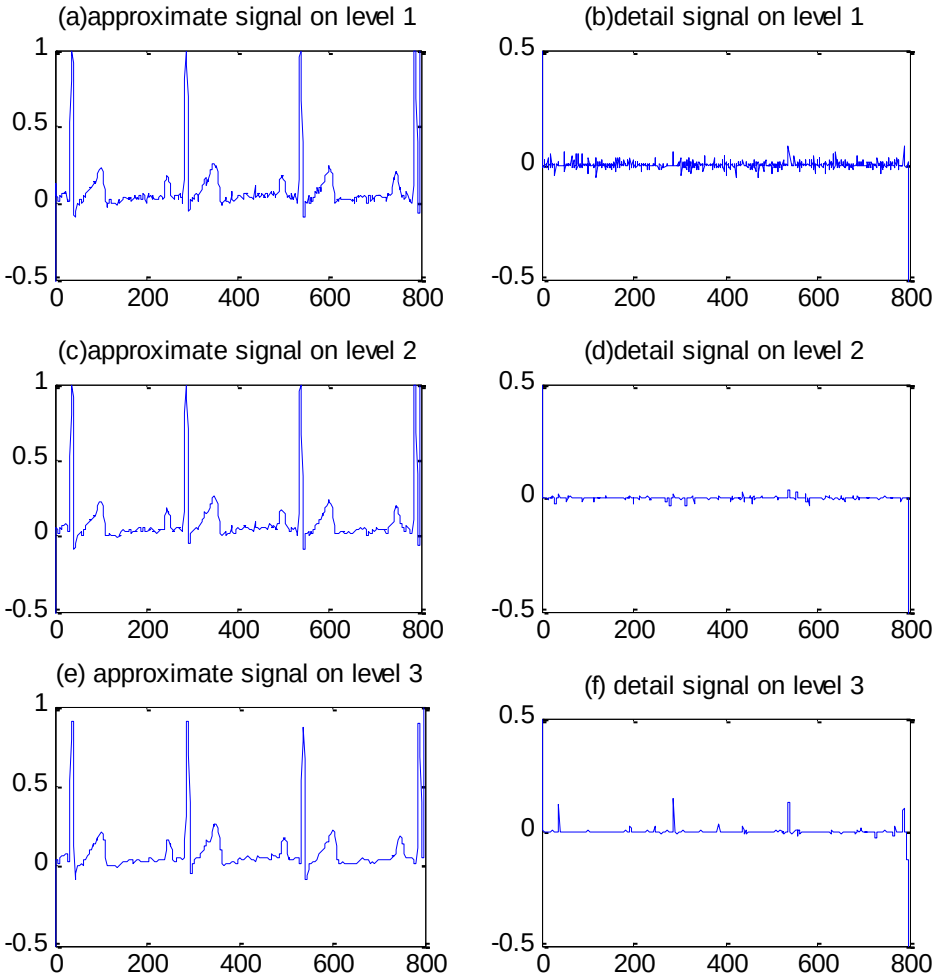

Figure 3-7 Decomposition of ECG signal by MMD method. (a) Approximate signal on level 1. (b) Detail signal on level 1. (c) Approximate signal on level 2. (d) Detail signal on level 2. (e) Approximate signal on level 3. (f) Detail signal on level 3.

Table 3-2 Performance evaluation of noise suppression by three methods.

Baseline correction method	db6 wavelet transform	morphological operations	
Noise suppression method		MMD algorithm	LMMMD algorithm
MAD	0.0362	0.0531	0.0527
MaxD	4.11×10^{-4}	1.39×10^{-4}	1.29×10^{-4}
RMSE	0.0659	0.0567	0.0562
Computing time (s)	1.166	0.189	0.509

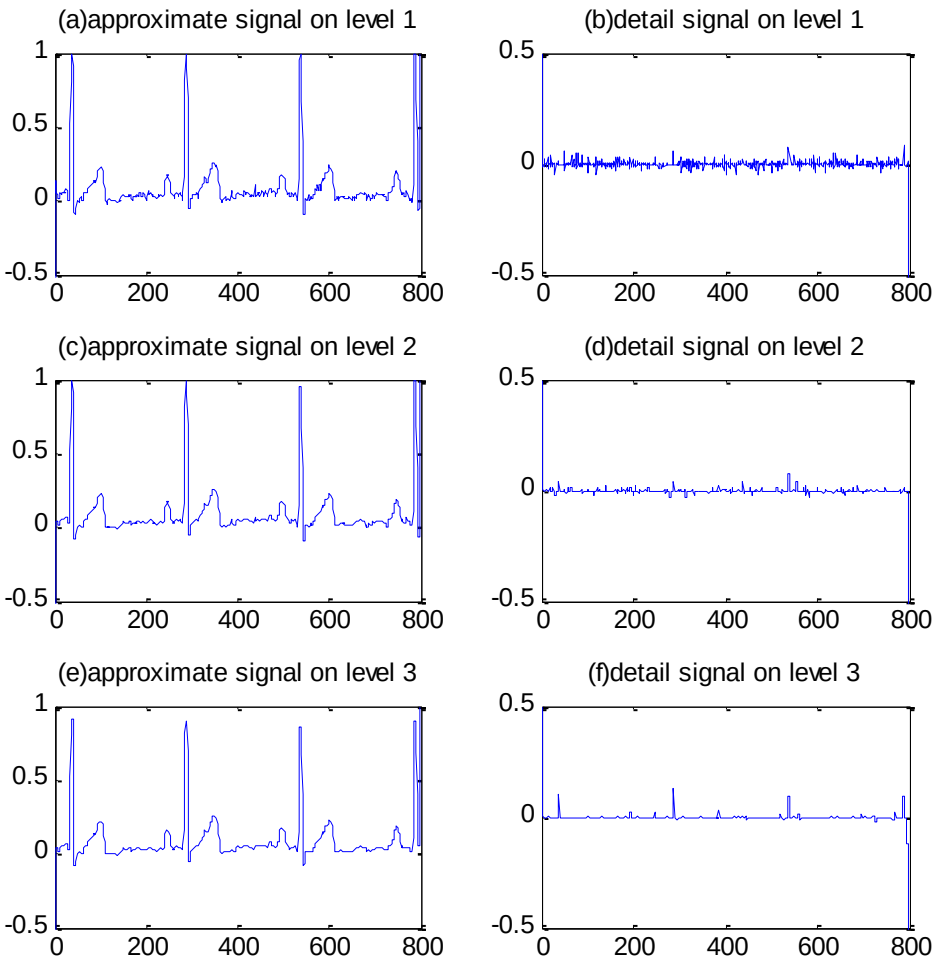

Figure 3-8 Decomposition of ECG signal by LMMD method. (a) Approximate signal on level 1. (b) Detail signal on level 1. (c) Approximate signal on level 2. (d) Detail signal on level 2. (e) Approximate signal on level 3. (f) Detail signal on level 3.

ECG signal pre-precession can be divided into two steps: baseline correction and noise suppression. Baseline correction based on high-pass filter is easy to realize by hardware, but useful clinic information in ECG signal is apt to be filtered at the same time. Adaptive filters also have been developed to address this issue, yet they are inflexible to deal with diverse ECG morphology. Baseline correction based on wavelet transform can smoothly remove baseline component. However, to clearly separate baseline component, the ECG signal should be analyzed to relatively high level. It greatly aggravates the computing burden of the pre-processing system. Furthermore, waveform distortions cannot be avoided. Although baseline correction based on morphological operations cause extra block effect, it can remove the drift properly with acceptable waveform distortions.

Noise suppression based on digital filters can remove noise with small computing cost. However, high frequency information in ECG signal, such as R peaks, are usually mixed with noise, and waveform distortion cannot be avoided. Wavelet transform method also cannot separate noise and information clearly and QRS complex are apt to be partially filtered. Noise suppression based on morphological operations or multi-resolution morphological decomposition cannot solve block effect brought by

linear SE. Based on simulation results in this paper, the noise suppression performance of LMMMD algorithm have better performance on noise suppression than method based on db6 wavelet transform and multi-resolution morphological decomposition although the weakness in baseline correction by morphological operations. On the other hand, by adopting lifting scheme based on cubic spline interpolation, block effect caused by linear SE was improved, which was visually distinguishable and reflected in values of performance evaluation criterions. Furthermore, the waveform distortion in LMMMD algorithm was smaller than the other two algorithms, which was both acknowledged visually and numerically. The computing time increased by lifting scheme was acceptable when comparing with method based on db6 wavelet transform.

3.5 Simulation applied to MIT-BIH database and clinical ECG signals

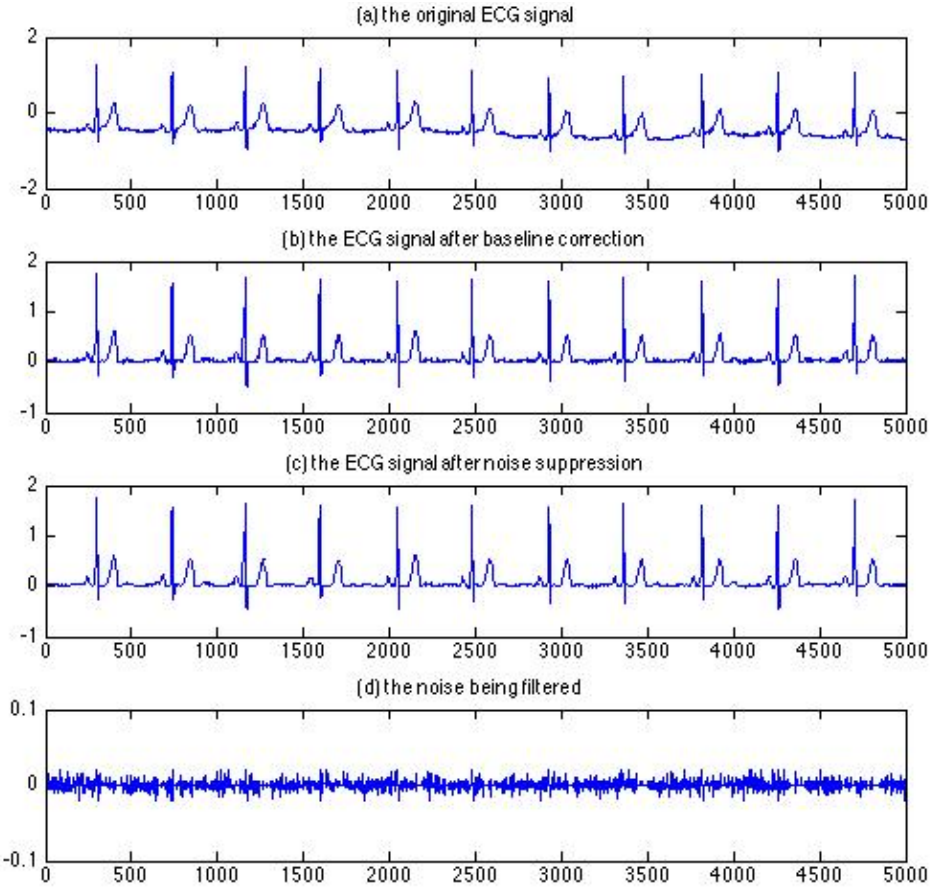

Fig. 3-9 the pre-processing results of Sample No. 117 in MIT-BIH Arrhythmia Database by the proposed method

It is very important to test the algorithm in the database to evaluate its effectiveness. And it is also critical to test the algorithm for clinical ECG signals collected from the hospital. Because comparing with ECG signals in the database, the clinical ECG signals have more random range and noise interference. In this paper,

first the MIT-BIH Arrhythmia Database has been chosen as the testing database. The MIT-BIH Arrhythmia Database contains 48 half-hour excerpts of two-channel ambulatory ECG recordings, which were sampled at 360Hz with 11-bit resolution over a 10mV range. And each beat in this database has been annotated as references for applications such as QRS complex detection and ECG auto diagnosis. In this chapter, we adopt Sample No. 117, No. 118 and No. 222 to demonstrate the efficiency of the proposed method.

Fig. 3-9, 3-10 and 3-11 present the pre-processing results of Sample No. 117, No. 118 and No. 222 by the proposed method respectively. As illustrated in (b) of these three figures, baseline drift has been removed almost completely and waveform distortion is visually ignorable. And from (d) in these three figures, the filtered noise mainly consists of high frequency noise, and we can hardly see useful clinical information in it, especially in Fig. 3-10 (b).

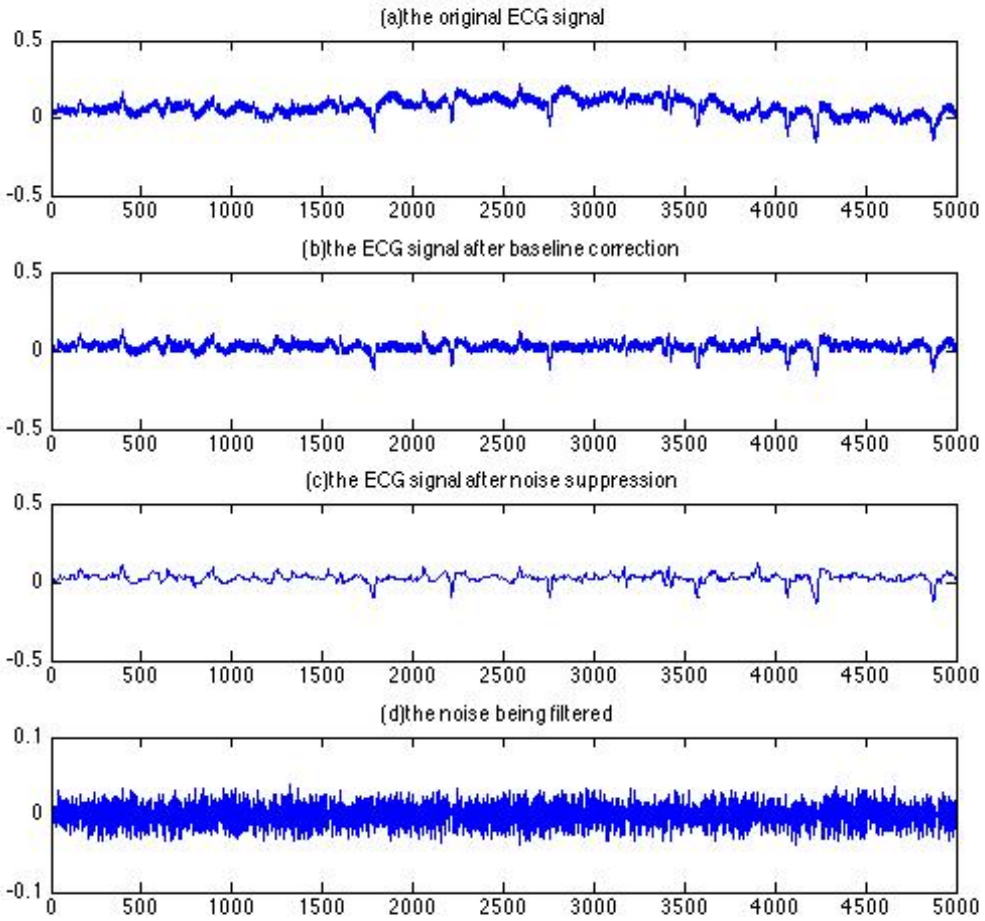

Fig. 3-10 the pre-processing results of Sample No. 118 in MIT-BIH Arrhythmia Database by the proposed method

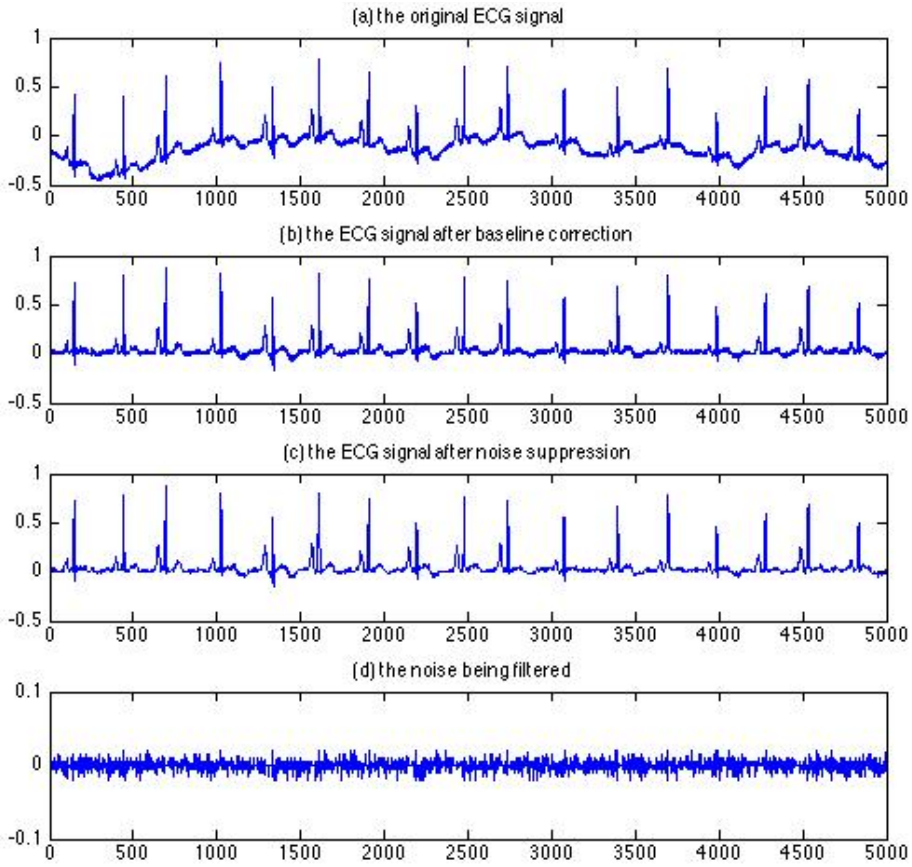

Fig. 3-11 the pre-processing results of Sample No. 222 in MIT-BIH Arrhythmia Database by the proposed method

Then the algorithm was tested on clinical ECG signal collected in the hospital, the sample rate is 250Hz. Comparing with ECG signals in the MIT-BIH Arrhythmia Database, these signals have lower high frequency noise, but may contain EMG with very high amplitude. We collected 60 objects with two postures (sitting and standing), and both ECG and PPG are recorded to estimate the blood pressure of them. In this chapter, we only take ECG signals for example, but this method is also suitable for PPG pre-processing, and the only thing we need to do is to adjust the length of SE.

Fig. 3-12 and 3-13 are two examples from the collection. As illustrated in (b) of these two figures, baseline drift has been removed almost completely. And from (d) in these three figures, the filtered noise mainly consists of high frequency noise, and we can hardly see useful clinical information in it. However, for Fig. 3-13, this sample contains high amplitude EMG interference, and the proposed method cannot completely filter them and the waveforms in these areas are distorted, which will cause QRS detection false.

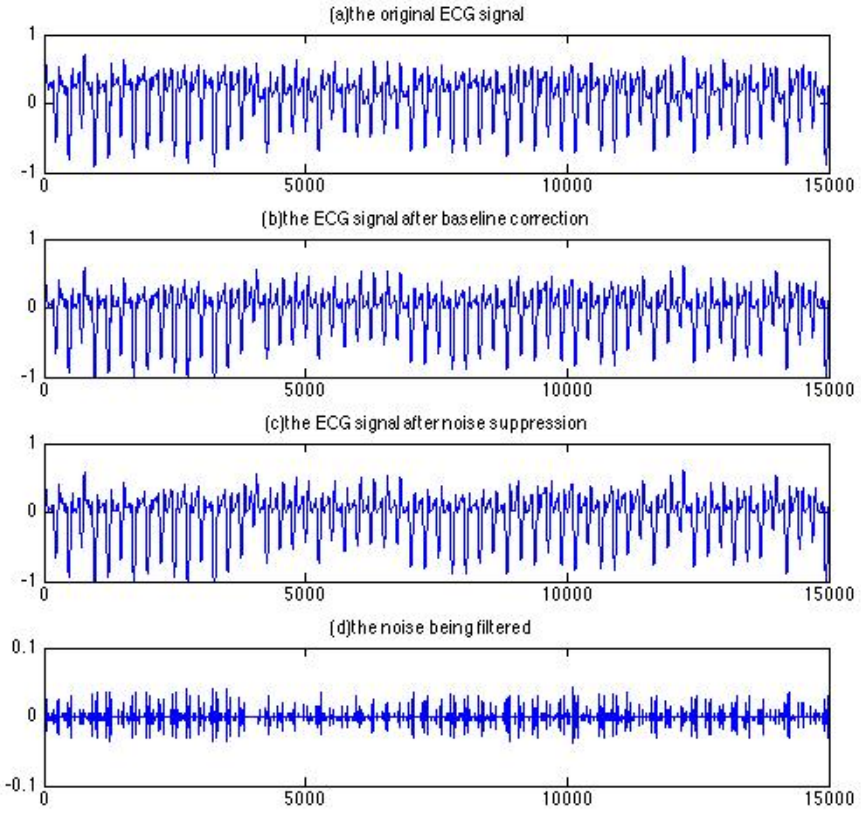

Fig. 3-12 The pre-processing of Sample 1 from ECG collection from hospital

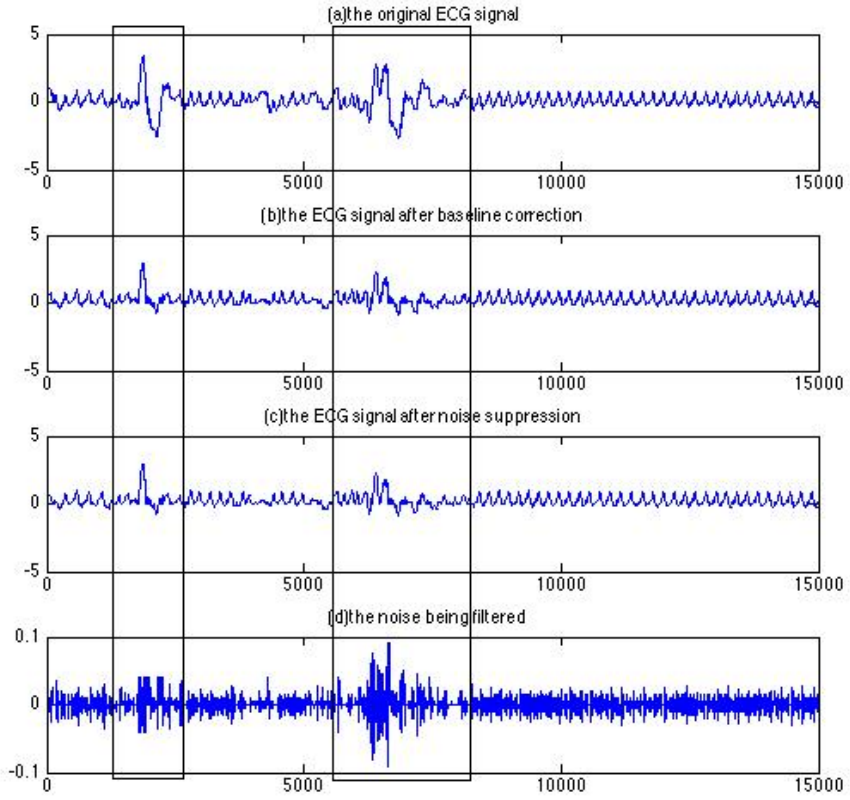

Fig. 3-13 The pre-processing of Sample 2 from ECG collection from hospital

Chapter 4 Research on QRS detection methods

QRS complex detection is the foundation of ECG auto classification and diagnosis. It also provides important premise to realize compression and reconstruction system. On the other hand, it can help to estimate blood pressure.

I channel of normal ECG signals has QRS complex with highest amplitude and slope, which corresponds to ventricular depolarization. Normal QRS of an adult last about 0.06~0.10s, while children and people doing sports have shorter duration. The duration, amplitude and morphology are important diagnosing characteristics for arrhythmia, conduction abnormalities, myocardial infarction, ventricular hypertrophy, electrolyte disorder and so on. Besides, QRS morphologies are very different from each channel, while physiological and pathological state and individual difference will also cause complex variation of the morphology of QRS complex. The common waveform patterns of QRS complex are shown in Figure 4-1. Although the QRS complex mainly consists of Q wave, R wave and S wave, but the direction amplitude, and even appearance of these characteristic waves are varied.

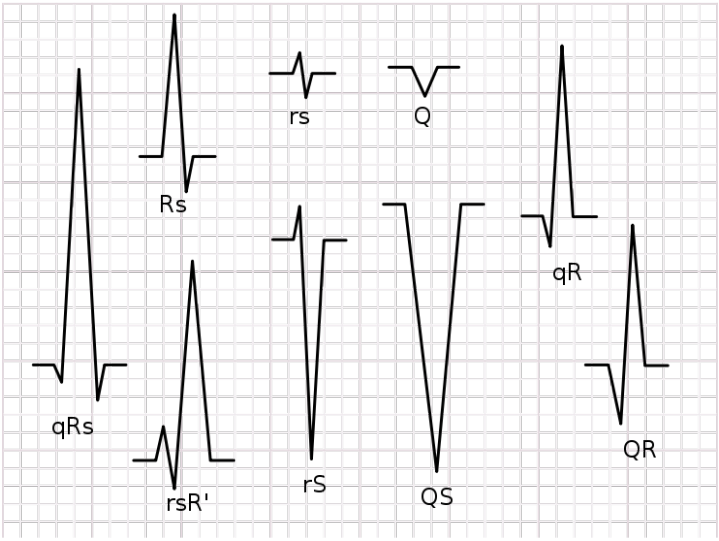

Figure 4-1 Common morphologies of QRS complex.

QRS Complex detection is the most important stage in ECG analyzing process. Accurate detection of QRS Complex is the precondition of detecting other ECG waves. This is the basis of ECG automatic classification and diagnosis [54,55]. Meanwhile, it ensures dividing cardiac cycles correctly, which is usually the first step before ECG compression, and has deep impact on utilization of correlations between cardiac cycles or different leads. QRS Complex detection consists of R peak detection and onset/offset decision, and we focus on R peak detection in this paper.

There are many algorithms designed for QRS detection purpose. Before Wavelet techniques are adopted, the derivative and its related information of ECG are mainly used for QRS detection, as it can access the deep slops of the R waves. Such kind of

methods has the characteristics of less calculation and easy implementation, but with lower positive rate and noise immunity. QRS detection algorithms based on Wavelet Techniques have been popular since last decade. The main idea is that QRS Complex's analyzing components are different between levels, and by choosing the level with local maximum, it is easier to distinguish modulus maximum that are related to QRS Complexes. However, for QRS Complex with steep slope, methods based on Wavelet techniques are likely to mix it with EMG or other noise, and result in leak detection. Mathematical morphology (MM) methods have been introduced into ECG signal processing field in 1980s. Mostly, algorithms based on MM methods are adopted in the pre-processing for its robustness and self-adaptability in extracting morphological information. And then QRS detection based on MM method was mainly implemented by triangle structure elements (SE). In 2002, Goutsias et al proposed nonlinear multi-resolution signal decomposition scheme based on MM, which can achieve good performance for ECG signals, especially in ECG pre-processing. QRS complex detection can also be realized by multi-resolution decomposition scheme based on MM (MDMM). However, QRS complex detection methods based on MM distinguish steep R peaks more easily than gentle ones.

4.1 QRS detection method based on lifting scheme constructing multi-resolution decomposition based on MM

Define ECG signal as $\mathrm{f(n)}, \mathrm{n} = 0,1, \dots, \mathrm{N}-1$, symmetrical SE as $\mathrm{B(m)}, \mathrm{m} = 0,1,2, \dots, \mathrm{M}-1$, erosion and dilation of ECG signal can be denoted as following

$$(\mathrm{f\Theta B})(\mathrm{n}) = \min\{\mathrm{f(n+m)} - \mathrm{B(m)}\} \quad m\epsilon 0,1, \dots, M-1 \tag{4-1}$$

$$(\mathrm{f\oplus B})(\mathrm{n}) = \max\{\mathrm{f(n-m)} + \mathrm{B(m)}\} \quad m\epsilon 0,1, \dots, M-1 \tag{4-2}$$

Opening operator is $\mathrm{f} \circ \mathrm{B} = (\mathrm{f\Theta B})\oplus \mathrm{B}$ while closing operator is $\mathrm{f} \cdot \mathrm{B} = (\mathrm{f\oplus B})\Theta \mathrm{B}$.

According to multi-resolution morphological decomposition theory, ECG signals at level j can be decomposed as following

$$x_{j+1} = \psi_j^{\uparrow}(x_j) = MF_j(x_j) \tag{4-3}$$

$$y_{j+1} = \omega_j^{\uparrow}(y_j) = x_j - MF_j(x_j) \tag{4-4}$$

where $\mathrm{MF_j(f)}$ is defined as multi-resolution morphological filter at level j.

$$MF_j(f) = \frac{1}{2}\left(f \circ B_j \cdot B_j + f \cdot B_j \circ B_j\right) \tag{4-5}$$

where $\mathrm{B_j}$ is a linear SE with length equals to $\mathrm{j}+1$ while $\mathrm{x_j}$ is the approximate

signal and y_j is the detail signal at level j.

More improvements in specified performance of algorithms such as noise suppression and QRS detection accuracy and so on, are able to be achieved by adopting lifting scheme constructing method with appropriate operators. Consider lifting scheme constructing new detail and approximate component at level j as

$$y_j' = y_j - \pi(x_j) \tag{4-6}$$

$$x_j' = x_j - \lambda(y_j') \tag{4-7}$$

where $\pi: V_j \to W_j$ is the predicting operator and $\lambda: W_j \to V_j$ is the updating operator. Reconstructions at level j and $j-1$ are defined as

$$\hat{x}_j = x_j' + \lambda(y_j') \tag{4-8}$$

$$\hat{x}_{j-1} = \psi_j^{\downarrow}(\hat{x}_j) + \omega_j^{\downarrow}\left(y_j' + \pi(\hat{x}_j)\right) \tag{4-9}$$

Noise suppression in ECG signals can be divided into two steps: (1) remove the baseline wander caused by electrodes movement and respiration; (2) Suppress high frequency noise caused by EMG and other interference. Therefore, LMW algorithm first does baseline wander correction by using the following MM filter

$$f_b = f_0 \circ B_0 \cdot B_c \tag{4-10}$$

where f_0 is the original ECG signal, f_b is the detected baseline wandering, B_0 and B_c are two linear SEs which depend on the duration of characteristic waveforms in ECG signals T_ω and sampling rate F_s. Commonly, $T_\omega < 0.2s$, therefore, let $B_0 = 0.2F_s$ and $B_c = 1.5B_0 = 0.3F_s$. ECG signals after baseline correction can be decomposed at level j as following

$$x_0 = f_0 - f_b \tag{4-11}$$

and let $x_1 = x_0$.

Then high frequency noise suppression is conducted by lifting scheme constructing MDMM. Block effect is the main cause of waveform distortion in morphological filter based ECG pre-processing method. To address this issue, a novel updating and predicting operator based on cubic spline interpolation is proposed as

$$\pi(x_j)(n) = x_j(n) - x_j(n+1) \tag{4-12}$$

$$\lambda(y_j)(n) = \mathrm{spline}\big(x_j(n-1), x_j(n+1)\big) \tag{4-13}$$

where the predicting operator is the difference between adjacent samples; and updating operator is the interpretation according to the forward and backward sample. Because of the smoothing characteristic of cubic spline interpolation, LMW algorithm can reduce the block effect and improve the waveform distortion. The good performance in noise suppression is also proved by our previous work.

Take Sample 222 in MIT-BIH with visible baseline wander and high frequency noise as example, as is shown in Figure 4-2: baseline wander is corrected firstly, then

ECG signals are decomposed to level 2 by lifting scheme constructing MDMM, finally we choose approximation component at level 2 as the pre-processing results and original data for QRS detection, because the root mean square is the least among level 1 to level 3 decomposition.

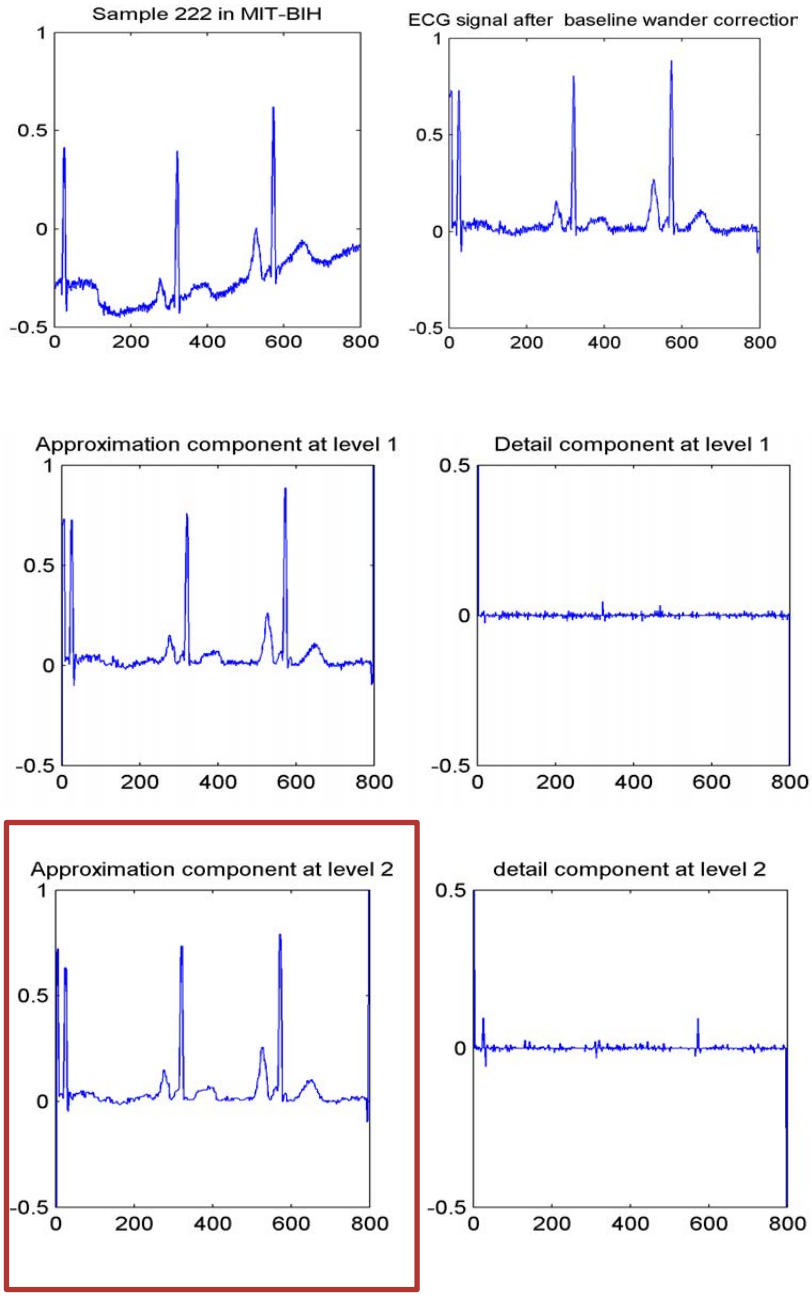

Figure 4-2 Sample 222 in MIT-BIH database. Preprocessing by LMW algorithm. Take Approximation component at level 2 as preprocessing results.

After ECG signal pre-processing, it becomes apt to detect QRS complex more easily. Then we consider detecting QRS complex accurately by lifting scheme constructing MDMM with maximization operator (LMS algorithm for short). Let predicting operator is the difference between adjacent samples; and updating operator is the maximum of adjacent three samples, as describe in "(4-14)" and "(4-15)":

$$\pi(x_j)(n) = x_j(n) - x_j(n+1) \tag{4-14}$$

$$\lambda(y_j)(n) = \max(x_j(n-1), x_j(n), x_j(n+1)) \tag{4-15}$$

and ECG signals can be decomposed through "(4-3)-(4-8)". Furthermore, a search back method is encompassed in our proposed QRS detecting algorithm, which is called LM Algorithm for short and can be summarized by the application of the following steps, and the flow chart is illustrated in Figure 4-3:

1) Divide every 10 seconds ECG data as a segment. Set initial value of threshold as one-tenth the maximum of samples in the segment.

2) Decompose segment by using LM Algorithm up to level 4 (i.e. do twice lifting scheme constructing with maximization operator after pre-processing).

3) Locate modulus maxima of detail component at level 3 (D3) and detail component at level 4 (D4); D3 and D4 of Sample 222 is shown in Figure 4-4. Then do "OR" operation between D3 and D4 as the input to search back algorithm.

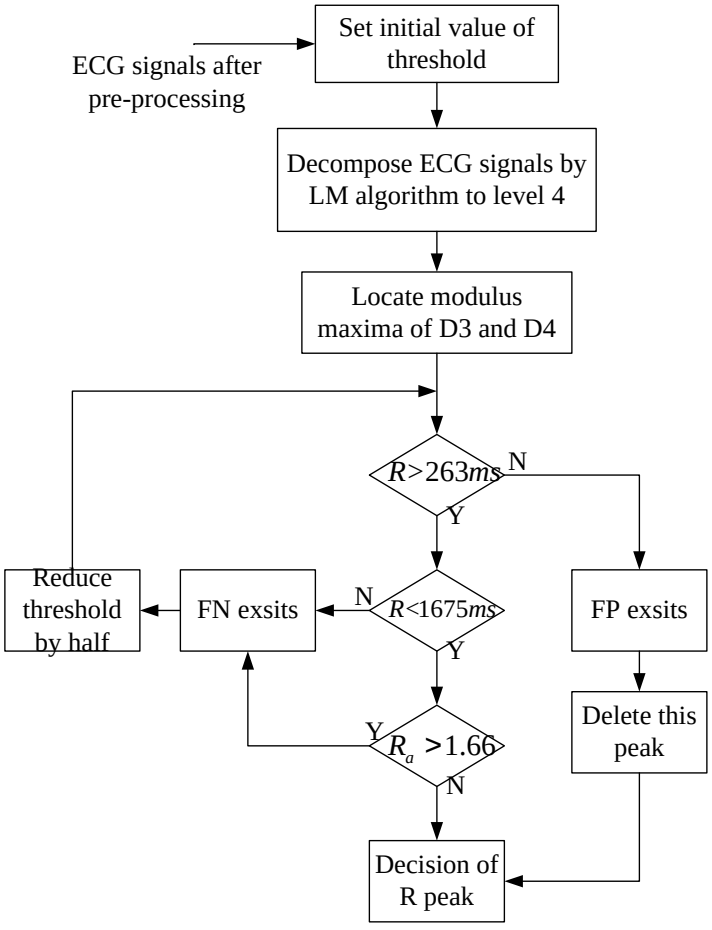

Figure 4-3. Flow chart of LMS Algorithm

4) Define R is RR interval, and aveR is the average RR intervals of two preceding segments. It is critical for both medical staff and researchers to restrict R and aveR in reasonable ranges. In [54], it presents that $R < 250\text{ms}$ is an important symbol of sudden death; and in [55], it is proved that only 5% of patients have $R > 1750\text{ms}$ occasionally. Therefore, we consider reasonable range is

$250\text{ms} < \text{R} < 1750\text{ms}$. Because the sampling rate of MIT-BIH Arrhythmia Database is 360Hz, we set the limits of R are 263ms and 1675ms, which means if $\text{R} < 263\text{ms}$, there's a false peak (FP); if $\text{R} > 1675\text{ms}$, there's a leak detection (FN). Define $\text{R}_\text{a} = \text{R}/\text{aveR}$, if $\text{R}_\text{a} > 1.66$, we consider there's a FN. When there's a FP, the peak is deleted; when there's a FN, then the threshold is reduced by half and the search back algorithm is conducted one more time, until the values of R and R_a are reasonable and R peaks will be decided.

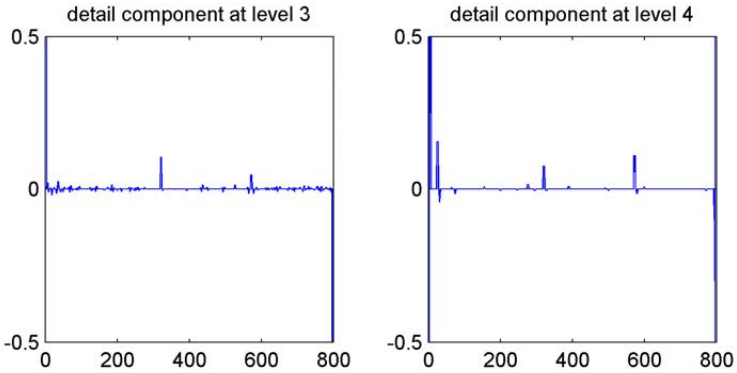

Figure 4-4 Detail components at level 3 and level 4

4.2 QRS detection based on Hilbert transform

As described in 2.3.1, the Hilbert transform of the first differential of ECG signals can be used for QRS detection. The peaks in the Hilbert transformed sequence $h(n)$ represent regions of high probability of finding a real QRS peak.

Take Sample No. 100 in MIT-BIH Arrhythmia Database for example, the QRS detection results is shown in Figure 4-5. We can see, when the interference is not severe, the detection accuracy is very high, as we choose the first 10000 samples in Sample No. 100, the R peaks can be 100% recognized. However, several detected peaks have shift from the true R wave peak position by a few milliseconds.

But for Sample No. 200 in MIT-BIH Arrhythmia Database, three peaks have been detected two times. This is because that there are jitters caused by high frequency noise or other interference. Therefore, it is very important to adopt noise suppression algorithm. Also, the R peak search back algorithm is very necessary to be added into the QRS detection method to delete the repeated peaks.

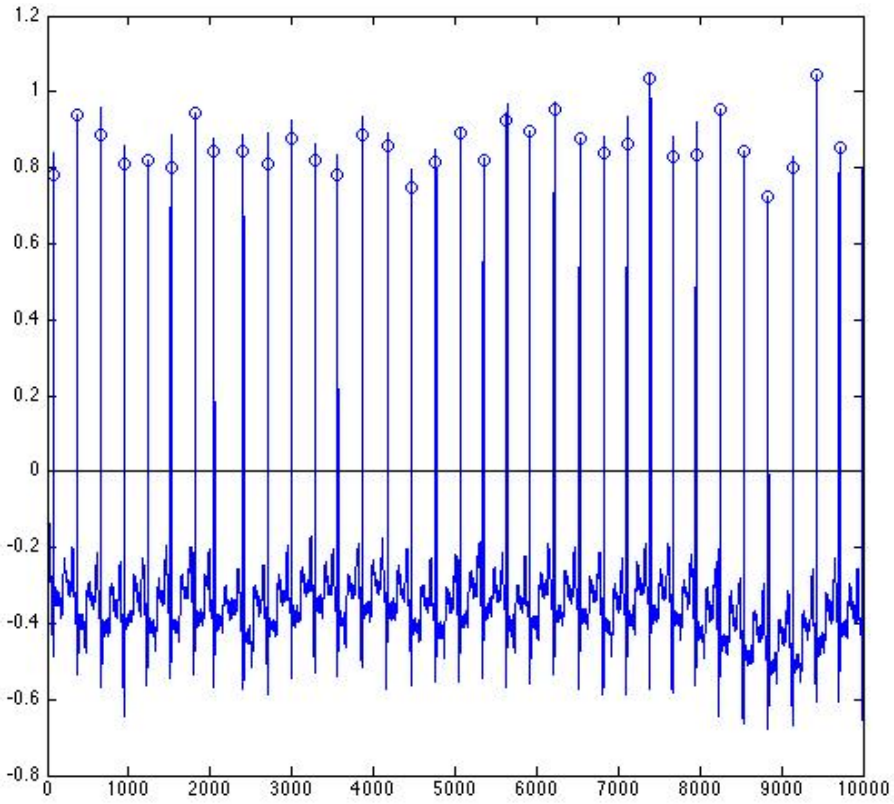

Figure 4-5 QRS detection results by using Hilbert transform of Sample No. 100 in MIT-BIH Arrhythmia Database

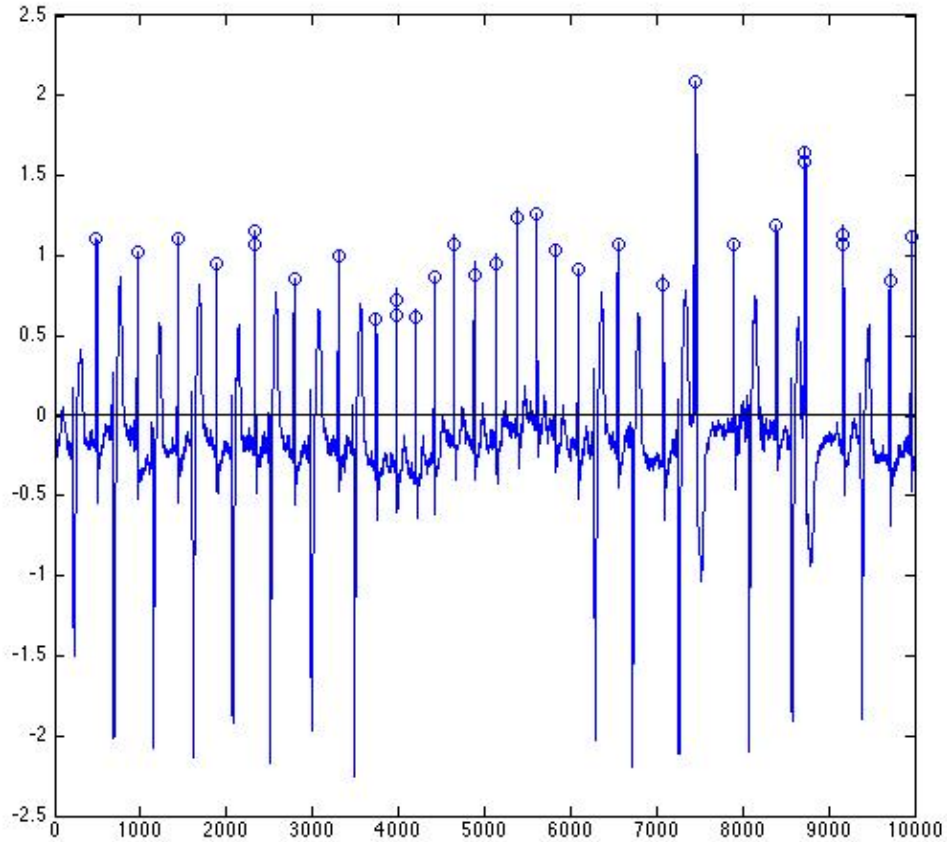

Figure 4-6 QRS detection results by using Hilbert transform of Sample No. 200 in MIT-BIH Arrhythmia Database

4.3 QRS detection method based on MMMD and Wavelet Decomposition

To improve the detection accuracy of QRS complex with gentle peaks, the proposed QRS complex detection algorithm (WMR algorithm) adopts wavelet transform and multi-resolution morphological decomposition and can be summarized by the application of the following steps, and the flow chart is illustrated in Figure 4-5:

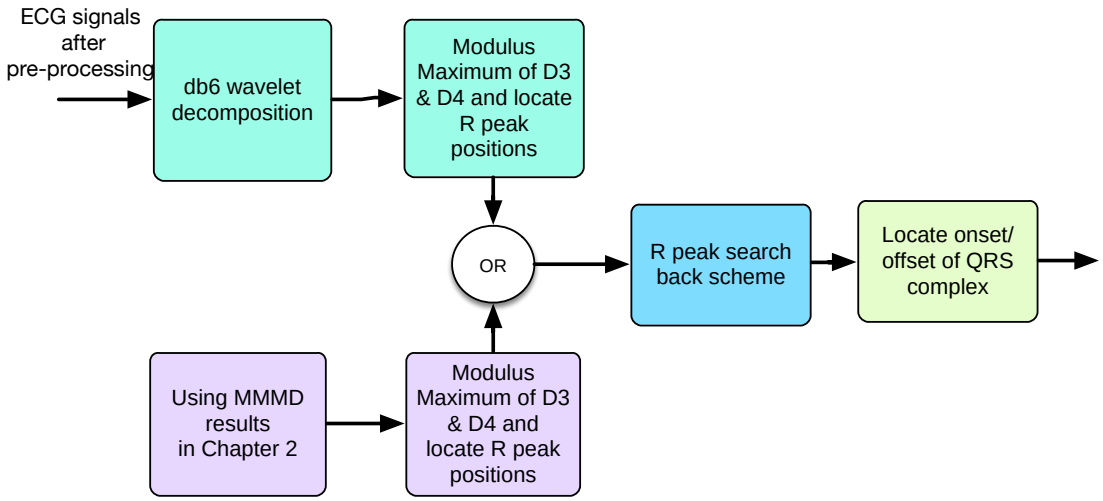

Figure 4-5 Flat chart of WMR algorithm.

(1) Correct baseline and suppress noise by LMMMD method from chapter 3, then segment ECG data every 10 seconds as a result of compromise between data size and the number of calculation;

(2) apply wavelet decomposition up to level 4 by db6 wavelet. Specific to ECG signals in MIT-BIH database with sampling rate of 360Hz, frequency component of QRS complex mainly focuses on detail signals on level 3 and 4 (D3 and D4). Therefore, we search modulus maximum of D3 and D4 and the corresponding zero crossing points, and feed back to original signals as R peaks;

(3) Using LSM results in 4.2.

(4) R peak search back scheme is the same with LMS algorithm described in 4.2.

(5) Locate onset/offset of QRS complex. According to step (2), choose extremum nearest the zero crossing points as the onset/offset of QRS complex.

(6) Update threshold. Let θ_3 be D3 threshold, define it as root of mean square (RMS) of previous 3 seconds samples including the sample; while θ_3 be D4 threshold, define it as half the RMS of previous 3 seconds samples including the sample; as are shown in (4-16) and (4-17). Where $W_3x[m]$ and $W_4x[m]$ are ECG components at D3 and D4, k is ECG sample number per second. For MIT-BIH Arrhythmia Database, $k = 360$.

$$\theta_3(n) = RMS(W_3x[m]), if\ n < 3k, 1 \le m \le n$$

$$otherwise, n-3k \le m \le n \quad (4\text{-}16)$$

$$\theta_4(n) = \frac{1}{2} RMS(W_4 x[m]), if\ n < 3k, 1 \le m \le n$$

$$otherwise, n-3k \le m \le n \quad (4\text{-}17)$$

4.4 Simulation and Discussion

The proposed QRS complex detection algorithm (WMR algorithm) is applied to 48 ECG signals in MIT-BIH Arrhythmia Database which have been preprocessed by LMW Algorithm. Three evaluation index have been chosen: FP, FN, and sensitivity that is define as follows,

$$S_+ = \left(1 - \frac{(FP+FN)}{\text{RR Numbers}}\right) \times 100\% \quad (4\text{-}18)$$

where RR Numbers denotes overall RR Numbers, i.e. heart beats in the sample. The algorithm was compared with Method 1 [56] based on wavelet decomposition, Method 2 [57] based on positive and negative slope of QRS complex, Method 3 [58] based on sparse derivatives, Method 4 [59] based on first-derivative, and Method 5 [60] based on topological mapping.

The performances of above algorithms are shown in Table 4-1. Although the overall heart beats for simulation were different, it was obvious to conclude that, compared with other algorithms; the proposed algorithm achieved better performance on FP, FN and sensitivity. Not only the improving QRS detection method, but also the good pre-processing performance contributed to this result.

Table 4-1 The performance of WMR algorithm and comparison with 5 algorithms.

QRS detection methods	***Overall beats***	***FP***	***FN***	S_+**(%)**
WMR (mixed method)	109494	103	121	99.80
Method 1 (Bahoura et al, 1997) based on wavelet decomposition	109819	135	184	99. 71
Method 2 (Adname et al, 2009) based on positive and negative slope of R peaks	109494	393	253	99.41
Method 3 (Ning and Selesnick, 2013) based on sparse derivatives	109452	127	138	99.76
Method 4 (Arzeno et al, 2008) based on first-derivative	109456	405	354	98.53
Method 5 (Lee et al 1996) based on topological mapping	109267	240	340	99.46

We also focus on Sample with abnormal waveforms and serious noise. Table II chooses Sample 104 (with PB), 108 (with abnormal P waves), 203 (with irregular RR and QRS MC) for instance to inspect the QRS detection performance.

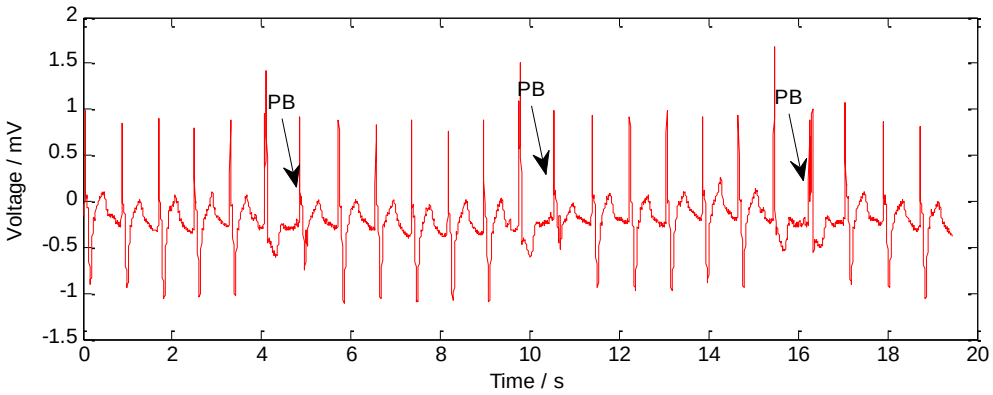

Figure 4-6(a) Sample No. 104 with PB

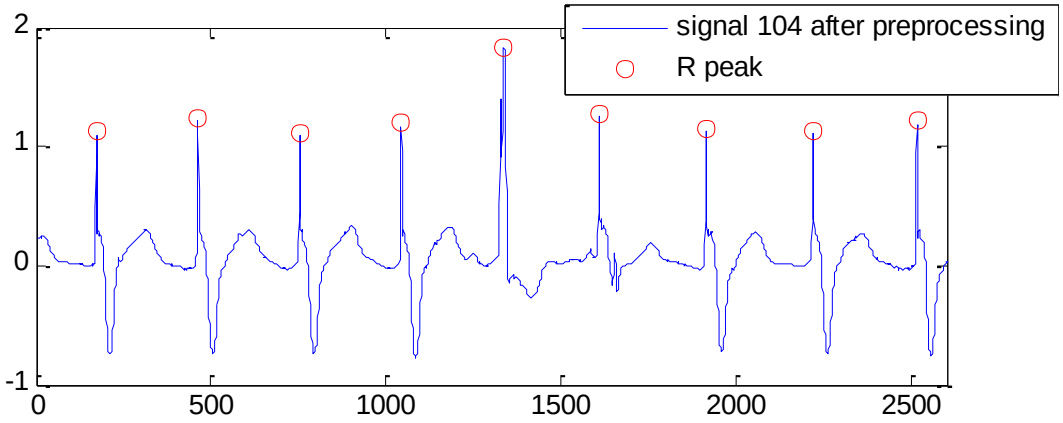

Figure 4-6(b) Segment of R peak detection in signal 104.

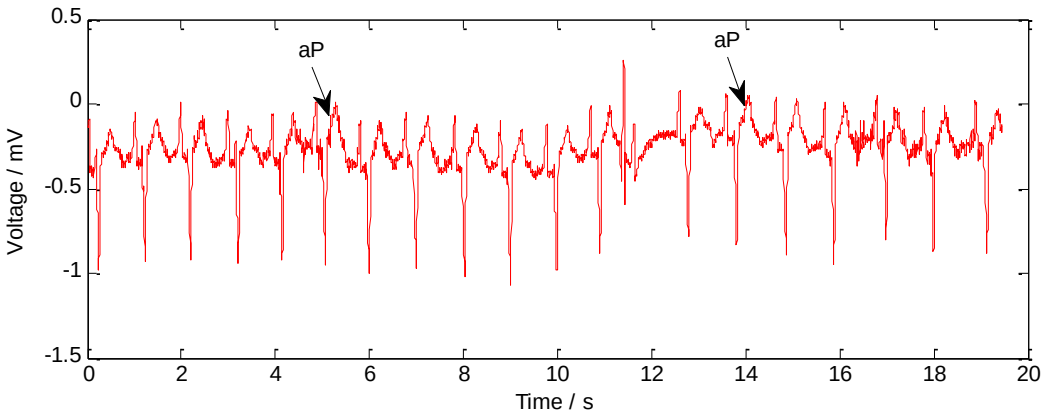

Figure 4-7(a) Sample No. 108 with abnormal P waves

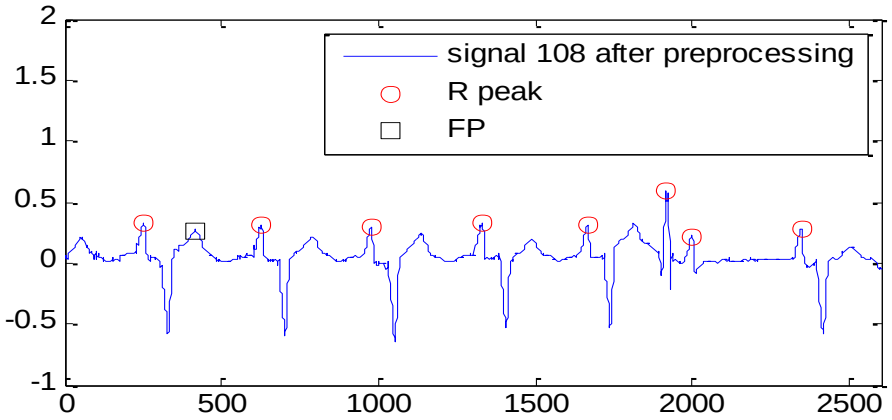

Figure 4-7(b) Segment of R peak detection in signal 108.

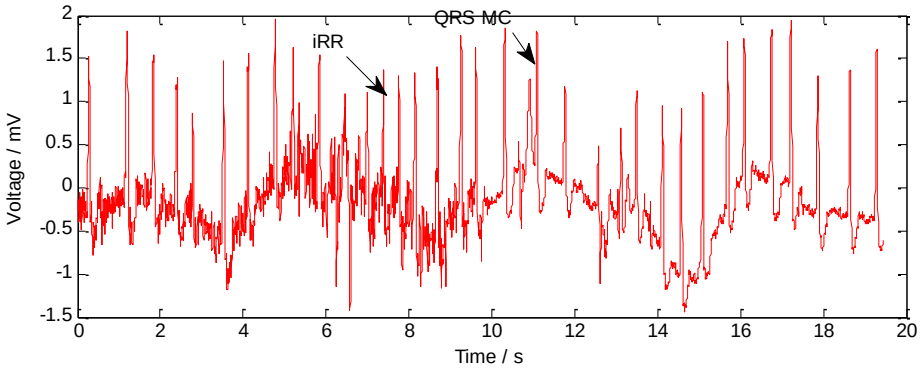

Figure4-8(a) Sample No. 203 with irregular RR intervals and QRS MC

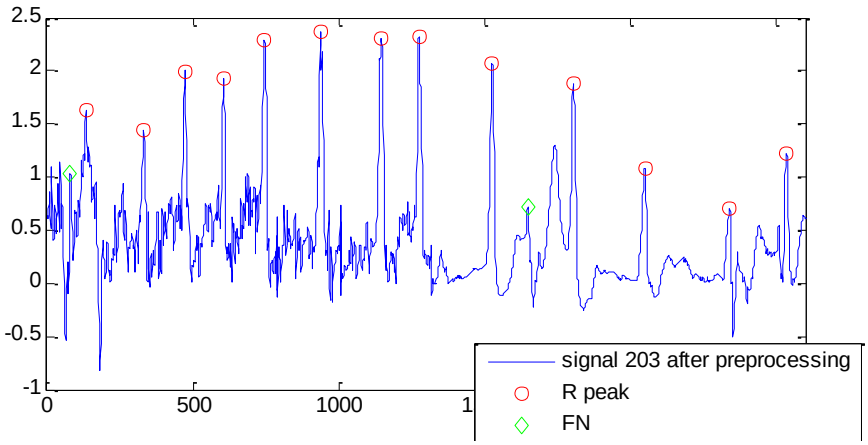

Figure 4-8(b) Segment of R peak detection in signal 203.

From Figure 4-6, we can see after pre-processing, the periodicity becomes stronger, the waveform pattern of R peaks are distinguish with other characteristic waves. Therefore, FP and FN are hard to find.

Figure 4-7 shows Sample 108 with abnormal P waves. Generally, high P waves do not cause false detection (FP); but when RR intervals become longer suddenly and high P waves exist, it is possible to cause FP, as samples between 400 and 500. On the other hand, for samples around 2000, two adjacent R peaks are very close, $RR = 230ms, R_a \approx 1.724$. Therefore, if there's no search back process, a leak detection (FN) will definitely occur.

Figure 4-8 shows Sample 203 with irregular RR intervals (iRR) and QRS multiple changes (QRS MC). Obviously, irregular RR intervals and noise interference are the reason that causes the first FN, and amplitude changes rapidly causes the second FN.

4.5 Pulse Transit Time by WMR algorithm

Continuous measurements of blood pressure (BP) have critical meaning to both clinical diagnosis and medical researches. However, traditional method is cuff-based, which cannot realize continuous measurement and is uncomfortable. Therefore, nowadays, researchers focus on invasive measurement based on sensors. The pulse transit time (PTT) [61-66] and its variability reflect the change of vascular resistance, Therefore, it can be used as the most important parameter for establishing BP estimating model.

PTT can be measured between the characteristic points of the electrocardiogram (ECG) and photoplethysmogram (PPG) at peripheral sites [66,67], as is shown in Figure 4-9.

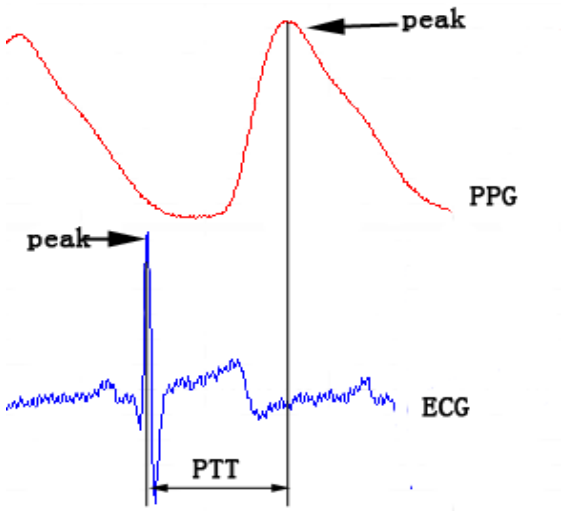

Figure 4-9 Pulse transit time is defined as the time interval between the R-peak of ECG and the peak of PPG within the same cardiac cycle

By using WMR algorithm proposed in 4.3, the R peaks can be accurately located, and PPG peaks can be located by turning point method. Take Sample 1 in our collected clinical data for example, Figure 4-10 (a) shows the ECG after locating peak detection. (b) shows the PPG after locating peak detection (c) shows the PPT calculated by ECG and PPG. In this sample, there are 191 R peaks in all, and by using the proposed algorithm, they are all detected with no FP and FN. And there are 189 PPG peaks being detected with 2 FNs. After correction, the PTT waveform is calculated by ECG and PPG. Therefore, the proposed method is effective in detecting R peaks of ECG signals both in MIT-BIH Arrhythmia Database and clinical collected data.

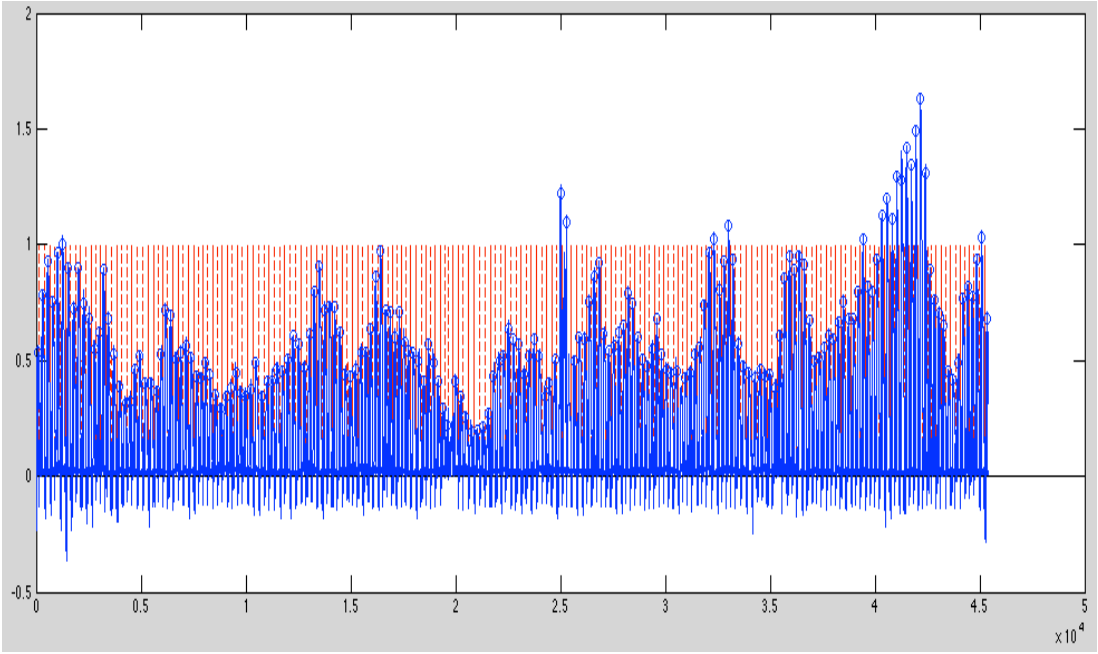

(a) R peak detection of Sample 1 ECG signal from our collected clinical data

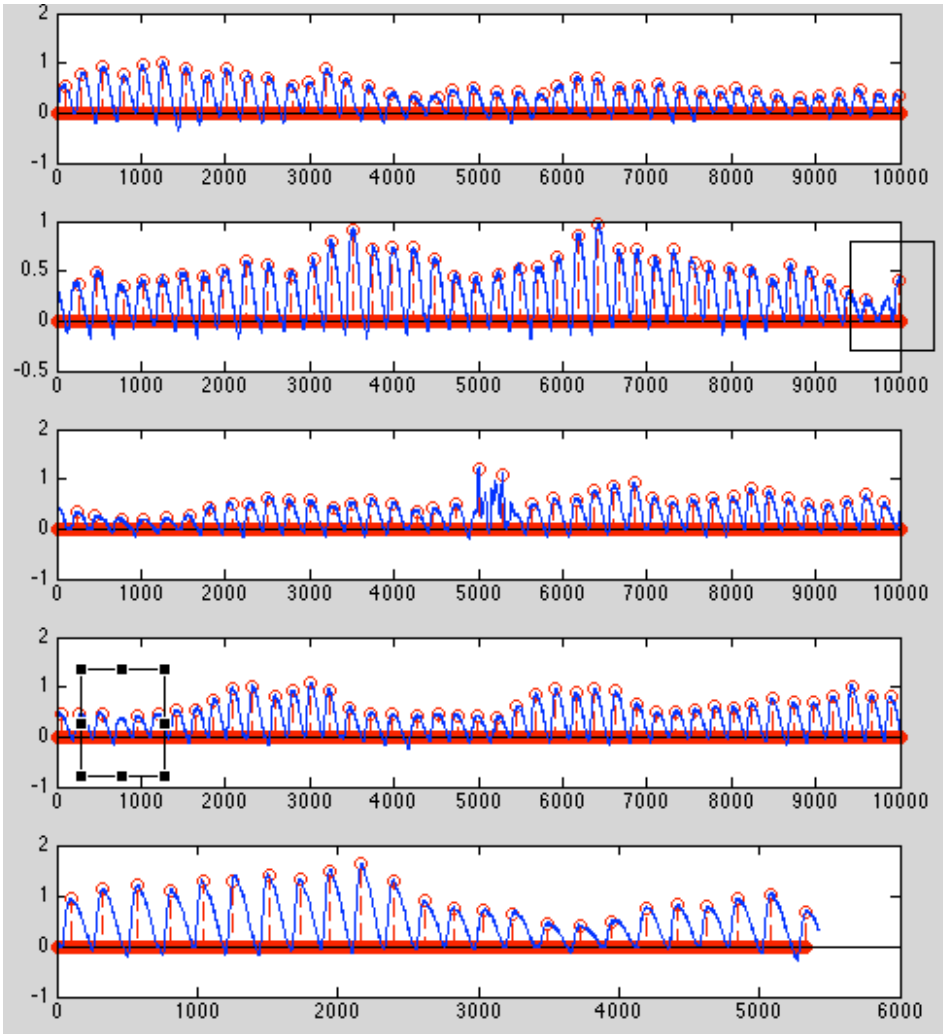

(b) PPG peak detection of Sample 1 signal from our collected clinical data

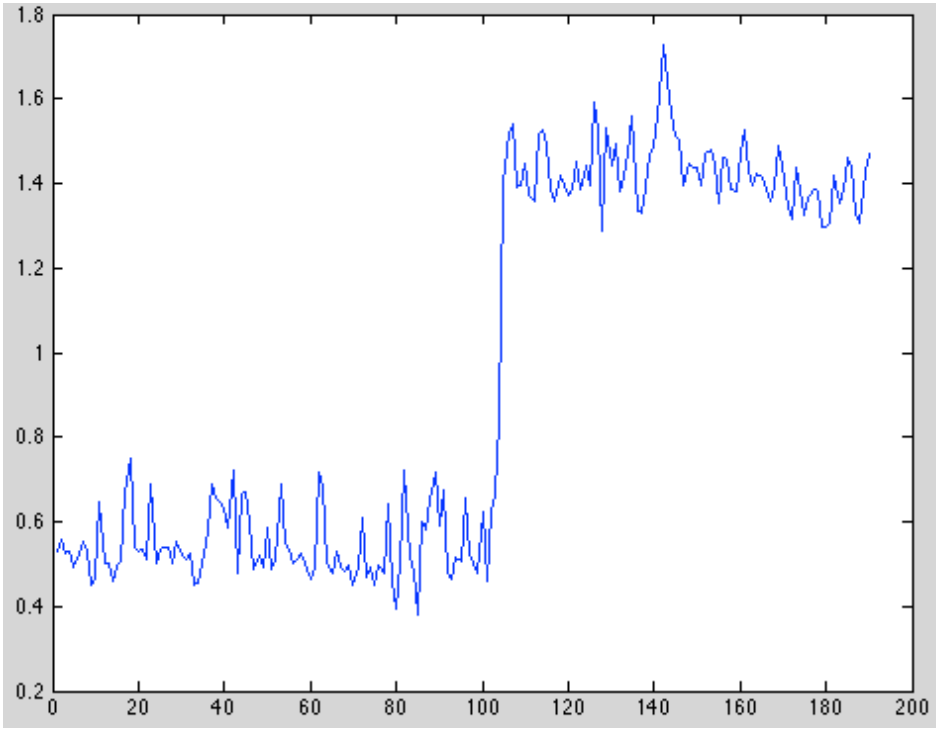

(c) PTT calculated by ECG and PPG

Figure 4-10 Peak detection of ECG and PPG signals from Sample 1 and the PTT result.

Chapter 5 ECG Signal Compression based on Compressive Sensing

ECG signals are non-invasive heart disease diagnosis tool and long-term monitoring can achieve more accurate information of physiological and pathological conditions. However, the large amount of ECG data size is heavy burden for both storage and transmission in Telemedicine and routine medical services. Therefore, it is necessary to compress the ECG signals before transmission and storage to reduce time and cost.

Traditional ECG signal compression methods are mainly divided into three types: direct method, transform method and nonlinear method. Compression methods based on wavelet transform, which can be classified as transform method, is widely adopted by researchers, because they have merits such as simple implementation, good locating performance in time and frequency domain, and so on. In this field, embedded zero tree wavelet coding (EZW) [68] and Set Partitioning in Hierarchical Trees coding (SPIHT) [69] are popular compression methods for their good compression ratio and easy implementation.

Traditional compression methods are limited by Nyquist sampling theorem. For sparse signals such as ECG signal, this kind of compression method will produce a lot of redundancy samples and consume transmission and storage cost. Therefore, researchers wish to compress the sparse signal further by using nonlinear technology, i.e., reducing the information rate by sparse characteristic of the signal. Compressive sensing (CS) realizes the aforementioned idea: it can reconstruct the original signal from samples, whose number is much lower than the limitation of the Nyquist sampling theorem. Comparing with traditional methods, it has the following super priorities [70]:

(1) The calculation is mainly done at the receiver and the algorithm adopted at the transmitter becomes simpler. For wireless medical devices in telemedicine system, it has important meanings such as minminaturization of the transmitter and extension the working hours of the system.

(2) There's no need to code the positions of the maximum coefficients in wavelet domain.

However, the difficulty in ECG signal compression method based on CS is the optimization of the reconstruction algorithms, because they often associative with large matrix and dense matrix calculation. It will cause hard realization of real-time processing of the ECG signals.

In this chapter, an ECG signal compressing algorithm based on Compressive Sensing (CS) is proposed. This method sufficiently takes advantage of pseudo-periodicity and correlation between leads. It has been tested in MIT-BIH Arrhythmia Database and can achieve balances between compression ratio (CR) and waveform distortion with acceptable computing complexity.

5.1 Compressive Sensing

Traditional signal and image sampling methods are base on Nyquist sampling theorem:

If a function $x(t)$ contains no frequencies higher than B hertz, it is completely determined by giving its ordinates at a series of points spaced $1/(2B)$ seconds apart.

This criterion almost covers all signal sampling models in voice, visual system and medical image device, wireless transmitters, and so on. However, this kind of uniform sampling has the following disadvantages:

(1) If the signal source is high frequency signal, 2 times than the highest frequency sampling rate may be impossible to implement because of the complexity of the device;

(2) For some sparse signals, it may cause a lot of redundancy in samples because of the uneven distribution of the signal information. And it will be a lot of waist in storage and transmission.

Compressive Sensing Theory (CS) was presented by Donoho, Candes, et al [71,72] in 2006. The main idea is that it can perfectly reconstruct the original signal from samples, whose number is much lower than Nyquist sampling rate. To realize this target, two principles should be established: signal is sparse and sensing model is uncorrelated. The sparsity of the signal is mainly in that the information rate of continuous signal is much lower than its bandwidth, and for discrete signal, number of the degree of freedom is much smaller than its length. CS expands the meaning of the sparsity: many signals can be simply denoted by appropriate basis Ψ, and in the transform domain, they are sparse and can be compressed. Many orthogonal basis are meeting this condition, such as Fourier basis, wavelet basis and so on. Uncorrelation extends relations between time and frequency domain, and if a signal can be sparsely presented by Ψ, it definitely can be unfolded in its original sampling domain, and the sampling/sensing waveforms of Ψ have very complicated expressions.

In this thesis, CS mechanics is based on that the signal $f(t)$ can be recorded by linear function, as is shown in 5-1:

$$y_k = \langle f, \varphi_k \rangle, \qquad k=1,\ldots,m \tag{5-1}$$

where $f \in R^n$. We are interested in the undersampling condition, i.e. $m < n$. It is very important assuming in practice. For example, the number of sensors limited, the time cost for MRI images is very long, and so on. In this thesis, we discuss the telemedicine system with limited transmission, storage and energy resources. Therefore, to realize real-time monitoring of ECG signals, we should adopt compression step to lower transmission time delay, extend working hours, and save storage space.

A typical CS procession is as illustrated in Figure 5-1. Let $x \in R^n$ be K sparse under some orthogonal basis Ψ, and x can be approximately denoted by linear combination by vectors in Ψ, as is shown in 5-2:

$$x \approx \sum_{i=1}^{K} s_i \psi_i \tag{5-2}$$

Where $K = n$. Let Φ be an $m \times n$ measurement matrix, and $m < n$. The compressed signal (measured signal) can be denoted by 5-3:

$$y = \Phi x = \Phi \Psi S \tag{5-3}$$

At the receiver, we need to reconstruct the received signal y according to 5-3 under the condition of $\min \|x\|_0$, where $\|x\|_0$ is 0-norm, represents the number of non-zero elements in x [73]. According to CS theory, when column vectors in Ψ can not represent the row vectors in Φ sparsely, and measurement m is bigger than $O(K \log(n/K))$, the signal can be reconstructed.

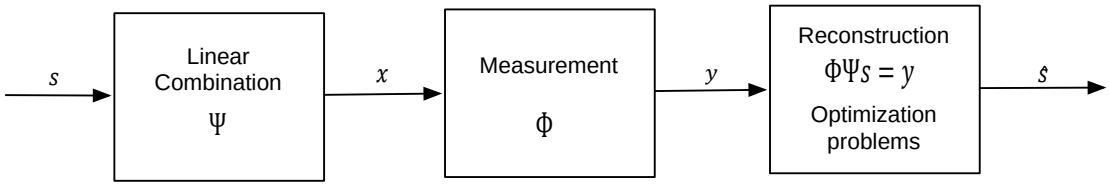

Figure 5-1 Typical Compressive sensing procession diagram.

The reconstruction process of CS can be actually considered as that when knowing the sparsity of the original signal in the sampling domain without other priori conditions, and solve optimization problems under some constraint condition. Observe 5-3 isolated, we need to solve n unknowns from m equations, which is an undetermined linear equations problem, i.e. NP-hard Problem. However, combine sparsity of the original signal, characteristic of measurement matrix and the structure of the reconstructed algorithm, we can achieve the only solution under the constraint condition, i.e. complete the signal reconstruction process.

5.1.1 Sparsity of the signal

Several natural signals can be transformed to very simple expressions by some basis. For instance, ECG signals can be transformed by orthogonal wavelet basis, and the most of wavelet coefficients achieved equals or approaches to zero while relatively rare big ones contain the vast majority information of the signal.

Assuming signal $f \in R^n$, unfold it by orthogonal basis $\Psi = [\psi_1, \psi_2, \ldots, \psi_n]$, as is shown in 5-4:

$$f(t) = \sum_{i=1}^{n} x_i \psi_i(t) \tag{5-4}$$

Where x is the coefficient sequence of f, $x_i = \langle f, \psi_i \rangle$, and 5-4 can be written as $f = \Psi x$. Then **Sparsity** is defined as: if a signal has a sparse expression, there's not much distortion felt when small coefficients are discarded. Considering that $f_S(t)$ represents the signal corresponding to only reserving the biggest S coefficients of

$\{x_i\}$, define $f_s = \Psi x_s$, where x_s is a vector related to $\{x_i\}$, except for the biggest S coefficients, the rest is zero. This vector is sparse strictly, and the vector with no more than S non-zero elements is called as S-sparse.

For orthogonal basis Ψ, we have:

$$\left\| f - f_S \right\|_{l_2} = \left\| x - x_s \right\|_{l_2} \tag{5-5}$$

If (x_i) is decreasing, i.e. x_i is lined up from big to small: $|x_1| > |x_2| > \cdots > |x_n|$, existing $C, q > 0$, make x_i satisfying 5-6:

$$\left| x_i \right| \le C i^{-q} \tag{5-6}$$

From this point of view, x is sparse or compressed, and when q is bigger, x_i decreases faster, and the signal is more compressive. Then x can be approached by x_S. Therefore, $\left\| f - f_S \right\|_{l_2}$ is very small and can be discarded without causing obvious distortion.

The aforementioned theory forms a simple compression method: calculate x according to f, then encode the positions and values of the S important coefficients. In this process, information of all n coefficients is needed to be known, because the positions of the coefficients that contain important information of the signal cannot be known in advance. More commonly, sparsity is efficient basic modeling tool, and can be adopted in basic signal processing such as accurate estimation and classification, valid data compression and so on. Meantime, sparsity has tolerance in signal sampling process and decides effectiveness of non-adaptively gotten signals.

5.1.2 Measurement matrix

Signal compressing process are also sampling process for CS method, as is shown in 5-3. Two factors should be considered for measurement matrix Φ: the correlation with orthogonal basis and the value of m.

Φ and orthogonal basis Ψ construct a pair (Φ, Ψ) on R^n. Define correlation between Φ and Ψ as 5-7:

$$\mu(\Phi, \Psi) = \sqrt{n} \cdot \max_{1 \le k, j \le n} \left| \langle \phi_k, \psi_j \rangle \right| \tag{5-7}$$

If Φ and Ψ contain correlated elements, the correlation is big. $\mu(\Phi,\Psi) \in [1, \sqrt{n}]$. The CS method wishes to use (Φ, Ψ) with small correlation. For example, unit impulse basis $\phi_k(t) = \delta(t-k)$ and Fourier basis $\psi_j(t) = \frac{1}{\sqrt{n}} e^{\frac{2\pi j t}{n}}$, will get $\mu(\Phi,\Psi) = 1$, i.e., this time-frequency pair has the smallest correlation. Besides, random matrix and arbitrary basis have weak correlation. Select arbitrary normalized orthogonal basis Φ, which can be obtained by orthogonalizing n vectors, which can

be gotten by independent and random sampling on the unit sphere. $\mu(\Phi,\Psi)$ probably equals to $\sqrt{2\log n}$. So the random waveform $\left(\phi_k\left(t\right)\right)$ with independent and normalized elements, has weak correlation with arbitrary measurement matrix Ψ.

Restricted isometry property (RIP) is the sufficient condition to construct the measurement matrix, as is shown in 5-8:

$$\left(1-\delta_S\right)\|x\|_{l_2}^2 \le \|\Phi x\|_{l_2}^2 \le \left(1+\delta_S\right)\|x\|_{l_2}^2 \tag{5-8}$$

Where x is S-sparse vector, define the isometry constant δ_S of Φ is the minimum meeting 5-8, if $\delta_S \in (0,1), \Phi$ is called meeting S-level RIP. And Φ approximately reserves the Euler length of S-sparse signal, which means S-sparse vector is not included in the zero space of Φ. Therefore, these vectors can be reconstructed.

However, in practice, it is very difficult to prove whether Φ meeting RIP. Reference [74] provides the relationship between the uncorrelation of (Φ,Ψ) and RIP characteristic: if (Φ,Ψ) has smaller correlation, the sensing matrix $\Theta=\Phi\Psi$ has a high probability of meeting RIP, i.e., reconstructing the original signal.

For $f \in R^n$, assuming that the coefficient sequence x of f under the orthogonal basis Ψ is S-sparse, m measurements in Ψ are uniform random, then m should satisfy the following:

$$m \ge C \cdot \mu^2(\Phi,\Psi) \cdot S \cdot \log n \tag{5-9}$$

The correlation of (Φ,Ψ) is weaker, the measurements needed are fewer. If $\mu(\Phi,\Psi)$ equals or approaches to 1, about $S \cdot \log n$ samples are sufficient to replace the primary n samples. In practice, for general signals or images, we usually choose $m \approx 4S$ to ensure sufficient reconstruction accuracy and acquire relatively more structure information from the signal.

5.1.3 Reconstruction algorithm

The design of reconstruction algorithm is the core of CS theory. Reconstruction accuracy, calculation complexity and measurements needed should be considered critically. Meanwhile, the convergence and stability of the algorithm should be ensured. According to context, reconstruction process can be transformed as optimization problem under specific condition, as is shown in 5-10:

$$\min\|s\|_0 \quad s.t. \quad y=\Phi\Psi s \tag{5-10}$$

However, it is proved that under the minimize 0-norm condition, the optimized solution of the equation is also a NP-hard problem. C_n^S non-zero elements lining should be exhausted to find the optimized solution, which can not realized in practice. Therefore, RIP should be further weaken or matching pursuit algorithm should be iterated to get the solution. Reconstruction algorithm can be divided into three types: l_1-norm convex optimization method, greedy algorithm and combine

method.

5.1.3.1 l_1-norm convex optimization method

In ideal condition, we hope that we can obtain all n coefficients of f, but we only observe its subset, and collect measurements by 5-11:

$$y_k = \langle f, \phi_k \rangle, k \in M \tag{5-11}$$

Where $M \subset \{1, \ldots, n\}$ is the subset of the basis $m < n$. According to this information, minimizing l_1-norm to reconstruct the signal [75,76]. Reconstruction signal is $\hat{f} = \Psi\hat{x}$, and $\hat{x}$ is the coefficient sequence meeting 5-12 and minimizing l_1-norm, i.e., the reconstruction process meeting 5-10 transforms an NP-hard problem to convex optimization process, which is easier to implement.

$$\min_{\tilde{x} \in R^n} \|\tilde{x}\|_{l_1} \qquad s.t. \qquad y_k = \langle \phi_k, \Psi\tilde{x} \rangle, \ \forall k \in M \tag{5-12}$$

Where $\|x\|_{l_1} = \sum_i |x_i|$. If f is sufficiently sparse, it can accurately reconstruct the original signal by minimizing l_1-norm method. Linear equation restriction under minimizing l_1-norm condition can be transformed to linear programming problem and by 5-9 we can have the lower limit of the measurements.

Meanwhile, if RIP is satisfied, the linear programming problem as is shown in 5-13 can be accurately reconstructed:

$$\min_{\tilde{x} \in R^n} \|\tilde{x}\|_{l_1} \qquad s.t. \qquad A\tilde{x} = y \tag{5-13}$$

Considering $\delta_{2S} < \sqrt{2}\text{-}1$, the optimized solution $\hat{x}$ meets 5-14 [77,78], for some constant C_0. And x_S is a vector, which includes the significant S elements in x, and the rest are zero.

$$\|\tilde{x} - x\|_{l_2} \le C_0 \cdot \|x - x_S\|_{l_1} / \sqrt{S}$$
$$\|\tilde{x} - x\|_{l_2} \le C_0 \cdot \|x - x_S\|_{l_1} \tag{5-14}$$

This conclusion is stronger than the limitation condition of m given by 5-9. If x is S-sparse, we have $x = x_S$, accurate reconstruction is possible. If x is not S-sparse, according to 5-14, the reconstructed signal and pre-known the positions of S significant coefficient of x, ensure that the reconstruction results are as good as direct measurement on the basis of we having a sensing matrix A meeting 5-14, and S significant elements in the sparse vector.

If we consider reconstructing the original signal from received signal with noise $y=Ax+z$, 5-13 has been transformed as reconstruction loose restriction, as is shown in 5-15:

$$\min_{\tilde{x} \in R^n} \|\tilde{x}\|_{l_1} \ \text{ s.t. } \ \|A\tilde{x} - y\|_{l_2} \le \varepsilon \tag{5-15}$$

Where ε determines the noise level. This problem is also a convex optimization problem. Considering $\delta_{2S}<\sqrt{2}$-1, and C_0, C_1 are constants, the optimized solution $\hat{x}$ meeting 5-15 are satisfying 5-16:

$$\|\hat{x}-x\|_{l_2} \leq C_0 \cdot \|x-x_S\|_{l_1}/\sqrt{S} + C_1 \cdot \varepsilon \quad (5\text{-}16)$$

The reconstruction error is determined by two terms. The first is the error without noise, and the second is proportion to noise level. The typical values of C_0 and C_1 are small. The result shows that CS is a sensing mechanic with practicality and robustness. It is not only suitable for sparse signal, but also is tolerant to noise.

Many fast and effective algorithms can be used to solve 5-15 and 5-16. Such as FPC (Fixed-Point Continuation) [79], FPC_AS (FPC Active Set) [80], FISTA (Fast Iterative Shrinkage-Thresholding Algorithm [81], Spa-RSA (Sparse Reconstruction by Separable Approximation) [82] and GPSR (Gradient Projection for Sparse Reconstruction) algorithm [83] and so on.

5.1.3.2 Greedy Algorithm

Different from convex optimization method, the greedy algorithms do not have standard reconstruction formulas. Instead, it chooses a local optimized solution at every iteration, and approaches the original signal by several iterations. Matching pursuit [84] algorithm is the earliest approximation method designed for solving minimizing l_0-norm problem. The main idea is to search for several vectors in measurement matrix Φ and these vectors have higher contribution. At every iteration, vectors that have strongest correlation with residue component of the signal, are added to the support vector, and minus the contribution of these vectors from the residue component. After limited time iterations, the optimized solution for minimizing l_0-norm problem can be obtained.

And there are other improved MP algorithms, such as Orthogonal Matching Pursuit (OMP) algorithm [85], which chooses only one column vector at every iteration; Compressive Sampling Matching Pursuit (CoSaMP) algorithm [86], which chooses 2K vectors that have the strongest correlation with the residue component; Orthogonal Least Square (OLS) algorithm [87], which chooses the column vector that can minimize the residue component at every iteration; Normalized Iteration Hard Thresholding (NIHT) algorithm [88], which chooses the column vector that can both meet minimizing residue component and maximizing the difference between current and previous iteration.

There are also combine algorithms, which can realize fast reconstruction by group testing, such as Fourier sampling, Chain Pursuit (CP) algorithm [89] and so on.

5.2 Distributed Compressive Sensing Method

Distributed Compressive Sensing (DCS) theory is based on Joint Sparse Model

(JSM), which is one kind of signal combination method. This model is built on basis of correlation in signals and between different signals: for example, for one-channel ECG signal, the pseudo periodicity shows correlation between cardiac cycles; and for multi-channel ECG signals, which measure the electrical activities of the heart from different directions, also have very strong correlation among them. These correlations can improve compressing performance further.

A typical DCS method is based on that for specific basis, measurements from different sensors are independently sparse and correlated. By projecting to another sensor, every sensor encodes independently, then transmits very few joint coefficients to the receiver, and the decoder can accurately combine reconstruct all the signals. Based on JSM of joint sparse signal, the presented algorithm can jointly reconstruct several signals from uncorrelated projections and describe the measurements of every sensor for accurate reconstruction.

According to CS theory, a group of *J* signals can be processed as follows: let $x_j(n)$ be the *n*th sample of *j*th sample, where $j \in \{1, \dots, J\}, x_j \in R^n$. Assuming that there's a known sparse basis Ψ, and x_j can be sparsely represented in R^n, Φ_j is $M_j \times N$ measurement matrix for the *j*th signal. Therefore, $y_j = \Phi_j x_j$ consists of M_j ($M_j < N$) uncorrelated measurements of x_j. Φ_j in the following denotes Gaussian matrix with random independent and identical distribution.

5.2.1 JSM-1 Model

Define additive model (JSM-1) [90] is: all the signals have the same sparse component, and include respective sparse components, as is shown in 5-17:

$$x_j = z + z_j \qquad j \in \{1, \dots, L\} \tag{5-17}$$

where $z = \Psi\theta_z, \|\theta_z\|_0 = K, z_j = \Psi\theta_j, \|\theta_j\|_0 = K_j$. Therefore, z is the common component in x_j when basis Ψ is K-sparse; z_j is the characteristic component of x_j, under the same basis is K_j-sparse. From the last section, to acquire optimized solution by minimizing l_1-norm problem, which is also called as basis pursuit (BP), the linear programming technology with complexity of $O(N)$ is adopted. In the BP algorithm, typical value of measurements is $M \geq cK$, where $c > 1$ is oversampling parameter.

Considering the simplest $J = 2$, one joint coding is needed. We can predict from CS mechanics:

(1) $(K + K_1)c$ coefficients are sufficient for reconstruction of x_1;

(2) $(K + K_2)c$ coefficients are sufficient for reconstruction of x_2;

(3) $(K + K_1 + K_2)c$ coefficients are sufficient for reconstruction of x_1 and x_2,

because there are $(K+K_1+K_2)$ non-zero elements in x_1 and x_2, which is more efficient than encoding and transmitting separately.

5.2.2 JSM-2 Model

In common support model (JSM-2) [91], all the signals are constructed by the same sparse set of the sparse basis, but with different coefficients, as is shown in 5-18:

$$x_j = \Psi\theta_j, \qquad j \in \{1, \dots, J\} \tag{5-18}$$

Where, each support of θ_j is $\Omega \subset \{1,2, \dots, N\}$ and $|\Omega| = K$. Therefore, all the signals are K-sparse and constructed by K elements in Ψ with different coefficients. This model is appropriate for ECG sign processing, because it can accurately reconstruct every signal.

For JSM-2, cK measurements are needed to reconstruct every signal by minimizing l_1-norm. The number of measurements can be further reduced through joint reconstruction algorithm, which adopts common coefficients support Ω and the correlation inner and inter signals. The reconstruction algorithms can be divided into One Step Greedy Algorithm and multi-step iterated greedy pursuit algorithm:

(1) One step greedy algorithm (OSGA)

For signals with correlation, by using a simple non-iterated greedy algorithm based on inner product, the joint reconstruction can be implemented. Let $\Psi=I_N$, the signals have the same measurements $M_j=M$, the measure matrix is $\Phi_j = [\phi_{j,1}, \phi_{j,2}, \dots, \phi_{j,N}]$, calculated the statistical value ξ_n, as is shown in 5-19:

$$\xi_n = \frac{1}{J}\sum_{j=1}^{J}\langle y_j, \phi_{j,n}\rangle^2 \qquad n = \{1,2, \dots, N\} \tag{5-19}$$

Where J is the signal number. The common coefficient support is evaluated by 5-20:

$$\widehat{\Omega} = \{n\ that\ makes\ \xi_n\ having\ the\ biggest\ K\ significant\ coefficients\} \tag{5-20}$$

Theorem 5-1:

Let Ψ is the orthogonal basis on R^n, and the measure matrix Φ_j contains independent identically distributed Gaussian elements. Assuming that the non-zero elements in θ_j are Gaussian random variables, then for each signal, by using $M \geq 1$ measurements, when $J \to \infty$, OSGA can reconstruct Ω with the probability approaching to 1.

In other words, by using JSM-2, for each sensor, it is possible to reconstruct sparse support Ω by measurements less than K. But it is obvious that this method cannot completely reconstructed K coefficients for each signal.

Theorem 5-2:

Assuming that non-zero elements in θ_j are independent identically distributed Gaussian random variables, we have the following conclusion:

a) If measure matrix Φ_j contains independent identically distributed Gaussian

elements, the oversampling constant for each matrix is c=1, i.e. M_j=K, then all of the signals can be reconstructed by OSGA with the probability approaching to 1 when $J \to \infty$.

b) If the oversampling constant for each matrix is c>1, i.e., M_j<K, then all of the signal cannot be reconstructed uniquely whatever the value of J and algorithm is.

Theorem 5-2 presents the condition and limitation of OSGA. But when J is small, the performance of OSGA is not satisfying, and is hardly possible to reconstruct all the signals. Therefore, multi-step iterated greedy pursuit algorithm is needed to improve the performance.

(2) Iterated greedy pursuit algorithm

In fact, the common sparse support of J signals makes joint reconstruction all the signals possible by fast iteration algorithm. Synchronous Orthogonal Matching Pursuit algorithm (SOMP) [92] is an improved version of Orthogonal Matching Pursuit algorithm (OMP), and determines one element of Ω at each iteration step. This algorithm has been adopted in the frame of DCS, and is called as DCS-SOMP algorithm. In the following, it is used in JSM-2.

To make DCS-SOMP be appropriate for JSM-2, first, extend different measure matrix basis Φ_j for each signal; second, at each iteration, select the sequence number $n \in \{1,2,\dots,N\}$ of the column vector, which maximizing the residue signal energy; third, orthogonalize the residue column vectors after each iteration. The algorithm is described as follows:

a) Initialization: set initial value of the iteration counter is 1. To every signal index $j \in \{1,2,\dots,J\}$, set initial value of the orthogonalized coefficient vectors $\hat{\beta}_j = 0, \hat{\beta}_j \in R^M$, and initialize the set of selected indices $\widehat{\Omega} = \emptyset$. Let $r_{j,l}$ represent the residual of the measurement y_j remaining after l iterations and set $r_{j,0} = y_j$.

b) Selection of dictionary vector: the selected one maximizes the value of the sum of the magnitudes of the projections of the residual, then update the selected index set as 5-21 and 5-22:

$$n_l = \arg\max_{n=1,2,\dots,N} \sum_{j=1}^{J} \frac{\left|\langle r_{j,l-1}, \phi_{j,n}\rangle\right|}{\left\|\phi_{j,n}\right\|_2} \tag{5-21}$$

$$\widehat{\Omega} = \left\{\widehat{\Omega}, n_l\right\} \tag{5-22}$$

c) Orthogonalization of the selected basis vector against the orthogonalized set of previously selected dictionary vectors, as shown in 5-23:

$$\eta_{j,l} = \phi_{j,n_l} - \sum_{j=1}^{l-1} \frac{\left|\langle \phi_{j,n_l}, \eta_{j,l}\rangle\right|}{\left\|\eta_{j,l}\right\|_2^2} \eta_{j,l} \tag{5-23}$$

d) Iteration: update evaluations of selected vectors and residuals as 5-24

and 5-25:

$$\hat{\beta}_j(l) = \frac{\langle r_{j,l-1}, \eta_{j,l} \rangle}{\|\eta_{j,l}\|_2^2} \tag{5-24}$$

$$r_{j,l} = r_{j,l-1} - \frac{\langle r_{j,l-1}, \eta_{j,l} \rangle}{\|\eta_{j,l}\|_2^2} \eta_{j,l} \tag{5-25}$$

e) Convergence: if $\|r_{j,l}\|_2 > \varepsilon \|y_j\|_2$ for $\forall j$, let $l = l + 1$, go back to b); otherwise, go to f). ε determines target error, and step c) limits maximum iteration M.

f) Deothogonalization: define Φ_Ω is subset of $\Phi = [\phi_1, \phi_2, \dots, \phi_N]$, indices given by $\Omega = \{n_1, n_2, \dots, n_M\}$, i.e. $\Phi = [\phi_{n_1}, \phi_{n_2}, \dots, \phi_{n_M}]$. By QR matrix decomposition, reach 5-26:

$$\Phi_{j,\hat{\Omega}} = Q_j R_j = \Gamma_j R_j \tag{5-26}$$

where $y_j = \Gamma_j \beta_j = \Phi_{j,\hat{\Omega}} x_{j,\hat{\Omega}} = \Gamma_j R_j x_{j,\hat{\Omega}}$, and $x_{j,\hat{\Omega}}$ is the corresponding coefficient vector of $\Phi_{j,\hat{\Omega}}$. Therefore, it is possible to use 5-27 and 5-28 to estimate $\{x_j\}$ and $\hat{\theta}_{j,\hat{\Omega}}$ is residual of $\hat{\theta}_{\hat{\Omega}}$.

$$\hat{\theta}_{j,\hat{\Omega}} = R_j^{-1} \hat{\beta}_j \tag{5-27}$$

$$\hat{x}_j = \Psi \hat{\theta}_j \tag{5-28}$$

In practice, in each sensor, $\Phi_j x_j$ is used to project the signal x_j, and $\hat{c}K$ measurements are generated, where $\hat{c}$ is the oversampling coefficient, and usually set to $(K+1)/K$. Then the decoder joint reconstructs J signals by DCS-SOMP. Besides, Regularized Orthogonal matching pursuit (ROSP) [93] and Sparse Adaptive Matching Pursuit (SAMP) [94] algorithms can also be used in DCS systems.

For multi-channel ECG signals, because they are from different directions and one heart, JSM-2 is more appropriate for ECG signal compression.

5.3 DCS-SOMP multi-lead ECG signals compressing method (multi-lead DCS-SOMP)

The correlation of ECG signals is mainly manifested inner, inter RR intervals and inter different channels. And these are the basis for designing compressing method based on DCS. In this thesis, a multi-lead ECG signals compressing method is presented, first, the ECG signals are segmented; second, JSM-2 is adopted to establish joint model for DCS; third, at the decoder, SOMP algorithm is used for search one element in reconstruction support at each iteration; finally, the signals are joint reconstructed.

The work flow of the proposed algorithm is illustrated in Figure 5-2. First, the data are divided by RR intervals and sliding windows; second, the JSM-2 Model in Distributed compressive sensing theory (DCS) is adopted to construct joint sparse signals of multi-lead ECG signals; Third, Simultaneous Orthogonal Matching Pursuit algorithm is used to reconstruct the ECG signals. The specific descriptions are as follows:

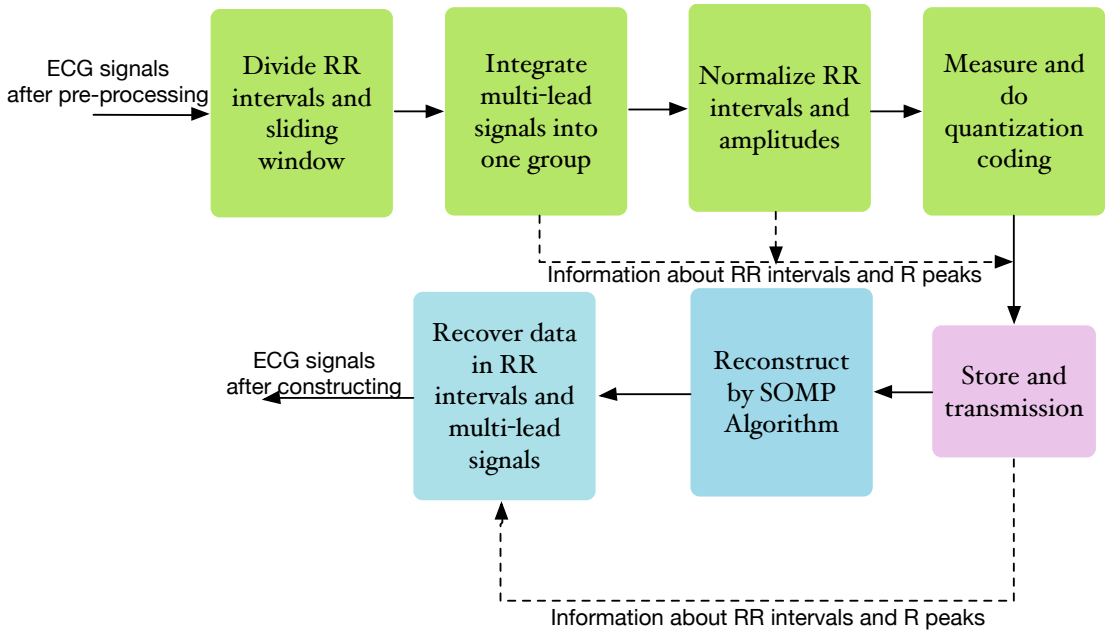

Figure 5-2 Multi-lead ECG signal compression algorithom based on DCS-SOMP.

(2) Define the length of sliding windows: according to results in chapter 3, RR intervals are divided and as references when sliding windows are determined. A balance between real-time conducting and CR should be considered. Take MIT-BIH Sample No.100 for example, the relationship between RR intervals and common support ratio (CSR) of MLII lead is shown in Figure 5-3(a) while the relationship between RR intervals and common support ratio of MLII and V5 leads is shown in Figure 5-3(b). The db6 wavelet is adopted to construct sparse signal representation. From Figure 5-3(a), when the number of RR intervals (No. RR) is smaller than 5, the declining of CSR is fast, otherwise that is slow. In Figure 5-3(b), increasing No. RR will not bring much decreasing in CSR. Therefore, I choose the length of sliding windows equals to 5 RR intervals to achieve balance between real-time conduction and CR.

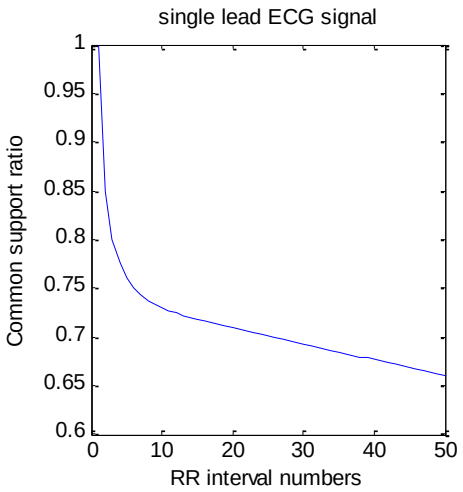

Figure 5-3(a) Common support ratio of MLII-lead in No. 100 ECG signal.

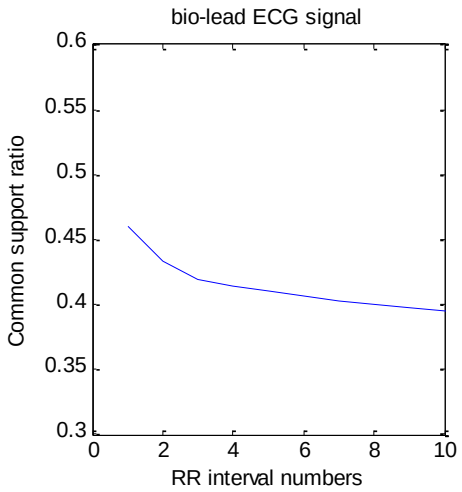

Figure 5-3(b) Common support ratio of MLII-lead and V5-lead in No. 100 ECG signal.

(3) Integrate multi-lead ECG signals into groups: if transmission data is 12-lead clinical ECG signals, the segments from each leads can be treated as one measuring sample for Compressive Sensing. However, ECG signals in Telemedicine systems are usually not more than 3 leads, while ECG signals in MIT-BIH Arrhythmia Database are bio-lead. To ensure real-time conducting, it is necessary to synchronize the multi-lead signals. In this thesis, the multi-lead signals in the same sliding window are integrated. Take bio-lead ECG signals for example, data in some sliding window are denoted as $x_i(n), n = 1,2,\dots,N_i$, and $y_i(n), = 1,2,\dots,N_i$, and the integrated signal becomes $z_i(k) = [x_i(n),\ y_i(n)],\ k = 1,2,\dots,2N_i$.

(4) Normalize RR intervals and amplitudes: define normalized RR interval N_a as average value of RR intervals in the first sliding window. Therefore, the normalized values in the RR intervals can be denoted by:

$$x_{ia}(m) = \hat{x}_i(m \cdot N_i/N_a),\ y_{ia}(m) = \hat{y}_i(m \cdot N_i/N_a) \qquad (5\text{-}29)$$

where $\hat{x}_i$ and $\hat{y}_i$ are cubic spline interpolation of x_i and y_i to decrease distortion. Data in every RR interval are transformed as an N_a vector, and data in one sliding window for bio-lead ECG signals can be transformed as an $N_a \times 10$ matrix X. Meanwhile, N_i will be sent to the receiver too. Besides, to normalize amplitudes, let maximum in one RR interval equals to $a \times 2^L$, where L is wavelet decomposition levels, a is the integer nearest the average value of maximum in RR intervals in the first sliding window.

(5) Measure and quantization encode: according to CS theory, matrix Φ meeting Restricted Isometry Property (RIP) requirement is chosen to make $Y = \Phi X$. And given that random matrix are probably meeting the above condition. Therefore, choose elements of matrix Φ following independent sampling of normal distribution with mean value 0 and variance $1/m$. Then Y is easily quantization encoded and transmitted together with information about RR intervals and R peaks from step (3).

(6) Reconstruct ECG signals by DCS-SOMP algorithm: is described as follows.

a) Initialization: set initial value of the iteration counter is 1. To every signal

index $j \in \{1,2,\dots,J\}$, set initial value of the orthogonalized coefficient vectors $\hat{\beta}_j = 0, \hat{\beta}_j \in \mathbb{R}^M$, and initialize the set of selected indices $\widehat{\Omega} = \emptyset$. Let $r_{j,l}$ represent the residual of the measurement y_j remaining after l iterations and set $r_{j,0} = y_j - \Phi_{j,\Omega_0}\left(\Phi_{j,\Omega_0}^{+} y_j\right)$. This is based on PKS theory, i.e. according to known condition that positions of important wavelet coefficients are fixed, define known support Ω_0 and $\Omega = \Omega_0 \cup \Delta \backslash \Delta_e$, where $\Delta_e \subset \{1,2,\dots,n\}$ is error between known support and real support, $\Delta \subset \{1,2,\dots,n\}$ is unknown support. Φ_{j,Ω_0} is subset of Φ_j with support of Ω_0 and Φ_{j,Ω_0}^{+} is the pseudo-inverse matrix of Φ_{j,Ω_0}.

b) Selection of dictionary vector: the selected one maximizes the value of the sum of the magnitudes of the projections of the residual, then update the selected index set as:

$$n_l = \underset{n=1,2,\dots,N}{\arg\max} \sum_{j=1}^{J} \frac{\left|\langle r_{j,l-1}, \phi_{j,n} \rangle\right|}{\left\|\phi_{j,n}\right\|_2} \tag{5-30}$$

$$\widehat{\Omega} = \left\{\widehat{\Omega}, n_l\right\} \tag{5-31}$$

c) Orthogonalization of the selected basis vector against the orthogonalized set of previously selected dictionary vectors, as shown in:

$$\eta_{j,l} = \phi_{j,n_l} - \sum_{j=1}^{l-1} \frac{\left|\langle \phi_{j,n_l}, \eta_{j,l} \rangle\right|}{\left\|\eta_{j,l}\right\|_2^2} \eta_{j,l} \tag{5-32}$$

d) Iteration: update evaluations of selected vectors and residuals as:

$$\hat{\beta}_j(l) = \frac{\langle r_{j,l-1}, \eta_{j,l} \rangle}{\left\|\eta_{j,l}\right\|_2^2} \tag{5-33}$$

$$r_{j,l} = r_{j,l-1} - \frac{\langle r_{j,l-1}, \eta_{j,l} \rangle}{\left\|\eta_{j,l}\right\|_2^2} \eta_{j,l} \tag{5-34}$$

e) Convergence: if $\left\|r_{j,l}\right\|_2 > \varepsilon \left\|y_j\right\|_2$ for $\forall j$, let $l = l + 1$, go back to b); otherwise, go to f). ε determines target error, and step c) limits maximum iteration M.

f) Deothogonalization: define Φ_Ω is subset of $\Phi = [\phi_1, \phi_2, \dots, \phi_N]$, indices given by $\Omega = \{n_1, n_2, \dots, n_M\}$, i.e. $\Phi = \left[\phi_{n_1}, \phi_{n_2}, \dots, \phi_{n_M}\right]$. By QR matrix decomposition, reach:

$$\Phi_{j,\widehat{\Omega}} = Q_j R_j = \Gamma_j R_j \tag{5-35}$$

where $y_j = \Gamma_j \beta_j = \Phi_{j,\widehat{\Omega}} x_{j,\widehat{\Omega}} = \Gamma_j R_j x_{j,\widehat{\Omega}}$, and $x_{j,\widehat{\Omega}}$ is the corresponding coefficient vector of $\Phi_{j,\widehat{\Omega}}$. Therefore, it is possible to use 5-36 and 5-37

to estimate $\{x_j\}$ and $\hat{\theta}_{j,\hat{\Omega}}$ is residual of $\hat{\theta}_{\hat{\Omega}}$.

$$\hat{\theta}_{j,\hat{\Omega}} = R_j^{-1}\hat{\beta}_j \tag{5-36}$$

$$\hat{x}_j = \Psi\hat{\theta}_j \tag{5-37}$$

(7) Finally, recovery data in RR intervals and reconstruct multi-lead ECG signals.

5.4 Simulation and Discussion

Multi-lead DCS-SOMP method is applied to MIT-BIH Arrhythmia Database and compared to embedded algorithms such as EZW, SPIHT; and distributed compressive sensing methods, such as DCS-CoSaMP, DCS-NIHT and DCS-ROLS. Three estimation indices are introduced:

(1) Compressing ratio (CR):

$$CR = \frac{R_{org}}{R_{rec}} \tag{5-38}$$

where R_{org} and R_{rec} denote original and reconstruction sample numbers.

(2) Percentage of root mean square difference (PRD):

$$PRD = \left\{\frac{\sum_{i=1}^{n}[x_{org}(i)-x_{rec}(i)]^2}{\sum_{i=1}^{n}[x_{org}(i)]^2}\right\}^{\frac{1}{2}} \times 100\% \tag{5-39}$$

where $x_{org}(i)$ and $x_{rec}(i)$ denote the original and reconstructed signals respectively.

(3) Peak signal to noise ratio (PSNR):

$$PSNR = 10log_{10}\left[\frac{(2^n-1)^2}{e_{rms}^2}\right] \tag{5-40}$$

where e_{rms} is mean square error, and n is gray level of pixels.

After using results from chapter 2 and chapter 3, 48 samples in the database are simulated. Choose No. 100, 108, 117, 203 samples for illustration. Figure 5-3(a) shows MLII lead signal of No. 100 after pre-processing; Figure 5-3(b) shows CR as a function of the PRD for 5 algorithms; and Figure 5-3(c) shows CR as a function of the PRD for 3 algorithms, where DCS-SOMP1 denotes applying DCS-SOMP on separate lead while DCS-SOMP2 denotes applying proposed multi-lead DCS-SOMP on bio-lead together. No. 100 is normal ECG signal with average RR intervals and clear characteristic waveforms.

For bio-lead ECG signals, DCS methods achieve better performance than embedded algorithms. This is because DCS methods concentrate on not only correlation inner leads, but also inter leads. When requiring high reconstruction performance, i.e. PRD value is small, DCS methods can achieve relatively better CR than embedded algorithms, which cannot ensure availability as PRD is lower than 2%. Among DCS methods, when PRD is small, DCS-ROLS has lower CR with worse robustness, this is because the algorithm searches vectors that minimized residual error after orthogonalization. Without regard to computing complexity, DCS-CoSaMP

usually can achieve better performance, especially when requiring high CR.

From Figure 5-4(c), multi-lead DCS-SOMP has advantage of dealing with bio-lead ECG signals for its utilization of correlations inner and inter RR intervals as well as between different leads. This priority also can be testified by other samples in the database.

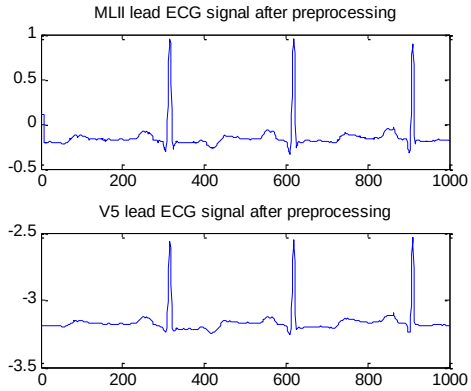

Figure 5-4(a) Sample No. 100 2-lead ECG signals after preprocessing.

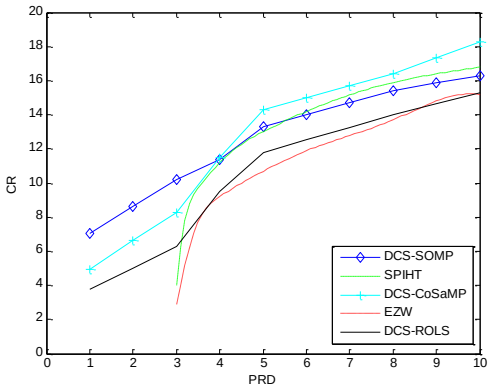

Figure 5-4(b) CR as a function of the PRD for 5 algorithms.

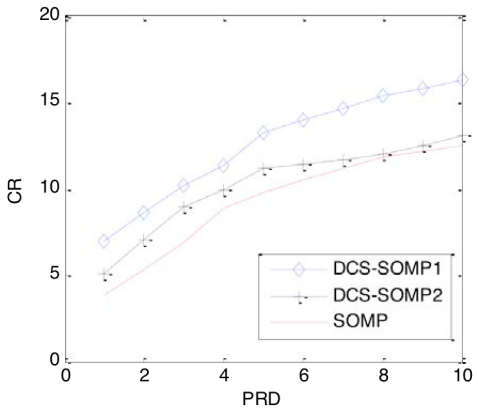

Figure 5-4(c) CR as a function of the PRD for 3 algorithms

Figure 5-5, 5-6, 5-7 choose another 3 samples in database and compare CR as a function of PRD for the 5 algorithms. Figure 5-5 selects Sample No. 108 with abnormal high P wave, long RR intervals and deep noise interference; Figure 5-6 shows Sample No. 117 with typical PVC and large amplitudes; and Figure 5-7 illustrates Sample No. 203 with multiple PVC patterns, changing QRS waveforms and severe interference of EMG and baseline wandering.

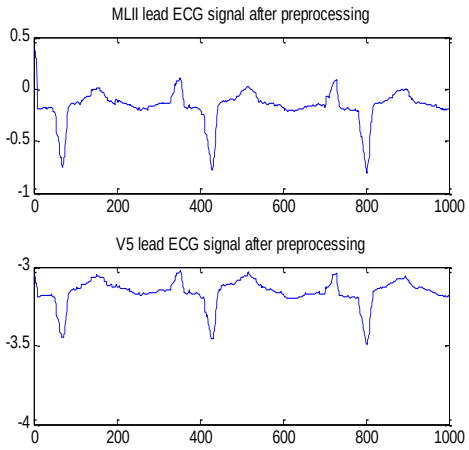

Figure 5-5(a) Sample No. 108 2-lead ECG signals after preprocessing.

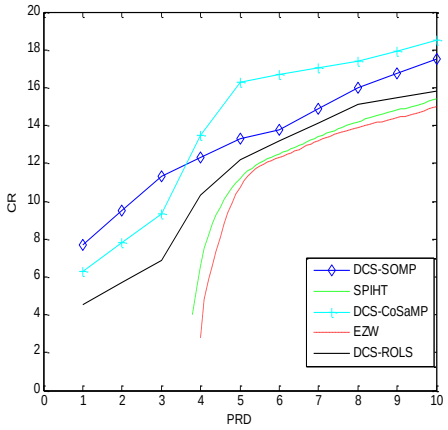

Figure 5-5(b) CR as a function of the PRD for 5 algorithms.

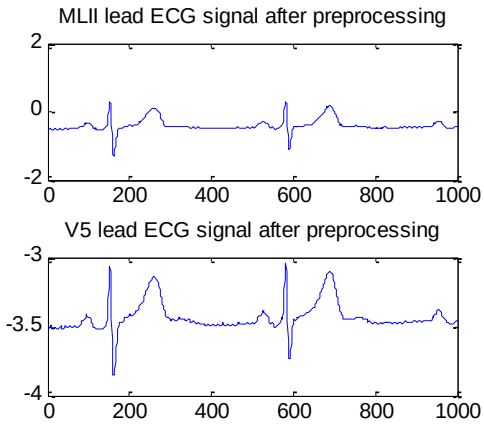

Figure 5-6(a) Sample No. 117 2-lead ECG signals after preprocessing.

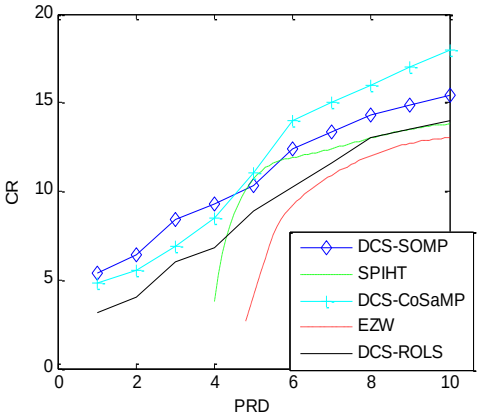

Figure 5-6 (b) CR as a function of the PRD for 5 algorithms.

From Figure 5-5, it is obvious that performance is better than that of No. 100 by using multi-lead DCS-SOMP. It is because that the RR intervals are longer and waveform pseudo-periodicity is stronger. When PRD is small, the proposed method can achieve best performance. However, the abnormal high P waves cause non-zero coefficients increasing, embedded algorithms cannot reach better PRD.

As is shown in Figure 5-6, the waveform patterns in Sample No. 117 are not stable, and amplitudes are large. There are reasons that the number of non-zero coefficients increase heavily and performance of all algorithms decline, especially the embedded algorithms. The DCS-CoSaMP algorithm works stable in this condition.

From Figure 5-7, Although ECG signals in Sample No. 203 have been pre-processed, because of severe baseline wandering and high frequency noise, characteristic waveforms are missing or difficult to distinguish. Meanwhile, RR intervals change significantly. Therefore, the performance of all algorithms declines a lot. Only DCS-CoSaMP algorithm is robust. But when PRD is small, multi-lead DCS-SOMP can achieve good performance too.

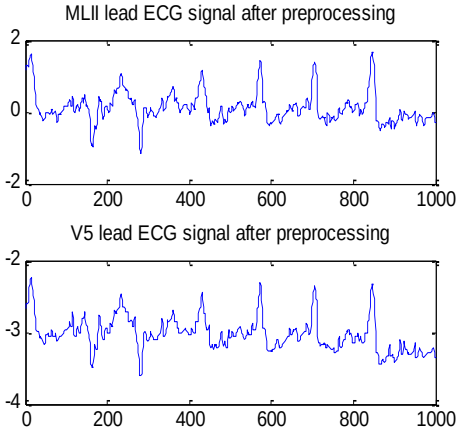

Figure 5-7(a) Sample No. 203 2-lead ECG signals after preprocessing.

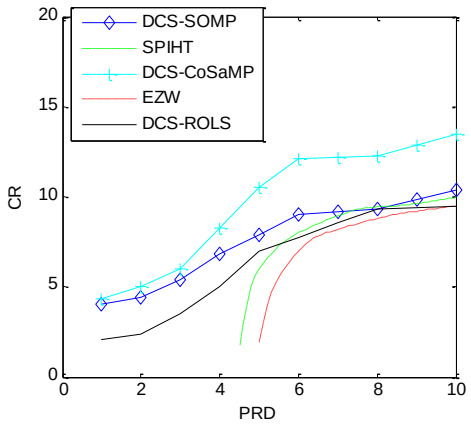

Figure 5-7(b) CR as a function of the PRD for 5 algorithms.

Table 5-1 CS and PSNR value of 48 ECG signals in MIT_BIH using multi-lead DCS-SOMP algorithm with PRD=2%

Sample No.	CS	Sample No.	CS	Sample No.	CS	Sample No.	CS
100	8.25	113	5.33	201	5.35	217	6.73
101	8.05	114	7.44	202	7.56	219	7.25
102	7.34	115	8.10	203	4.34	220	7.71
103	8.34	116	7.12	205	5.23	221	6.14
104	6.74	117	5.90	207	5.21	222	6.39
105	7.35	118	6.11	208	4.23	223	5.12
106	7.48	119	6.86	209	7.34	228	4.96
107	5.54	121	7.23	210	7.88	230	7.38
108	7.63	122	5.67	212	8.00	231	8.22
109	8.01	123	7.56	213	7.45	232	6.20
111	7.34	124	7.23	214	7.32	233	5.18
112	6.45	200	8.34	215	6.26	234	7.35

In conclusion, when $PRD < 5\%$, DCS-CoSaMP and Multi-lead DCS-SOMP algorithms are good options for multi-lead ECG signals compression.

In the following, CS and PSNR of 48 samples in the database are considered when $PRD = 2\%$, as is shown in Table 5-1. Exception of Sample No. 203 and 208, applying Multi-lead DCS-SOMP to bio-lead ECG signals can reach $CR > 5$, and $PSNR >$

$30dB$ according to calculation results, which ensures desirable CR and PSNR with sufficient reconstruction accuracy.

Besides, in Telemedicine system, computing complexity should be considered, theoretical computing time of several DCS algorithms are listed in Table 5-2.

Table 5-2 Theoretical Computing time of several DCS compressive sensing algorithm

DCS alogorithms	Theoretical computing time
Multi-lead DCS-SOMP	$O(k_1 mn)$
DCS-CoSaMP	$O(\log(k)mn)$
DCS-ROLS	$O(kmn)$

where k is sparse coefficients, m and n are row and column numbers respectively, k_1 is the number of partial known support and $k_1 < k$. From Table 5-2, Multi-lead DCS-SOMP and DCS-ROLS are appropriate for Telemedicine systems with limited resources. According to above simulation, Multi-lead DCS-SOMP achieves better performance and robustness than DCS-ROLS.

In conclusion, Multi-lead DCS-SOMP is suitable for Telemedicine systems and can reach balance between compression performance, waveform distortion and computing complexity.

Conclusion

The thesis focused on ECG processing methods in Telemedicine systems, including pre-processing, QRS complex detection, compression and reconstruction. Besides containing clinical information of reconstructed signal, computing complexity should also be taken into consideration. This thesis mainly adopted Wavelet transform, Hilbert transform, Mathematical Morphology, multi-resolution decomposition and compressive sensing, researched on wavelet transform based ECG processing methods, Hilbert transform based ECG characteristics extraction, ECG signal pre-processing method based on lifting scheme constructing multi-resolution mathematical morphological decomposition (LMMD); proposed QRS complex detection based on LMMD, Hilbert transform and combination of LMMD and wavelet transform (WMR algorithm), with an efficient R peak search back scheme; and presented a multi-lead DCS-SOMP compressing and reconstructing method for ECG signals. According to theoretical analysis, simulation and comparison results, these methods are not only achieve good performance on baseline correction, noise suppression, QRS detection accuracy and compression ratio, they also have priorities in reserving clinical information and reducing computing complexity. Therefore, these methods are appropriate to implement in Telemedicine system.

References

[1] World Health Organization, “Cardiovascular diseases (CVDs),” http://www.who.int/mediacentre/factsheets/fs317/en/，2013.

[2] Wikipedia, “Telemedicine,” http://en.wikipedia.org/wiki/Telemedicine, 2014.

[3] A. W. Martinez, Phillips S T, Carrilho E, et al. Simple Telemedicine for Developing Regions: Camera Phones and Paper Based Microfluidic Devices for Real-Time, Off-Site Diagnosis. Analytical Chemistry, 2008, 80(10): 3699-3707.

[4] Ekeland A G, Bowes A, and Flottorp S. Effectiveness of Telemedicine: A Systematic review of reviews[J]. International Journal of Medical Informatics, 2010, 79(11): 736-771.

[5] Anker S D, Koehler F, Abraham W T. Telemedicine and Remote Management of Patients with Heart Failure. The Lancet, 2011, 378(9792):731-739.

[6] Nicolini D. Medical Innovation as a Process of Translation: a Case from the Field of Telemedicine[J]. British Journal of Management, 2010, 21(4): 1011-1026.

[7] Gherardi S. Telemedicine: A Practice-based Approach to Technology. Human Relations, 2010, 63(4): 501-524.

[8] Shan F. Providing Telemedicine Services in an Infrastructure-based Cognitive Radio Network. IEEE Wireless Communications, 2010, 17(1): 96-103.

[9] Tyrer H W. Satellite Wide-area-network for Telemedicine]. IEEE Aerospace and Electronic Systems Magazine, 2009, 24(2): 20-26.

[10] Chen W, Yeh M F, Chang K C, et al. Real-time Telemonitoring System Design with Mobile Phone Platform. Measurement, 2008: 463-470

[11] De Capua C, Meduri A, Morello R. A Smart ECG Measurement System Based on Web-Service-Oriented Architecture for Telemedicine Applications. IEEE Transactions on Instrumentation and Measurement, 2010, 59(10): 2530-2538.

[12] Setyono A, Alam M L, Eswaran C. Development of Streaming Application for Mobile Telemedicine System Using Multimedia Messaging Service Technology. In Proceedings of 2011 IEEE Communication Software and Networks, 2011: 574-578.

[13] Wikipeadia, “Eletrocardiography,” http://en.wikipedia.org/wiki/Electrocardiography, 2014

[14] Hargittai S. Efficient and Fast ECG Baseline Wander Reduction without Distortion of Important Clinical Information. Computers in Cardiology, 2008: 841-844.

[15] Christov-Dotsinky I I, Dotsinsky I A, Daskalov I K. High Pass Filtering of ECG Signals Using QRS Elimination. Medical and Biological Engineering and Computing, 1992, 30(2): 253-256.

[16] Ferrara E, Widrow B. The Time-sequenced Adaptive Filter. IEEE Transaction on Circuits and Systems, 1981, 28(6): 519-523.

[17] Thakor N V, Zhu Y S. Applications of Cardiac Filtering to ECG Analysis: Noise Cancellation and Arrhythmia Detection. IEEE Transaction on Biomedicine Engineering, 1991, 39(8): 785-794.

[18] Strobach P, Fuchs K A, Harer W. Event-synchronous Cancellation of the Heart Interference in Biomedical Signals. IEEE Transaction on Biomedicine Engineering, 1994, 41(4): 343-350.

[19] Smital L, Vitek M, Kozumplik J, et al. Adaptive Wavelet Wiener Filtering of ECG Signals. IEEE Transactions on Biomedical Engineering. 2013, 60(2): 437-445.

[20] Khan M, Aslam F, Zaidi T, et al. Wavelet Based ECG Denoising Using Signal-Noise Residue Method. In Proceedings of 5th International Conference on Bioinformatics and Biomedical Engineering, 2011: 1-4.

[21] Raj V N P, Venkateswarlu T. ECG Signal Denoising Using Undecimated Wavelet Transform. In Proceedings of 3rd International Conference on Electronics Computer Technology, 2011, 3: 94-98.

[22] Sun P, Wu Q H, Weindling A M, et al. An Improved Morphological Approach to Background Normalization of ECG Signals. IEEE Transaction on Biomedical Engineering, 2003, 50(1): 117-121.

[23] Zhang Q, Zhao C H. A Morphological Filtering Approach to Removing Noise in ECG Signal. Applied Science and Technology, 2002, 29 (9): 9-11.

[24] J. Pan, and W. J. Tompkins, "A Real-time QRS Detection Algorithm," IEEE Trans. Biomed. Eng., vol. 32, pp: 230-236, 1985.

[25] F. Bereksi Reguig, and Z. E. Hadj Slimane, "A powerful algorithm to aid cardiac arrhythmia diagnosis," Comput. Methods. Biomec., vol. 3, pp: 119-127, 2000.

[26] R. Cautam, and A. K. Sharma, "Detection of QRS complexes of ECG recording based on wavelet transform using Matlab," Int. J. Eng. Sci., vol. 2, pp: 3038-3044, 2010.

[27] S. A. Chouakri, F. Bereksi-Reguig, and A. Taleb-Ahmed, "QRS complex detection based on multi wavelet packet decomposition". Appl. Math. Comput., vol. 217, pp: 9508-9525. 2011.

[28] A. Zidelmal, A. Amirou, M. Adnane, and A. Belouchrani, "QRS detection based on wavelet coefficients," Comput. Meth. Prog. Bio., vol. 107, pp: 490-496, 2012..

[29] C.H.H. Chu, and E.J. Delp, "Impulsive noise suppression and background normalization of Electrocardiogram signals using morphological operators," IEEE Trans. Biomed. Eng., vol. 36: pp: 262-273, 1989.

[30] Y. Sun, K.L. Chan, and S.M. Krishnan, "ECG signal conditioning by morphological filtering," Comput. Biol Med., vol. 32, pp: 465-479, 2002.

[31] P.E. Trahanias, "An approach to QRS complex detection algorithm using mathematical morphology," IEEE Trans. Biomed. Eng., vol. 40, pp: 201-205, 1993.

[32] P. Zhang, Q.Y.Zhang, M. Akutagawa, Y. Kinouchi, S. Konaka, "ECG signal pre-processing by lifting scheme constructing multi-resolution morphological decomposition," Information Technology Journal, vol. 12(2), pp: 315-322, 2013.

[33] J. Goutsias, and H.J.A.M. Heijmans, "Nonlinear multiresolution signal decomposition scheme-part I: Morphological pyramids". IEEE Trans. Image Process., vol. 9, pp: 1862-1876, 2000.

[34] Ebrahimzadeh A, Azarbad M. ECG Compression Using Wavelet Transform and Three-Level Quantization. In Proceedings of 6th International Conference on Digital Content, Multimedia Technology and its Application, 2010: 250-254.

[35] Reddy B R S, Murthy I S N. ECG Data Compression Using Fourier Descriptors. IEEE Transactions on Biomedical Engineering, 1986, 33(4): 428-434.

[36] Olmos S, Millan M, Garcia J, et al. ECG Data Compression with the Karhunen-Loeve Transform. In Proceedings of Computers in Cardiology, 1996: 253-256

[37] Allen V A, Belina J. ECG Data Compression Using the Discrete Cosine Transform. In

Proceedings of Computers in Cardiology, 1992: 687-690.

[38] Iwata A, Nagasaka Y, Suzumura N. Data Compression of the ECG Using Neural Network for Digital Holter Monitor. Medical Engineering and Physics, 2008, 30(4): 523-530.

[39] McAuliffe D. Data Compression of the Exercise ECG Using a Kohonen Neural Network. Journal of Electrocardiology, 1993, 26(Supplement): 80-89.

[40] Madhukar B, Murthy I S. ECG Data Compression by Modeling. Computers and Biomedical Research, 1993, 26(3): 310-317.

[41] Zigel Y, Cohen A, Abu-Ful A, et al. Analysis by Synthesis ECG Signal Compression. In Proceedings of Computers in Cardiology, 1997, 9: 279-282.

[42] Carmona R A, Hwang W L, Torresani B. Characterization of Signals by the Ridges of Their Wavelet Transform[J]. IEEE Transaction on Signal Processing. 1997, 45(10): 2586-2590.

[43] Bruce L M, Adhami R R. Classifying Mammographic Mass Shapes Using the Wavelet Transform Modulus-Maxima Method[J]. IEEE Transactions on Medical Imaging, 1999, 18(12): 1170-1177.

[44] Mallat S G. A Theory for Multiresolution Signal Decomposition: the Wavelet Representation[J]. IEEE Transactions on Pattern Analysis and Machine Intelligence, 1989, 11(7): 674-693.

[45] Kadambe S, Murray R, Boudreaux-Bartels G F. Wavelet Transform-Based QRS Complex Detector[J]. IEEE Transaction on Biomedical Engineering, 1999, 46(7): 838-848

[46] Kohli S S, Makwana N, Mishra N, and Sagar B. Hilbert transform based adaptive ECG R-peak detection technique. International Journal of Electrical and Computer Engineering, 2012, 2(5): 639-643;

[47] Benitez D, Gaydecki P A, Zaidi A and Fitzpatrick AP. The use of the Hilbert transform in ECG signal analysis. Computers in Biology and Medicine, 2001, 31: 399-406.

[48] Huang, N E, Attoh-Okine, N O. The Hilbert-Huang Transform in Engineering. CRC Taylor & Francis, 2005.

[49] Huang, N E, Shen, S S P. Hilbert-Huang Transform and its Applications. World Scientific, 2005.

[50] Heijmans H J A M, Goutsias J. Nonlinear Multiresolution Signal Decomposition Scheme-part II: Morphological Wavelets[J]. IEEE Transaction on Image Processing, 2000, 9(11): 1897-1913.

[51] Sweldens W. The Lifting Scheme: A New Philosophy in Biorthogonal Wavelet Constructions[C]. In Proceedings of SPIE Wavelet Applications Signal Image Processing III, 1995, 2569: 68–79.

[52] Sweldens W. The Lifting Scheme: A Custom-design Construction of Biorthogonal Wavelets[J]. Applied and Computational Harmonic Analysis, 1996, 3: 186–200.

[53] Sweldens W. The Lifting Scheme: A Construction of Second Generation Wavelets[J]. SIAM Journal on Mathematical Anylysis, 1998, 29: 511–546.

[54] M. R. Jezior, S. M. Kent, and J. E. Atwood, “Exercise testing in Wolff-Parkinson-White syndrome: Case report with ECG and literature review,” Chest Journal, vol. 127(4), pp: 1454-1457, 2005.

[55] P. Buerregaard. “Mean 24h heart rate, minimal heart rate and pauses in healthy subjects 40-79 years of age,” European Heart Journal, vol. 4, pp: 44-51, 1983.

[56] Bahoura M., Hassani M., and Hubin M., 1997. DSP Implementation of Wavelet Transform for Real Time ECG Wave Forms Detection and Heart Rate Analysis. In: Computer Methods and Programs in Biomedicine, vol. 52(1), pp: 35-44.

[57] Adname M., Jiang Z. W., and Choi S., 2009. Development of QRS Detection Algorithm Designed for Wearable Cardiorespiratory System. In: Comput. Meth. Prog Bio., vol. 93, pp: 20-31.

[58] Ning X. and Selesnick I. W., 2013. ECG Enhancement and QRS Detection Based on Sparse Derivatives. In: Biomedical Signal Processing and Control, vol. 8, pp: 713-723.

[59] Arzeno N. M., Deng Z. D., and Poon C. S., 2008. Analysis of First-Derivative Based QRS Detection Algorithms. In: IEEE Transactions on Biomedical Engineering, vol. 55(2), pp: 478-484.

[60] Lee J., Jeong K., Yoon J, et al. A Simple Real-time QRS Detection Algorithm, 1996. In: 18th Annual International Conference of the IEEE Engineering in Medicine and Biology Society, pp: 1396-1398.

[61] Nye, E. R. The effect of blood pressure alteration on the pulse wave velocity. British heart journal, 26(2): 261, 1964.

[62] Gribbin B., Steptoe A., Sleight P.. Pulse wave velocity as a measure of blood pressure change. Psychophysiology, 13(1): 86-90, 1976.

[63] Steptoe A., Smulyan H., Gribbin B., Pulse wave velocity and blood pressure change: calibration and applications. Psychophysiology, 13(5): 488-493, 1976.

[64] Lutter N., Engl H. G., Fischer, F. Bauer R. D., Noninvasive continuous blood pressure control by pulse wave velocity. Zeitschrift fur Kardiologie, 85: 124-126, 1995.

[65] Schneider J. A., Davidson D. M., Winchester M. A., Taylor C. B., The covariation of blood pressure and pulse transit time in hypertensive patients. Psychophysiology, 18(3): 301-306, 1981.

[66] Landowne, Milton, A method using induced waves to study pressure propagation in human arteries. Circulation research, 5(6): 594-601, 1971.

[67] Bazett H. C., Dreyer N. B., Measurements of pulse wave velocity. American Journal of Physiology--Legacy Content, 63(1): 94-116, 1922.

[68]

[69] Hilton M L. Wavelet and Wavelet Packet Compression of Electrocardiograms. IEEE Transactions of Biomedical Engineering[J]. 1997, 44(5): 394-402.

[70] Lu Z, Kim D Y, Pearlman W A. Wavelet Compression of ECG Signals by the Set Partitioning in Hierarchical Trees Algorithm[J]. IEEE Transactions on Biomedical Engineering, 2000, 47(7): 849-856.

[71] Polania L F, Carrillo R E, Blanco-Velasco, et al. Compressed Sensing based Method for ECG Compression[C]. In Proceedings of IEEE International Conference on Acoustics, Speech and Signal Processing, 2011, 761-764.

[72] Donoho D. Compressed sensing[J]. IEEE Transactions on Information Theory. 2006, 52(4): 1289-1306.

[73] Candes E, Romberg J, Tao T. Rebust Uncertainty Principles: Exact Signal Reconstruction from High Incomplete Frequency Information[J]. IEEE Transactions on Information Theory, 2006, 52(2): 489-509.

[74] Candes E, Wakin M. An Introduction to Compressive Sampling[J]. IEEE Signal Processing Magazine, 2008, 25(2): 21-30.

[75] Baraniuk R G. Compressive sensing[J]. IEEE Transactions on Signal Processing, 2007, 24(4):118-121.

[76] Chen S S, Donoho D L, Saunders M A. Atomic Decomposition by Basis Pursuit[J]. SIAM Review, 2001, 43(1): 129-159.

[77] Candes E J, Romberg J. Sparsity and Incoherence in Compressive Sampling[J]. Inverse Problems, 2007, 23(3): 969-985.

[78] Candes E, Romberg J, Tao T. Stable Signal Recovery from Incomplete and Inaccurate Measurements[J]. Communications on Pure and Applied Mathematics, 2006, 59(8): 1207-1223.

[79] Candes E. Lecture on Compressive Sampling and Frontiers in Signal Processing. The Institute for Mathematics and its Applications[Online]. 2006. Available: http://www.ima.umn.edu/2006-2007/ND6.4-15.07/abstracts.html.

[80] Hale E, Yin W, Zhang Y. A Fixed-point Continuation Method for l_1 -regularized Minimization with Applications to Compressed Sensing[R]. Rice University Technical Report, 2007, 07.

[81] Wen Z, Yin W, Goldfarb D, et al. A Fast Algorithm for Sparse Reconstruction Based on Shrinkage, Subspace Optimization, and Contimuation[J]. SIAM Journal on Scientific Computing, 2010, 32(4): 1832-1857.

[82] Beck A, Teboulle M. A Fast Iterative Shrinkage-Thresholding Algorithm for Linear Inverse Problem[J]. SIAM Journal on Scientific Computing, 2009, 2(1): 183-202.

[83] Wright S J, Nowak R D, Fgueiredo M A T. Sparse Reconstruction by Separatable Approximation[J]. IEEE Transactions on Signal Processing, 2009. 57(7): 2479-2493.

[84] Fgueiredo M A T, Nowak R D, Wright S J. Gradient Projection for Sparse Reconstruction: Application to Compressed Sensing and Other Inverse Problems[J]. IEEE Journal of Selected Topics in Signal Processing, 2007, 1(4): 586-597.

[85] Mallat S G, Zhi Z F. Matching Pursuit with Time-frequency Dictionaries[J]. IEEE Transactions on Signal Processing, 1993, 41(12): 3397-3415.

[86] Tropp J A, Gilbert A C. Signal Recovery from Random Measurements via Orthogonal Mathing Pursuit[J]. IEEE Transactions on Information Theory, 2007, 53(12): 4655-4666.

[87] Needell D, Tropp J A. CoSaMP: Iterative Signal Recovery from Incomplete and Inaccurate Samples[J]. Applied and Computational Harmonic Analysis, 2009, 26(3): 301-321.

[88] Blumensath T, Davies M E. On the Difference between Orthogonal Matching Pursuit and Orthogonal Least Square[Online]. 2007. Available: http://eprints.soton.ac.uk/142469/1/BDOMPvsOLS07.pdf.

[89] Blumensath T, Davies M E. Normalized Iterative Hard Thresholding Guaranteed Stability and Performance[J]. IEEE Journal of Selected Topics in Signal Processing, 2010, 4(2): 298-309.

[90] Gilbert A, Strauss M, Tropp J, et al. Algorithmic Linear Dimension Reduction in the l_1 -norm for Sparse Vectors [Online]. 2006. Available: http://arxiv.org/pdf/cs/0608079v1.pdf.

[91] Baron D, Duarte M F, Sarvotham S, et al. An Information-theoretic Approach to Distributed Compressed Sensing[C]. In Proceedings of 43rd Allerton Conference on Communication,

Control, and Computing, 2005: 1-12.

[92] Duarte M F, Sarvotham S, Baron D, et al. Distributed Compressed Sensing of Jointly Sparse Signals[C]. In Proceedings of Conference Record of the Thirty-Ninth Asilomar Conference on Signals, Systems and Computers, 2005: 1537-1541.

[93] Needell D, Vershynin R. Signal Recovery from Inaccurate and Incomplete Measurements via Regularized Orthogonal Matching Pursuit[J]. IEEE Journal of Selected Topics in Signal Processing, 2010, 4: 310-316.

[94] Do T T, Tran T D, Gan L. Sparsity Adaptive Matching Pursuit Algorithm for Practical Compressed Sensing[C]. In Proceedings of 42nd Asilomar Conference on Signals, Systems and Computers, 2008: 581-587.

Acknowledgement

First of all, I would like to express my gratitude to all those who helped me during the writing of this thesis. I gratefully acknowledge to Professor Kinouchi, who gave me a lot of help during my overseas life in Japan, and let me attend many international conferences in Canada, Japan and China. I also would like to thank Professor Konaka and Professor Zhang for their advices in my academic research and without them, I cannot finish my research on time.
Last but not the least, my gratitude also extends to Akutagawa Sensei, who was in charge of all the fairs that are related to my graduation. I do appreciate his patience and kindness.

My husband and my son are my strength during sleepless nights for writing this thesis. Thank you all and I love all of you.